TECHNISCHE
UNIVERSITÄT
DARMSTADT

Designing Pickering Emulsions for Interfacial Catalysis

Design von Pickering Emulsionen zur Grenzflächenkatalyse

Dem Fachbereich Physik
der Technischen Universität Darmstadt

zur Erlangung des akademischen Grades

Doktor der Naturwissenschaften (Dr. rer. nat.)

genehmigte Dissertation von
M. Sc. Sebastian Stock
aus Fulda

Erstgutachterin: Prof. Dr. Regine von Klitzing
Zweitgutachter: Prof. Dr. Reinhard Schomäcker

Darmstadt 2022
D17

Stock, Sebastian: Designing Pickering Emulsions for Interfacial Catalysis
Darmstadt, Technische Universität Darmstadt,
Jahr der Veröffentlichung der Dissertation auf TUprints: 2022
URN: urn:nbn:de:tuda-tuprints-229395
Tag der mündlichen Prüfung: 23.11.2022

Promotionsausschuss:

1. Gutachten:	Prof. Dr. Regine von Klitzing
2. Gutachten:	Prof. Dr. Reinhard Schomäcker
3. Gutachten:	Prof. Dr. Benno Liebchen
4. Gutachten:	Prof. Dr. Thomas Walther
Tag der Disputation:	23.11.2022

Erklärung gemäß § 9 Promotionsordnung

Hiermit versichere ich, dass ich die vorliegende Dissertation selbstständig angefertigt und keine anderen als die angegebenen Quellen und Hilfsmittel verwendet habe. Alle wörtlichen und paraphrasierten Zitate wurden angemessen kenntlich gemacht. Die Arbeit hat bisher noch nicht zu Prüfungszwecken gedient.

_____

Datum und Unterschrift

Abstract

Pickering emulsions (PEs) are emulsions stabilized by solid or soft (nano-)particles. The high adsorption energy of the particles at the interface results in outstanding stability of PEs. This attribute makes them ideal candidates as an environment for interfacial catalysis. In PEs that are used for interfacial catalysis, usually, a water-soluble catalyst is enclosed in water droplets that are surrounded by the substrate/product containing oil phase. The reaction takes place at the interface of the droplets. The large internal interfacial area of PEs benefits the contact between substrate and catalyst, while the catalyst itself is conserved and protected in the dispersed phase. This increases the product yield and reduces the catalyst loss. Most important, the inherent stability of PEs allows the application of energy-efficient separation strategies, *e. g.*, membrane filtration, to retain the catalyst phase and simultaneously extract the product phase. Despite the growing interest in this topic over the last decade, the connection between emulsion structure and reaction performance remains unclear and general conclusions are missing.

This thesis addresses the influence of the emulsion structure on the reaction and filtration performance and suggests a new improved PE structure based on the gained findings. It resembles a bottom-up approach: First, the used nano-particles are characterized regarding their size, charge, hydrophobicity, density and other geometrical characteristics. As a model system, mono-disperse silica nano-spheres (SNs) are synthesized to enable the calculation of values for the particle coverage and the particle-liquid contact area in the PEs. Second, these particles are used to stabilize water in 1-dodecene emulsions and a connection between the nano-scale particle properties and the micro-scale PE structure is drawn. Third, the PEs are tested as an environment for the hydroformylation of 1-dodecene into tridecanal *via* the water-soluble ligand-metal catalyst Rhodium-Sulfoxantphos and subsequent membrane filtration is carried out. The knowledge about the geometry and structure of the PEs enables the development of a detailed and quantitative model of the reaction process. Finally, a novel emulsion structure is designed based on the findings by combining solid hydrophobic SNs and soft hydrophilic microgel particles (MGs) to synergistically stabilize PEs. The hydrophobic SNs enable the formation of water in oil emulsions while MGs act as a spacer between the SNs to improve the catalyst-substrate contact area. These findings may contribute to a fundamental understanding and offer new impulses for the optimization of interfacial catalysis in PEs.

Kurzzusammenfassung

Pickering Emulsionen (PEs) sind Emulsionen, die durch harte oder weiche Partikel stabilisiert werden. Die hohe Adsorptionsenergie der Partikel an der Grenzfläche, führt zu einer herausragenden Stabilität dieses Emulsionstyps. Diese Eigenschaft macht PEs zu idealen Kandidaten für den Einsatz als Umgebung in der Grenzflächenkatalyse. In PEs, die für die Grenzflächenkatalyse verwendet werden, befindet sich üblicherweise ein wasserlöslicher Katalysator in den Wassertropfen, die wiederum von der Ölphase umgeben sind, die das Substrat/Produkt enthält. Die Reaktion findet an der Grenzfläche der Tropfen statt. Die große interne Grenzfläche der PEs sorgt dabei für einen hohen Katalysator-Substrat-Kontakt, während der Katalysator selbst in der dispersen Phase geschützt wird. Dies führt zu einer erhöhten Produktausbeute und reduziert den Katalysatorverlust. Insbesondere erlaubt die inhärent hohe Stabilität von PEs die Anwendung von energieeffizienten Separationsstrategien zum Rückhalt des Katalysators und der Extraktion der Produktphase, wie der Membranfiltration. Auch wenn dieses Thema im letzten Jahrzehnt stark an Aufmerksamkeit gewonnen hat, bleibt die Verbindung zwischen der Emulsionsstruktur und dem Prozessverhalten in der Katalyse unklar und es fehlen übergreifende Schlussfolgerungen.
Diese Arbeit untersucht den Einfluss der Emulsionsstruktur von PEs auf ihr Prozessverhalten in der Grenzflächenkatalyse und der Filtration und schlägt basierend auf den Erkenntnissen eine neue verbesserte Emulsionsstruktur vor. Dabei wurde ein Bottom-up-Ansatz verfolgt: Im ersten Schritt wurden die verwendeten Nanopartikel auf Grundlage ihrer Größe, Ladung, Hydrophobizität, Dichte und anderer geometrischer Eigenschaften charakterisiert. Als Modelsystem wurden monodisperse Silikananokugeln (SNs) synthetisiert, um die Berechnung von Werten für die Partikelbelegung und die Größe der Kontaktfläche der Partikel mit den jeweiligen Flüssigkeiten zu ermöglichen. Im zweiten Schritt wurden die Partikel für die Stabilisation von Wasser in 1-Doedecen Emulsionen eingesetzt und eine Verbindung zwischen nano-skaligen Partikeleigenschaften und der mikro-skaligen Emulsionsstruktur hergestellt. Im dritten Schritt wurden die PEs im Bezug auf die Hydroformylierung von 1-Dodecen zu Tridecanal mit Hilfe des Katalysators Rhodium-Sulfoxantphos und der anschließenden Membranfiltration getestet. Das Wissen über die genaue Geometrie der Partikel und der sich daraus ergebenden Emulsionstruktur erlaubt die Entwicklung eines detailierten und quantitativen Models für den Reaktionsprozess. Zuletzt wurde basierend auf den Erkenntnissen eine neue Emulsionsstruktur entwor-

fen, bei der harte, hydrophobe SNs und weiche, hydrophile Mikrogelpartikel (MGs) synergetisch PEs stabilisierten. Die hydrophoben SNs garantieren dabei die Formation und Stabilität von Wasser-in-Öl-Emulsionen, während die MGs als Abstandshalter zwischen den SNs fungieren und so den Katalysator-Substrat-Kontakt verbessern. Diese Erkenntnisse tragen zu einem fundamentalerem Verständnis der Katalyse in PEs bei und schaffen Impulse für weitere Optimierung.

Contents

Symbols and Abbreviations

a	particle diameter
A	Amplitude
AAPH	2,2′-azobis-2-methyl-propanimidamide dihydrochloride
$A_{\varnothing}$	total (equatorial) particle cross-section
$a_{\varnothing}$	specific (equatorial) particle cross-section
$a_{\text{non eq}}$	specific non-equatorial particle cross-section
AFM	Atomic Force Microscopy
A_{eff}	effective membrane area
A_O	total particle surface area
a_O	specific particle surface area
$A_{\text{oil contact}}$	total oil contact area
ΔA_{inp}	created interfacial area
$A_{\text{P,tot}}$	total particle area
$A_{\text{single void}}$	single void area
$A_{\text{void, tot}}$	total void area
$A_{\text{PE,tot}}$	total emulsion interface
α	three phase contact angle
B	decay rate of emulsion height
BIS	*N*,*N*′-methylenbisacrylamid
β	scattering angle
β_s	effectiveness of decreasing the droplet size per microgel mass
C	final PE volume fraction
CA	contact angle
c_{P}	particle concentration
CRAA	conversion rate per active area

cryo-SEM	cryo-Scanning Electron Microscopy
D	diffusion coefficient
d_{32}	Sauter mean diameter
d_{H}	hydrodynamic diameter
DLS	Dynamic Light Scattering
d_{PE}	Sauter mean droplet diameter
$d_{\mathrm{p},i}$	diameter of particle i
DSA	dropshape analyzer
$\vec{E}$	electric field strength
E	minimal desorption energy
E_{oil}	desorption energy into the oil phase
E_{water}	desorption energy into the water phase
ϵ	interfacial energy
ϵ_0	electric constant
ϵ_{r}	relative permittivity
f_{PE}	Pickering emulsion volume fraction
f_w	volume water fraction
g^1	first order correlation function
g^2	second order correlation function
Γ	decay rate
$\gamma_{\mathrm{o/w}}$	interfacial tension between water and oil
h	indentation depth
h_{PE}	total emulsion height
HOSO	high oleic acid sunflower oil
I	measured intensity of the scattered light
J	membrane flux
k	coherence factor

k_B	Boltzmann's constant
k_N	ligand molecules per particle surface
κ	Debye-Hückel parameter
LCST	lower critical solution temperature
λ	wavelength
MAA	methacrylic acid
$m_{d,tot}$	total dispersion mass
m_{MG}	total microgel particle mass
MG	microgel particle
m_p	total weighed particle mass
$m_{PE,tot}$	total PE mass
$m_{product}$	product mass
m_ρ	slope of the reciprocal density over the particle mass fraction
m_s	solvent mass
MS	micellar systems
MWCO	molecular weight cut-off
μ_e	electrophoretic mobility
n	refractive index
NIPAM	*N*-isopropylacrylamide
NF	poly(*N*-isopropylacrylamide-*co*-fumaric acid)
N_P	total number of particles
$n_{catalyst}$	catalyst amount
$n_{product}$	product amount
$n_{substrate}$	substrate amount
η	viscosity
o/w	oil in water
PAC	Pickering assisted catalysis

PE	Pickering emulsion
PEI	polyethylenimine
PIC	Pickering interfacial catalysis
PNIPAM	poly *N*-isopropylacrylamide
q	swelling ratio
$\vec{q}$	scattering vector
r_{32}	Sauter mean radius
r_{H}	hydrodynamic radius
r_{NP}	particle radius
RH-SX	Rhodium-Sulfoxantphos
r_{shrunken}	radius of a shrunken microgel particle
r_{swollen}	radius of a swollen microgel particle
$\rho_{\mathrm{d,tot}}$	total dispersion density
ρ_{p}	average single particle density
ρ_{s}	solvent density
s	silica nanosphere coverage
S	selectivity
s_{limit}	final silica nanosphere coverage
s_{max}	amplitude of silica nanosphere coverage
SN	silica nano-sphere
STY	space time yield
SX	Sulfoxantphos
t	time
T	temperature
TEM	Transmission Electron Microscopy
TMS	thermomorphic systems
TON	turnover number

TOF	turnover frequency
τ	correlation time
$\vec{v}$	drift velocity
$V_{\mathrm{d,tot}}$	total dispersion volume
VIM	1-vinylimidazole
V_{P}	total particle volume
$V_{\mathrm{PE,tot}}$	total Pickering emulsion volume
V_{reactor}	reactor volume
VPT	volume phase transition
VPTT	volume phase transition temperature
V_{s}	total solvent volume
V_{shrunken}	volume of a shrunken microgel particle
V_{swollen}	volume of a swollen microgel particle
ΔW_{inp}	energy input
w/o	water in oil
WPM	whey protein microgel
X	conversion
x_{P}	particle mass fraction
x_{s}	solvent mass fraction
Y	yield
ζ	ζ-potential

Parts of this thesis are taken from the following publications of the author:

- Stehl, D.; Milojević, N.; Stock, S.; Schomäcker, R.; Klitzing, R. v.: Synergistic Effects of a Rhodium Catalyst on Particle-Stabilized Pickering Emulsions for the Hydroformylation of a Long-Chain Olefin. *Ind. Eng. Chem. Res.*, **2019**, 58, 2524–2536.

- Kempin, M.; Stock, S.; Klitzing, R. v.; Kraume, M.; Drews, A.: Influence of particle type and concentration on the ultrafiltration behavior of nanoparticle stabilized Pickering emulsions and suspensions. *Separation and Purification Technology*, **2020**, 252, 117457.

- Stock, S.; Schlander, A.; Kempin, M.; Geisler, R.; Stehl, D.; Spanheimer, K.; Hondow, N.; Micklethwaite, S.; Weber, A.; Schomäcker, R.; Drews, A.; Gallei, M.; Klitzing, R. v.: The quantitative impact of fluid vs. solid interfaces on the catalytic performance of pickering emulsions. *Physical chemistry chemical physics: PCCP*, **2021**, 23, 2355–2367.

- Stock, S.; Jakob, F.; Röhl, S.; Gräff, K.; Kühnhammer, M.; Hondow, N.; Micklethwaite, S.; Kraume, M.; Klitzing, R. v.: Exploring water in oil emulsions simultaneously stabilized by solid hydrophobic silica nanospheres and hydrophilic soft PNIPAM microgel. *Soft matter*, **2021**, 17, 8258–8268.

- Stock, S. ; Klitzing, R. v.: Microgels at droplet interfaces of water-in-oil emulsions — challenges and progress. *Current Opinion in Colloid & Interface Science*, **2022**, 58, 101561.

- Stock, S.; Kempin, M.; Hohl, L.; Petzold, M.; Hecht, K.; Klitzing, R. v.; Drews, A.: Chapter 4.3 Pickering Emulsions. In: Kraume M.; Enders S.; Drews A. , Schomäcker R.; Engell S. and Sundmacher K. (Hg.): *Integrated Chemical Processes in Liquid Multiphase Systems. From Chemical Reaction To Process Design and Operation*, **2022**, 1. Edition: DE GRUYTER, , 304–337.

- Stock, S.; Röhl, S.; Mirau, L.; Kraume, M.; Klitzing, R. v.: Maximum incorporation of soft microgel at water in oil emulsion droplet interfaces stabilized by solid silica spheres, *Nanomaterials*, **2022**, 12, 2649.

- Röhl, S.; Hohl, L.; Stock, S.; Klitzing, R. v.; Kraume, M.: Impact of aluminum particles on drop size distributions and phase separation in liquid multiphase systems, *Chemical Engineering Research and Design*, **2022**, 184, 603–613.
- Gräff, K.; Stock, S.; Mirau, L.; Bürger, S.; Braun, L.; Völp, A.; Willenbacher, N.; Klitzing, R. v.: Untangling effects of proteins as stabilizers for foam films, *Frontiers in Soft Matter*, **2022**. (submitted)
- Stock, S.; Mirau, L.; Rutsch, M.; Wismath, S.; Kupnik, M.; Klitzing, R. v.; Rahimzadeh, A.: Influence of ultrasonication on the interfacial adsorption of microgel , **2022**, *N.N.*. (in preparation)
- Stock, S.; Schneider, C.; Klitzing, R. v.: Structure formation of soft microgel with solid silica under lateral pressure, **2022**, *N.N.*. (in preparation)
- Röhl, S.; Hohl, L.; Stock, S.; Klitzing, R. v.; Kraume, M.: Application of population balance models in nanoparticle stabilized dispersions, *Nanomaterials*, **2022**. (in preparation)

1 Introduction

Emulsions are mixtures of two or more immiscible liquids without a macroscopic phase separation. In emulsions consisting of two liquids, one liquid is dispersed in the other in form of droplets. The other liquid constitutes the outer continuous phase. The droplets are stabilized against coalescence by surface active material that is adsorbed at the droplet interface. One class of emulsions are particle stabilized emulsions, so-called Pickering emulsions (PEs). PEs (or also called Ramsden-Pickering emulsions) are named after S. U. Pickering and W. Ramsden who discovered the stabilization of emulsions with (nano-)particles at the beginning of the 20th century [1, 2]. In contrast to classical surfactant stabilized emulsions, the particular stabilizers exhibit adsorption energies up to several thousand $k_{\mathrm{B}}T$ [3–5]. This results in an irreversible adsorption of the particles at the interface which is the reason for the superior stability of PEs compared to emulsions stabilized by surfactants.

Since their discovery in the early 1900s and improvements in their mathematical understanding in the 1950s and 1960s, the interest in PEs is steadily growing in the last two decades. The number of publications per year containing the key phrase "Pickering emulsion" increased from single digits to over 120 each year between the years 2000 and 2018 [6]. Especially their extraordinary stability against coalescence and the large variety of possible environment friendly and sustainable particular stabilizers is appreciated in a multitude of applications. Possible applications range from drug delivery vehicles in medicine [7, 8] or alternatives to fatty acid stabilized emulsions in the food industry [9–12], towards reaction environments for the interfacial catalysis [13]. The stabilizers themselves can consist of different materials including solid particles such as polysytrene-beads [14, 15], fumed [16–19] and spherical silica [20, 21], tubular clay [22–24], magnetic metal particles [25], synthetic soft particles such as microgel particles (MGs) [26–29] or biological particles such as starch [30, 31] and zein nanoparticles [32], proteins [11, 33] or even whole cells [34] and bacteria [35].

The investigation of PEs as reaction environments for interfacial catalysis is a surpris-

ingly young field of research. It started to gain interest only about 10 years ago but since then the number of possible catalytic reactions and applicable particle systems is steadily growing [13, 36]. The catalytic reactions proven to work in a PE environment range from bio-catalysis, *e.g.*, esterification catalyzed by enzymes, to metal-catalyzed industrial processes, *e.g.*, epoxidation or hydroformylation. In all cases, the concept of applying PEs as reaction environment is motivated by the intention to protect the precious catalyst in one phase while maximizing the contact area with the substrate in the other phase. PEs in this context provide a high stability of the droplets against coalescence while enlarging the contact area of the two phases significantly. The dispersion of a liquid with a volume of several milliliters into micrometer sized droplets enlarges the internal interface by a factor of about 10000. Conserving the catalyst in the dispersed phase while extracting the continuous phase that contains the substrate and later the product protects the catalyst, mitigates the catalyst loss and enables the application of a continuous process. In a continuous process, fresh substrate flows in and product flows out of the reaction cycle. In contrast to other emulsions, the outstanding stability against coalescence of PEs allows the application of rough but cheap and fast separation strategies such as membrane filtration without threatening the integrity of the PEs [24, 37–41].

This thesis aims for understanding the influence of the emulsion structure on the reaction performance with the intention of finding new designs for an optimal reaction environment. In contrast to previous studies, which relied on the iterative change of important emulsion parameters and the quantification of the consequences on the reaction performance, in this thesis a bottom-up approach was chosen. This approach aims for qualitative and quantitative connection of nano-scale particle properties, and the micro-scale emulsion structure, to quantify their impact on reaction and filtration performance. A fundamental characterization of the emulsion structure leads to a thorough understanding of the process and elucidates opportunities for improvements beyond trial and error. This thesis is structured as follows: **Chapter 2** provides a brief overview over the related scientific background. It starts with the state of knowledge about PEs in general, discusses previous works on their application in catalysis and closes with the discussion of new emulsion designs that include soft MGs at the droplet interface. **Chapter 3** introduces the applied materials and methods. Key feature of this work is the combination of various sample preparation and measurement techniques from particle synthesis, modification and characterization

over thorough emulsion structure determination up to evaluation of the catalysis and membrane filtration. **Chapter 4** summarizes the particle characterization for the particles used in the following chapters. **Chapter 5** introduces PEs solely stabilized by silica nano-spheres (SNs) as a model system and shows the findings about the impact of the emulsion structure on the reaction performance for it. Based on the conclusions of Chapter 5, **Chapter 6** proposes a new promising PE structure based on the combination of MGs and SNs for ensuring the w/o type and stability of the PEs while simultaneously improving the catalyst/substrate contact. Finally, **Chapter 7** summarizes and concludes the work and discusses directions for future research.

2 Scientific Background

This chapter provides a brief overview about the topic of PEs in general and the novel case of the incorporation of microgel particles at the interface of water in oil PEs as well as the application of PEs for interfacial catalysis. More detailed textbook knowledge can be found in *The Colloidal Domain* [42], *Intermolecular and Surface Forces* [43], *Emulsion Formation and Stability* [44] or other specific literature [45–47].

2.1 Pickering Emulsions

Emulsions are mixtures of two or more immiscible liquids where one phase (dispersed phase) is finely dispersed in the second phase (continuous phase). The natural tendency of the dispersed droplets to merge together back to a two phase system is hindered in emulsions by substances adsorbed at the interface of the droplets. The term Pickering emulsion (PE) describes particle stabilized emulsions and are named after after S. U. Pickering and W. Ramsden who independently discovered this stabilization mechanism in the beginning of the 20 th century [1, 2]. While often also used for soft particle stabilized emulsions, the terminology PE was originally introduced for emulsions stabilized by solid particles. The stabilization mechanism with (solid) particles relies on the high adsorption energy of the particles (up to several thousands $k_\mathrm{B}T$) at the water-oil-interface [3]. The particles are therefore considered as irreversibly attached to the interface and can sterically protect the droplets against coalescence. This distinguishes their stabilization mechanism from the one of (low-molecular) surfactant whose adsorption energy is usually in the range of the present thermal energy (several $k_\mathrm{B}T$) [3]. This causes significantly higher stability of the PEs compared to surfactant stabilized emulsions.
An important characteristic of PEs is, that they need a large initial energy input to create the necessary interface at which the particles adsorb spontaneously. This energy

can be provided by various techniques [48]. Common methods are shaking by hand or other shaking devices [49, 50], rotor-stator mixing [51–53] and ultra-sonication [54]. During the application of the energy input a detailed balance exists between the breakage of the droplets due to the energy input (increase of the total internal interface) and the coalescence of droplets that are insufficiently covered with particles (reduction of the total internal interface) [55]. After turning off the applied mixing application the coalescence of the droplets reduces the internal interface until the particle coverage is sufficient to prevent the droplets from further coalescence. This state of the emulsion is called *coalescence limit* and was first proposed by R. M. Wiley in the 1950s [14]. If the energy input is high and long enough so that all particles had the time and the space to adsorb at the interface, the droplet size is predictable by the geometry of the particles and their coverage parameter at the interface [14, 20, 50, 56–58].

PEs can be divided in two types which are oil in water (o/w) PEs, where the oil phase is dispersed in a continuous aqueous phase and water in oil (w/o) PEs, where the aqueous phase is dispersed in a continuous oil phase. In the late 1990s and in the beginning of the 21 st century, Binks *et al.* compared particle stabilized emulsions with their surfactant stabilized counterpart and found similarities for the prediction of the resulting emulsion type [3]. The PE type is determined by the initial phase composition and the hydrophobicity of the stabilizing particles - quantifiable by their contact angle against water [17, 18, 22, 59, 60]. For equal volumes of water and oil, hydrophilic particles lead to the formation of o/w PEs and hydrophobic particles lead to the formation of w/o PEs. This rule of thumb is called Bancroft rule [61], named after W. Bancroft, who had formulated this relation for classical surfactant stabilized emulsions earlier. The explanations in the following chapter focus on the case of water in oil emulsions where water is the dispersed phase and oil represents the continuous phase.

A large variety of different particle types were shown to be able to stabilize PEs. While the inner material of the particle plays only a secondary role for, their size and shape as well as their surface properties such as charge and water affinity are the dominating properties in emulsion stabilization [62]. The particle geometry such as size and shape determines the amount of area that the particles can cover in total (see section 2.1.3) as well as influences their adsorption speed and packing at the interface [15, 56, 57, 63–66]. While the focus of early investigations of PEs laid on spherical particles since they are easier to model [62] also a large variety of other particle shapes were tested in later studies including for example ellipse- [67, 68], rod- [69], tube- [24, 70–72], cube- [73], worm- [74], disk- [75] and even mushroom-shaped [76] particles. The surface proper-

ties of particles are mainly characterized by their charge and their wettability.
Ridel *et al.* [77] showed that the particle charge have various influences on the formation of PEs. Very strong electrostatic repulsion between the particles prevents the formation of PEs completely and may slow down the adsorption kinetics. In contrast, low charge leads to particle aggregation and enables the occurrence of particles multilayers at the interface. The charge itself is also strongly influencing the wettability of the particles with water that may or may not form hydrate shells around the particles. The wettability of the particles is one of the main determining particle property for the resulting emulsion type and stability because it determines the particle adsorption energy as well as the convexity of the interface [3]. Due to the high importance of the wettability, the findings regarding its effect on the particle adsorption and with that on the emulsion structure are discussed in section 2.1.1.

Figure 2.1 shows the adsorption characteristics of three different material classes at the interface. Classical surfactants such as polar-nonpolar molecules possess an adsorption energy lower or in the range of the present thermal energy $k_B T$ [42, 78]. Their adsorption is characterized by a detailed balance between the adsorbed and the desorbed bulk state (Figure 2.1 A). In contrast, the adsorption energy of nanoparticles is usually multiple magnitudes higher than the present thermal energy what makes their adsorption at the interface irreversible [3]. The behavior of layers of nanoparticles at interfaces is characterized on the one hand by their single particle adsorption behavior and on the other hand by their interaction at the interface (Figure 2.1 B). The adsorption of solid particles at the interface is determined by their hydrophobicity while the adsorption of soft particles is a matter of deformation and swellability by each liquid (Figure 2.1 C).

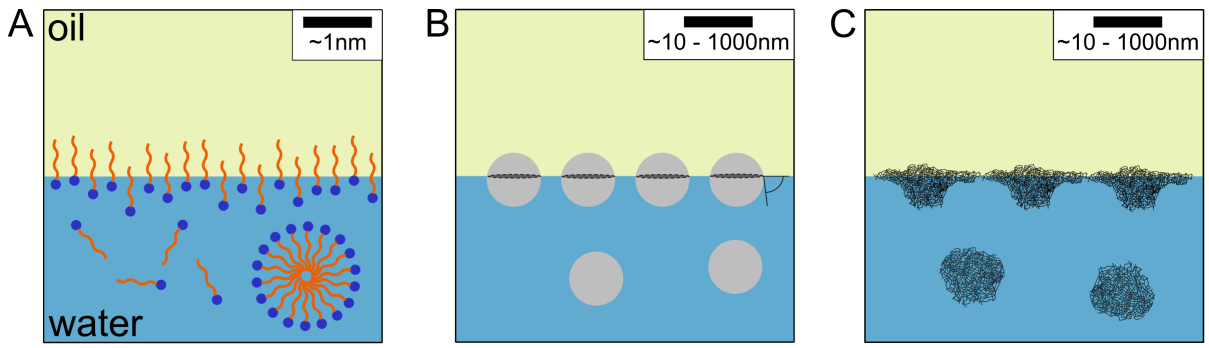

Figure 2.1: Depiction of the different adsorption types: (A) Surfactants are in a state of detailed balance between the adsorbed and the desorbed state because their adsorption energy lays in the range of $k_B T$. (C) Solid particles adsorb irreversibly at the interface in dependence of their wetting behavior (contact angle). Their adsorption energy is several orders of magnitude larger than $k_B T$. (C) Soft particles such as microgel particles display properties of both stabilization types. They have a high adsorption energy but deform at the interface and reduce the interfacial tension. Taken from Stock *et al.* [79] with permission from Elsevier.

2.1.1 Solid Particles adsorbed at the Liquid-Liquid Interface

Solid particles do not deform at the interface. Their response to the difference in interfacial energy between their surface and each of the liquids, respectively, is the penetration depth quantified by the contact angle. When defining this contact angle α as the contact angle with the water phase, this angle is equal to the contact angle of a water droplet (in oil) sitting on a macroscopic interface consisting of the same material as the solid particle. The described situation is depicted in Figure 2.2.

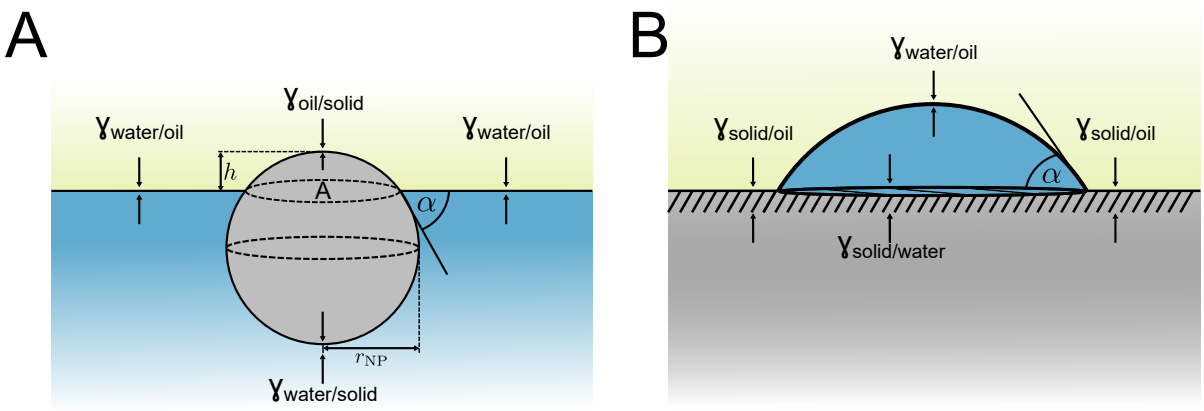

Figure 2.2: Depiction of the contact angle α between solid and water at the water/oil interface. (A) Contact angle of a single solid (nano-)sphere at the water/oil interface. The system gains energy by replacing the water/oil interfacial area A with solid/water and solid/oil interfacial area. (B) The same contact angle is found for a droplet of water on the surface of a solid interface consisting of the same material as the particle.

The penetration depth h for a spherical particle into the oil phase (as defined in Figure 2.2 A) is depending on the contact angle α by the following equation:

$$h = r_{\mathrm{NP}}(1 - \cos(\alpha)) \tag{2.1}$$

where r_{NP} is the particle radius. The contact angle α can be determined by setting a droplet on a spin coated particle layer. Hydrophobic particles with a higher contact angle tend to protrude rather into the oil phase than into the water phase while hydrophilic particles with a smaller contact angle act *vice versa*. The detachment energy E_{oil} that is necessary to remove a spherical particle from the interface into the oil phase is expressed by the contact angle α as the following [3, 4, 18]:

$$E_{\mathrm{oil}} = \pi r_{\mathrm{NP}}^2 \gamma_{\mathrm{o/w}} (1 + \cos\alpha)^2 \tag{2.2}$$

and the detachment energy E_{water} that is necessary to remove the same particle from the interface into the water phase is:

$$E_{\mathrm{water}} = \pi r_{\mathrm{NP}}^2 \gamma_{\mathrm{o/w}} (1 - \cos\alpha)^2 \tag{2.3}$$

where $\gamma_{\mathrm{o/w}}$ is the interfacial tension between the water and the oil phase. For finding an energy that describes how tight the particles are bond to the interface, it is more

important to find the minimal energy E, which is necessary to remove the particle into any of the two phase. $E(\alpha) = \min[E_{oil}(\alpha), E_{water}(\alpha)]$ describes the energy that is necessary to remove the particle into that phase in which it is easier to remove the particle into.

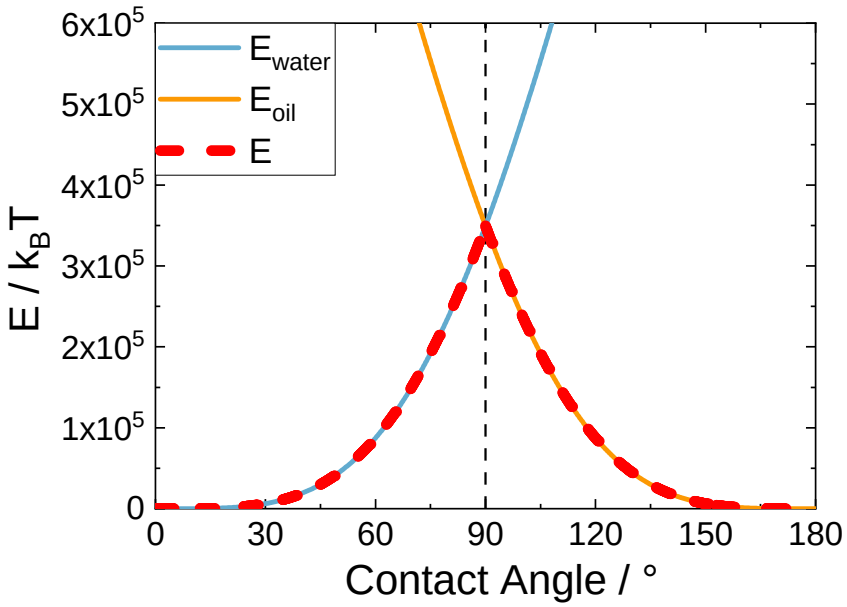

Figure 2.3: Detachment energies E_{oil}, E_{water} and E for a spherical particle with a size of $r_{NP} = 100\,nm$ at the water-dodecene interface ($\gamma_{o/w} \approx 45\,mNm^{-1}$) over the contact angle α against water.

Figure 2.3 shows the relation between E_{oil}, E_{water} and E for a spherical particle with a size of $r_{NP} = 100\,nm$ at the water-dodecene interface. E has a maximum at a contact angle of $\alpha = 90°$ because the same energy amount is necessary to move the particle fully in one or the other phase. Particles with a contact angle as close as possible to $\alpha = 90°$ are considered as the most effective interfacial stabilizer. For a spherical silica particle with a contact angle of 90° and a size of $r_{NP} = 100\,nm$ at the water-dodecene interface ($\gamma_{o/w} \approx 45\,mNm^{-1}$) the adsorption energy is $E \approx 3 \times 10^5\,k_B T$, which exceeds the present thermal energy by five orders magnitudes.
In addition to the single particle properties, the collective behavior of particle layers in terms of particle interaction and packing plays a major role for the internal emulsion geometry. Several authors showed that a layer of spherical solid particles at the inter-

face of a Langmuir trough is compressible until the limit of the hexagonal close packing when all the particles are in close contact with their neighbors [80–82]. Further compression leads to the collapse of the particle mono-layer and the eventual formation of multi-layers [83]. At the interface of PEs, the nanoscopic behavior of the nanoparticles leads to a microscopic bending of the interface of the emulsion droplets which defines the macroscopic emulsion type (o/w or w/o type) [3]. For a detailed description about the influence of the geometry of the particle layers on the droplet size see section 2.1.6.

2.1.2 Silica Nanoparticles

Nano-sized silica spheres are chosen in this work as the solid stabilizer for PEs. The term silica refers to the chemical compound of silicon dioxide. Silica is found in various forms. In nature, it is found as quartz and in various organisms [84, 85]. Examples for synthetic colloidal silica materials are fumed silica and silica nanospheres (SNs). Fumed silica is manufactured by combustion of silicon tetrachloride in an oxygen-hydrogen flame [86]. It is cheap and easy to produce, offers a wide range of industrial applications and, because of this, is produced in industry on a large scale, already. Because of its cheapness and availability in large amounts, it is most interesting for the application of emulsion stabilization but its irregular shape (Figure 2.4 A) makes it difficult to deal with from a scientific point of view.
In contrast, silica nanospheres are prepared by a seed grow process often called Stöber synthesis named after Werner Stöber, who introduced this procedure first [84, 87]. The most common approach for the Stöber synthesis route is the hydrolysis of tetraorthosilicate in an alcoholic solvent (usually ethanol) in presence of ammonia. Despite suffering from lower availability and reasonably higher production effort, SNs are a better choice for a scientific approach. Their spherical shape (Figure 2.4 B) allows to calculate necessary geometric values such as their specific surface or expected coverage parameter and therefore, they are found more frequently in fundamental research approaches [36].
Resulting from the detailed balance between protonation and de-protonation of their surface Si-O groups, silica exhibits in total a negative charge at the interface when in contact with water [88]. Untreated silica is very hydrophilic [58, 89]. Fortunately, their surface chemistry allows easy manipulation by silanization. This enables an easy tai-

loring of their surface properties without changing other particle parameters such as density, size and shape [85].

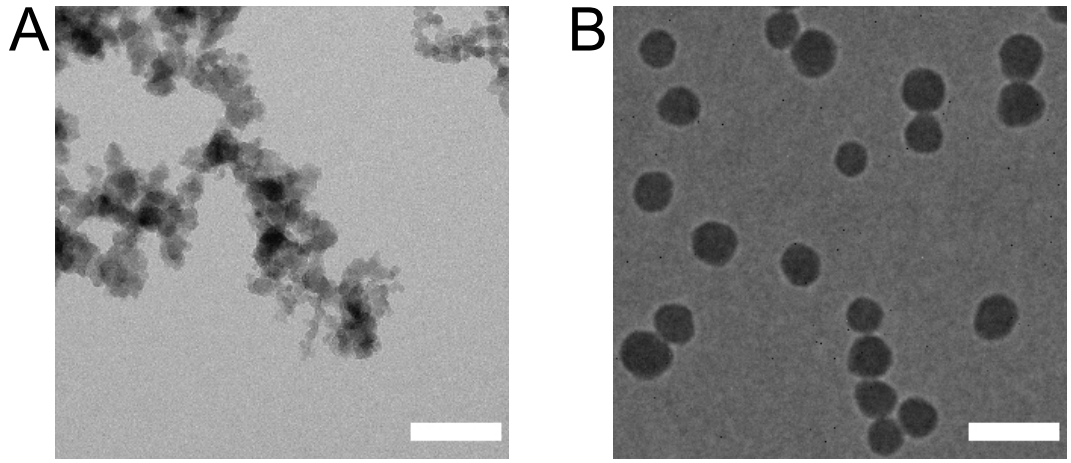

Figure 2.4: Transmission electron microscopy (TEM) images of fumed silica and silica nanospheres (SNs) [36]. Fumed Silica (A) is cheap and easy to produce but hard to describe due to its irregular shape. SNs (B) are more elaborate to produce but their convenient geometry allows the application of simple models. The white scale bars represent 100 nm.

2.1.3 Relation between Average Size and Cross-sectional Area in Ensembles of Nanospheres

For a detailed characterization of particle packing and emulsion efficiency it is necessary to characterize the stabilizing particles in terms of the area they can potentially physically cover at the interface and the amount of interface in contact with water or oil, respectively. For spherical particles it is possible to determine the total particle surface area and the total particle cross-section (= area potentially covered by the particles) from the Sauter mean diameter of the particles using simple geometric relations. For a system consisting of different sized spheres the definition of the Sauter mean diameter d_{32} is [90]:

$$d_{32} = \frac{6V_{\mathrm{p,tot}}}{A_{\mathrm{p,tot}}} = \frac{\sum_{i=1}^{N_\mathrm{p}} d_{\mathrm{p},i}^3}{\sum_{i=1}^{N_\mathrm{p}} d_{\mathrm{p},i}^2} \tag{2.4}$$

with the total number of particles N_p, the diameter of particle i $d_{\mathrm{p},i}$, the total particle area $A_{\mathrm{p,tot}}$ and the total particle volume $V_{\mathrm{p,tot}}$.
The specific particle (equatorial) cross-section $a_\oslash$ is the sum of the total (equatorial) particle cross-section area of all particles $A_\oslash$ per total weighed mass of the particles m_p and $a_\oslash$ is calculated by [58]:

$$a_\oslash = \frac{A_\oslash}{m_\mathrm{p}} = \frac{\sum_{i=1}^{N_p} \frac{\pi}{4} d_{\mathrm{p},i}^2}{\sum_{i=1}^{N_p} \frac{\pi}{6} \rho_\mathrm{p} d_{\mathrm{p},i}^3} = \frac{3}{2\,\rho_\mathrm{p}\,d_{32}} \tag{2.5}$$

with the average particle density ρ_p.
The generalized specific non equatorial particle cross-section area $a_{\text{non eq}}$ is connected with the contact angle α by:

$$a_{\text{non eq}} = a_\oslash \sin(\alpha)^2 \tag{2.6}$$

Because (a) the particles used in this thesis exhibit contact angles close to 90 ° ($\rightarrow \sin(\alpha) \approx 1$) and (b) the stabilized droplets are about two or three magnitudes larger than the stabilizing particles so that the interface on nanoscale is approximately planar (covered area = equatorial area), it is appropriate to use $a_\oslash$ instead of $a_{\text{non eq}}$ for further calculations (see section 2.1.6).
The specific particle surface area a_O of the particles is the sum of the total particle surface area of all particles A_O per total mass of the particles m_p. It is calculated analogously:

$$a_O = \frac{A_O}{m_\mathrm{p}} = \frac{\sum_{i=1}^{N_p} \pi d_{\mathrm{p},i}^2}{\sum_{i=1}^{N_p} \frac{\pi}{6} \rho_\mathrm{p} d_{\mathrm{p},i}^3} = \frac{6}{\rho_\mathrm{p}\,d_{32}} \tag{2.7}$$

The relation between $a_\oslash$ and a_O is in analogy to the relation between the surface and the equatorial cross-section of a sphere:

$$a_O = 4a_\oslash \tag{2.8}$$

The total surface area per mass of an ensemble of solid spheres is four times larger than their total cross-section per mass.

2.1.4 Coalescence and Ostwald Ripening

Large interfacial area is energetically unfavorable for mixtures of liquids with a non negligible surface tension. Energy is gained by reducing this interface. Coalescence is

a process that minimizes the internal interface and therefore the interfacial energy. It describes the process of two smaller droplets coming close together, forming a shared interface and finally merge together to a larger droplet [91]. This process leads to a reduction of the total water-oil-contact area because the larger sphere exhibits always less interface than the interface of two smaller spheres with the same volume combined. Substances that spontaneously adsorb at the interface are able to hinder the coalescence by electrostatics or steric hindrance [92]. For water-in-oil emulsions the steric hindrance plays a major role since charge effects are less pronounced in apolar solvents, *i. e.*, the continuous phase. In PEs, the particle layer around the droplets acts as a very effective hindrance for coalescence because of the enormous interfacial attachment energy of the particles. This makes PEs macroscopically very stable emulsions. Still, they do not represent a thermodynamically stable state in most cases [93]. Another mechanism of decay in emulsions is the Ostwald ripening [44, 45, 94]. It describes the process that on long time scales the larger droplets in the emulsion are growing in size while the smaller droplets are shrinking (coarsening). The result is an energetically favorable net loss in interfacial area. The explanation for this phenomenon is connected to the low but not negligible ability of the dispersed phase to solve in the continuous phase. The smaller droplets have a higher curvature so that their molecules have a higher chance to transfer into the continuous phase than those of the larger droplets. This leads to a net flow of molecules from smaller droplets to the larger ones. Since the solubility of the water molecules in an apolar oil is usually extremely low, this process takes up to several years to complete.

2.1.5 Limited Coalescence

The final PE structure depends on the quantitative ratio between two different area values, the amount of interface that the sum of all particles in the system is able to stabilize and the amount of interface created by the mixing process. The amount of interface that the particles are able to stabilize is not easy to predict in general, but for a system of spherical nanoparticles it may be calculated by simple geometrical considerations (eq. (2.5)). The amount of interface created by mixing depends very much on the applied mixing method, which are most commonly shaking by hand, rotor-stator mixing and ultra-sonication with an ultra-sonication tip [48]. Between these preparation methods lay several magnitudes of energy input. The relation between the energy input (ΔW_{inp}) and the created interface (ΔA_{inp}) is in case of PEs with solid nanoparticles

approximately defined by the interfacial energy ϵ of the water/oil interface [42]:

$$\epsilon = \frac{\Delta W_{\text{inp}}}{\Delta A_{\text{inp}}} \tag{2.9}$$

In practice, the achieved interface is difficult to determine, because the ability of the system to transform the energy into additional surface is reduced by the amount of energy loss in heat and streaming. Additionally, it does not reflect the total emulsion interface. The reason is that during the mixing step also heavy coalescence takes place which decreases the present amount of interface and acts against the interface formation (Figure 2.5 step 1) [92]. During this stirring process the particles spontaneously adsorb at the created interface. When the stirring is stopped, the coalescence reduces the free interface further until the particle coverage is sufficient to stop the coalescence (Figure 2.5 step 2). This process is happening usually quite rapidly within seconds or minutes. The end of this reduction of the excess interfacial area by coalescence to a semi-stable state is called *state of limited coalescence* [14, 50, 56, 95, 96]. If the applied mixing energy is high enough and the mixing time is sufficient, all particles in the system adsorb at the interface [97]. This allows the application of several simple models described in section 2.1.6. Nevertheless, even if the *state of limited coalescence* exhibits an outstanding stability against coalescence and has an extraordinary long-lastingness of up to several years, it is usually not thermodynamically stable [93]. The system will return to the two phase system on long time scales *via* Ostwald ripening and other mechanisms of decay such as stabilizer aging *etc.* (Figure 2.5 step 3).

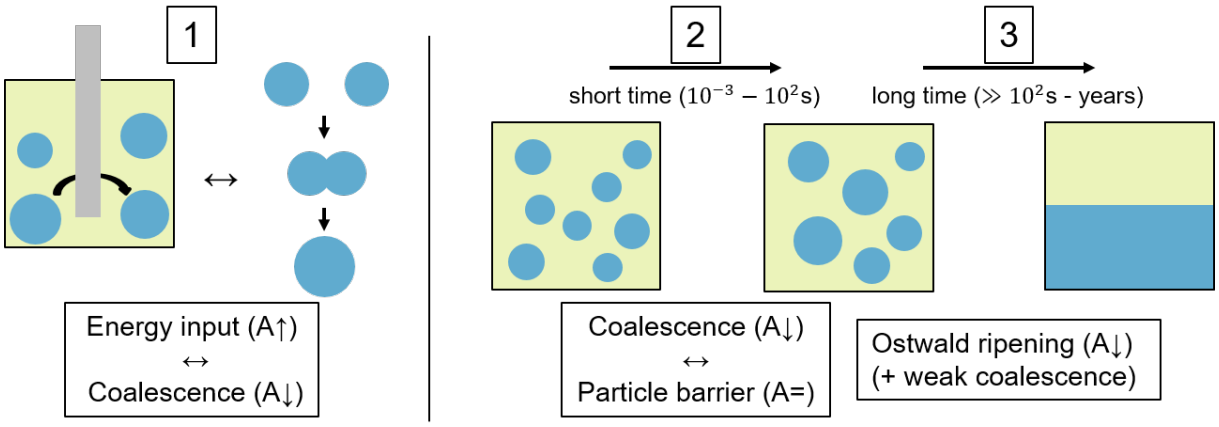

Figure 2.5: Preparation process of a Pickering emulsion. (1) Stirring the two phase system produces free interface A between oil and water that is occupied by the particles. Coalescence of unoccupied interface decreases the total interface. (2) When the stirring is stopped, the coalescence reduces the free interface further until the particle coverage is sufficient to stop the coalescence (*limited coalescence*). This state is usually not thermodynamically stable but exhibits outstanding long-lastingness. (3) Ultimately, the system decays back to the two phase system mostly by Ostwalt ripening. Depending on the system, this process can take several years.

2.1.6 Geometrical Considerations for Emulsion Droplets stabilized by Spherical Particles

In the *limited coalescence condition* the droplet size and the magnitude of internal interfaces can be predicted based on knowledge about the particle properties.
If the volume of the PE $V_{\mathrm{PE,tot}}$ is kept constant, the following expression for the total internal emulsion interface $A_{\mathrm{PE,tot}}$ as a function of the Sauter mean diameter d_{PE} of the PE droplets and the water fraction f_w is obtained by using the definition of the Sauter mean diameter (eq. (2.4)):

$$A_{\mathrm{PE,tot}} = \frac{6V_{\mathrm{PE,tot}}}{d_{\mathrm{PE}}} f_w \tag{2.10}$$

Assuming that all particles adsorb at the interface, the coverage parameter s connects the potential coverage area of the particles with the internal interface of the emulsion $A_{\mathrm{PE,tot}}$. The potential coverage area of the particles for spherical particles located

approximately equatorial at the interface is equal to the total particle cross-section $A_{\emptyset}$ [58]:

$$A_{\emptyset} = sA_{\mathrm{PE,tot}} \tag{2.11}$$

The densest physically possible packing for a two dimensional (2D) system with equally sized spheres is the hexagonal close packing (hcp) with a packing parameter of $s = \frac{\pi}{2\sqrt{3}} \approx 0.907$ (Figure 2.6 A). This leads to the following prediction for the droplet diameter d_{PE} in dependence of different measurable particle and emulsion properties:

$$d_{\mathrm{PE}} = \frac{6sV_{\mathrm{PE,tot}}}{a_{\emptyset}m_{\mathrm{p}}} f_w \tag{2.12}$$

With $c_{\mathrm{p}} = \frac{m_{\mathrm{p}}}{m_{\mathrm{PE,tot}}}$ as particle concentration eq. (2.12) is rearranged to:

$$d_{\mathrm{PE}} = \frac{6sf_wV_{\mathrm{PE,tot}}}{a_{\emptyset}m_{\mathrm{PE,tot}}} \frac{1}{c_{\mathrm{p}}} \tag{2.13}$$

with $m_{\mathrm{PE,tot}}$ as the total emulsion mass.
The interfaces relevant for the catalysis are only the interfaces with which the substrate (oil) is in contact with. This is on the one hand the water/oil contact area between the particles, the total void area ($A_{\mathrm{void,tot}}$), and on the other hand the interface between the particle caps and the oil (0.5 $A_{\mathrm{p,tot}}$, if the particles are located approximately equatorial at the interface). The relevant areas are depicted in Figure 2.6 B + C.

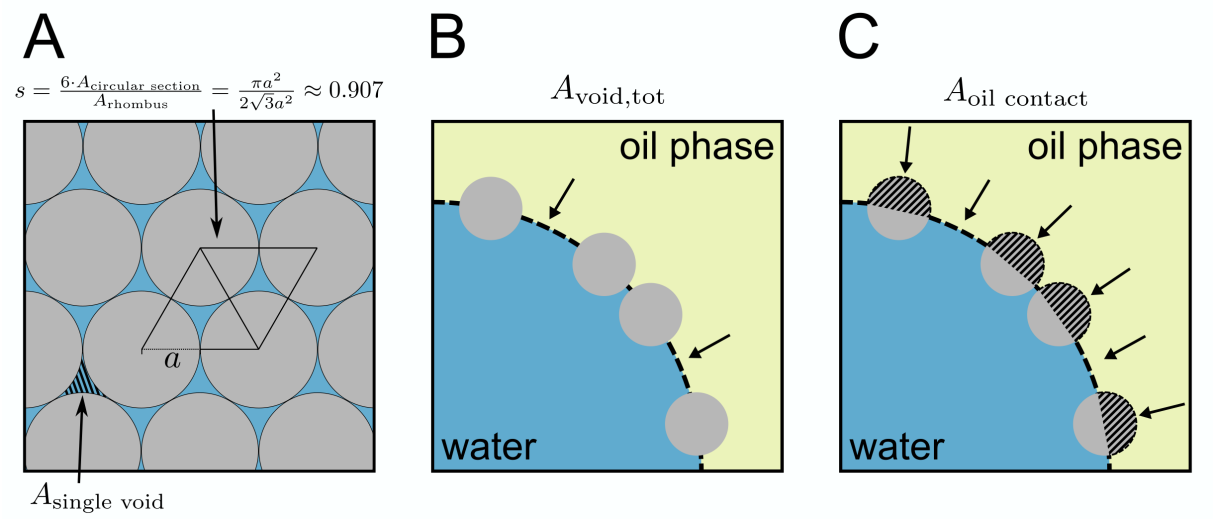

Figure 2.6: Geometry relations in w/o PEs. (A) The tightest possible packing of spherical (nano-)particles at the interface is the hexagonal close packing with a coverage parameter of $s \approx 0.907$. (B) The total free space between the particles is denoted $A_{\text{void,tot}}$. (C) The total contact area of the oil phase with the droplets (SN interface and w/o interface) is $A_{\text{oil contact}}$.

The total void area $A_{\text{void,tot}}$ (Figure 2.6 B) does not directly depend on the particle size:

$$A_{\text{void,tot}} = A_{\text{PE,tot}}\,(1-s) = A_{\emptyset}\frac{1-s}{s} \tag{2.14}$$

But the size of one gap $A_{\text{single void}}$ (Figure 2.6 A) is depending on the particle size:

$$A_{\text{single void}} = \left(\sqrt{3} - \frac{1}{2}\pi\right) r_{32}^2 \approx 0.16\, r_{32}^2 \tag{2.15}$$

The size of one void scales with the square of the particle diameter. Assuming the voids act like an ensemble of channels towards the interface that is described by Hagen-Poiseuille's law, the mass transport should be easier for larger particles systems at the same droplet size. This could indicate, whether the reaction system is limited by the mass transport through the particle layer or not.
The total substrate contact area $A_{\text{oil contact}}$ (oil-SNs + oil-water, Figure 2.6 C) can be calculated using the total particle surface $A_{\text{p,tot}}$ to:

$$A_{\text{oil contact}} = A_{\text{void,tot}} + \frac{1}{2}A_{\text{p,tot}} = A_{\emptyset,\text{tot}}\left(\frac{1-s}{s} + 2\right) = A_{\emptyset,\text{tot}}\frac{1+s}{s} \tag{2.16}$$

assuming that in average one half of the spheres extends into the oil phase (three phase contact angle 90°). This is again not depending on the particle size.

2.2 Microgel Particles at the Interface of Water in Oil Emulsions

The following section provides an overview on the scientific background regarding the incorporation of microgel particles (MGs) at the interface of w/o emulsions. It starts with basic knowledge about MGs and their adsorption behavior at interfaces. In case of soft particles used as stabilizers, the term PE is still under debate [96, 98–104]. However, most of the commonly used MGs are hydrophilic and are able to stabilize o/w emulsions [105]. Novel strategies are available to enable the w/o emulsion formation for applications, that benefit from MGs as a stabilizer but require the w/o emulsion type. Promising approaches range from novel microgel modifications to assisted stabilization with co-stabilizers. These approaches are presented and discussed at the end of this section. Large parts of the section were reproduced from the review paper *"Microgels at droplet interfaces of water-in-oil emulsions—challenges and progress"* by the author in *Current Opinion in Colloid and Interface Science* with permission from Elsevir.

2.2.1 Microgel Particles

Microgel particles (MGs) are nano- to micrometer sized polymeric cross-linked particles [106, 107]. A special characteristic of MGs is that they are swellable by the surrounding solvent [108]. Compared to solid particles like silica, MGs are soft and deformable. A very important influence factor on the macroscopic properties of the MGs is the choice of the monomer constituting the MG. Poly-*N*-isopropylacrylamide (PNIPAM) MGs - MGs that are based on the monomer *N*-isopropylacrylamid (NIPAM) - are the most common and broadly studied type of MGs. They are of high interest due to their responsiveness to outer stimuli such as temperature [106]. The monomer NIPAM has a lower critical solution temperature (LCST) at about 32 °C. Below the LCST the monomer is soluble in water but loses this solubility above the LCST. This property of NIPAM causes temperature responsivity for the polymerized final MG. PNIPAM MGs undergo a so-called volume phase transition (VPT) when their aqueous dispersion is heated over the volume phase transition temperature (VPTT) which is because originating from the LCST also at about 32 °C. Below the VPTT, the MGs are present in a swollen state with larger size. Heating the MGs above the VPTT the hydrogen bonds between the water and the MGs weaken and the water is expelled from the MG. This

causes the MGs to shrink. The swelling ratio q is the volume ratio between the swollen and shrunken state and quantifies the swellability of a MG:

$$q = \frac{V_{\text{swollen}}}{V_{\text{shrunken}}} = \frac{r^3_{\text{swollen}}}{r^3_{\text{shrunken}}} \tag{2.17}$$

V_{swollen} and r_{swollen} are the volume and the hydrodynamic radius of the MG in the swollen state, respectively. V_{shrunken} and r_{shrunken} are the volume and the hydrodynamic radius of the MG in the shrunken state, respectively.

Microgels at Interfaces

In contrast to solid particles, soft particles in general and MGs in particular are deforming significantly at the interface [98, 104, 109–115] and are able to reduce the interfacial tension [104, 109–114, 116–120]. At the interface, the MGs deform into a very flat state [121]. Most MGs are constituted as a core-shell system. Due to the polymerization process, the core of the MGs is higher cross-linked and therefore less deformable than the outer parts. This leads to a ”fried-egg” shape at the interface where the more cross-linked core remains vastly untouched while the polymer chains in the shell are stretched due to their adsorption (Figure 2.1 C). If the MG is better swellable by one liquid, it also shows a strong asymmetry in the vertical axis. The larger part of the MG is present in the liquid in which it is better swellable. The compressability of the MGs has important consequences for the behavior of their layers under compression. MG layers under compression show a non-trivial behavior. For MGs with a core-shell structure their morphology is also reflected in the compression behavior, for example in their Langmuir isotherms [112, 122, 123]. Initially, under low compression, the MG shells get in contact and the MG layer resists the compression solely by compressing the soft MG shells (Figure 2.7 A). With increasing compression more and more MG cores come into contact forming regular patterns at the interface (Figure 2.7 B). When all cores are in close contact only the elasticity of the cores resists the compression (Figure 2.7 C) until the film collapses into multi-layers or the MGs are pushed into the subphase. When MG attach spontaneously at a planar interface or at a droplet interface the state of core-core contact is not reached [124].

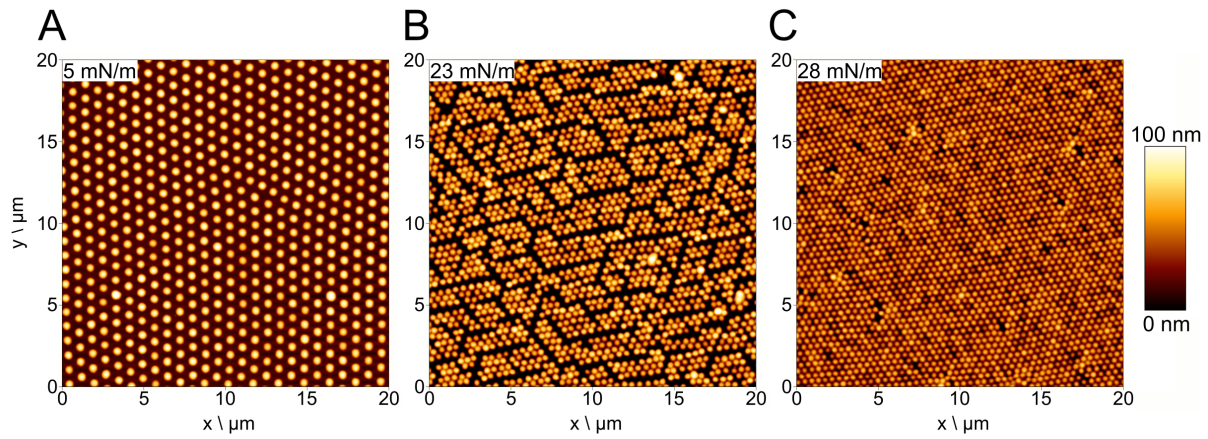

Figure 2.7: Atomic force microscopy images of MG layers that were compressed in a Langmuir trough and deposited on a wafer at three different stages of compression. For low compression (A) the outer shells are in contact and resist pressure. By further compression the MGs order themselves in increasingly tight patterns (B) until the cores are in contact at higher compression (C). Data were measured by Carina Schneider [125].

Similar to solid particles, MGs are also able to stabilize emulsions. Apart from the initial phase composition, the better wettability of the solid particles by one or the other liquid, *i. e.* the hydrophobicity, determines the emulsion type. As described in section 2.1.1, the contact angle towards water is the indicator for this hydrophobicity of the particles. W/o emulsions are preferred for a high contact angle with water (high wettability by oil, Figure 2.8 A) and o/w emulsions result from a low contact of the particles angle with water (high wettability by water, Figure 2.8 B). In analogy, the better swellability of the MGs by one or the other liquid decides about the emulsion type for MG stabilized emulsions. MGs, which are better swellable in the oil phase form w/o emulsions (Figure 2.8 C), while MGs, which are better or only swellable in water form o/w emulsions (Figure 2.8 D). W/o emulsions stabilized by MGs are very rare because most MGs are received from aqueous processes or are designed for aqueous applications [79].

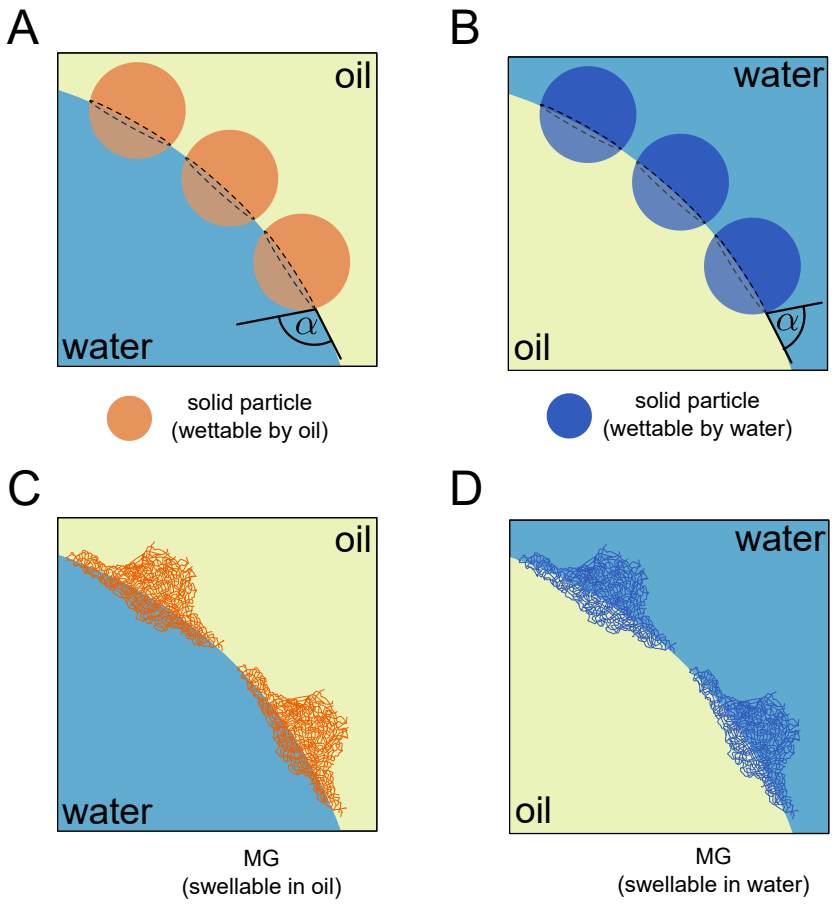

Figure 2.8: Depiction of the differences and similarities in the stabilization of emulsions with solid particles and soft MGs, respectively. While for solid particles the better wettability by one or the other liquid decides the emulsion type (A, B), for MGs the swellability by one or the other liquid decides the emulsion type (C, D) . Taken from Stock *et al.* [79] with permission from Elsevir.

2.2.2 Strategies for the Incorporation of Microgel at Interfaces of Water in Oil Emulsions

Table 2.1 provides an overview over all publications that document the presence of MGs at the interface of water in oil emulsions. The strategies to achieve this can be divided in using a highly polar oil as the continuous phase, modification of the microgel particles or introducing a second (hydrophobic) stabilizer.

Choice of the Oil Type

PNIPAM MGs are the MG species studied in most detail. They serve as a model MG for others and most of the found behavior might be generalizable to a variety of similar MGs. PNIPAM based MGs without further modification can only stabilize w/o emulsions in presence of polar oils. Destribats *et al.* [124] studied the resulting emulsion type of BIS cross-linked PNIPAM MGs (without co-monomer) in dependence of the oil type using a large variety of oils. Only the application of fatty alcohols (1-hexanol to 1-decanol), *i.e.* polar oils, led to the formation of w/o emulsions, while emulsions with non-polar oils (alkanes, ketones, aromatic hydrocarbon, halogenated oil, silicone oil) were either not stable at all or were of o/w type. Brugger *et al.* [126] and Schmidt *et al.* [26] found a similar behavior for PNIPAM based MGs with methacrylic acid as a co-monomer and BIS as cross-linker (PNIPAM-*co*-MAA MGs). These are able to stabilize water/1-octanol but also water/heptane emulsions at low water fractions ($<$50 vol%).

Table 2.1: Selection of reported cases of MGs at the internal interfaces of water-in-oil-emulsions. The publications are ordered after appearance in this section. $^{o}/^{w}$ initially dispersed in oil/water [a] High Oleic acid Sunflower Oil

MG type	co-stabilizer	oil type	reference
PNIPAM ^{w}	-	1-hexanol to 1-decanol	Destribats *et al.* (2011)[124]
PNIPAM-*co*-MMA ^{w}	-	heptane/octanol	Brugger *et al.* (2008)[126]
PNIPAM-*co*-MMA ^{w}		octanol	Schmidt *et al.* (2011)[26]
cellulose-based ^{o,w}	-	HOSO[a]	Lefreoy *et al.* (2021) [127]
PNIPAM-*co*-VIM ^{o,w}	-	silicon-oil	Zhang and Ngai (2021)[128]
PDEAEMA ^{w}	-	toluene	Jiang *et al.* (2021) [129]
PNIPAM-*co*-FA-NP hybrids ^{w}	-	various oils	Watanabe *et al.* (2019) [130]
WPM ^{w}	polyphenol crystal ^{o}	soy bean oil	Zembyla *et al.* (2019) [131]
PDEAEMA ^{w}	fumed silica ^{o}	toluene	Jiang *et al.* (2021) [129]
PNIPAM ^{w}	silica nanospheres ^{o}	1-dodecene	Stock *et al.* (2021) [132]

Stabilization with Modified Microgel

Because of their low swelling ability in many oil types, it is difficult to get w/o emulsions stabilized by hydrophilic MGs in general - and by pure PNIPAM MGs in particular. To achieve the formation of w/o emulsions, the interaction between the MGs and the oil needs to be adjusted in a way that the oil is able to swell the MGs. For most of the applications the choice of a suitable oil phase is not possible, since a certain oil type is in most cases essential for the intended application, *e. g.*, in interfacial catalysis, where the oil phase constitutes the substrate and the product, and both cannot be replaced. Therefore, some approaches were made to tailor the structure of the MGs for a better oil contact. This is done either by physisorption of functional molecules with an intended amphiphilicity, the co-polymerization of a second (co-)monomer, the choice of a better suitable monomer or other chemical manipulations such as the growing of hydrophobic particles inside the MGs. These modifications may reduce or induce surface charge, provide functional groups, add additional responsiveness or most important increase the hydrophobicity.
Especially, food technology made noticeable progress in the design and implementation of more hydrophobic MGs *via* physical adsorption: Ellis *et al.* [133] hydrophobized polysaccharide based (kappa carrageenan) MGs by attaching lauric arginate and could stabilize food-grade foams with the resulting complex, but did not test emulsification. Lefreoy *et al.* [127] compared High Oleic acid Sunflower Oil (HOSO) treated cellulose based microgel with untreated ones and showed that the hydrophobization with HOSO enables the formation of w/o emulsion up to a water content of 20%. Both authors emphasize the significant advantages of a bio-friendly and digestible stabilizer of w/o food-grade emulsions as an alternative for fatty acid based surfactant stabilizers. Studies with less emphasis on the food-grade aspect and less restrictions to biocompatibility focused more on the modification of the chemical structure of PNIPAM MGs for example by introducing functional co-monomers: Zhang and Ngai [128] synthesized PNIPAM based MGs and included 1-vinylimidazole (PNIPAM-*co*-VIM) or methacrylic acid (PNIPAM-*co*-MAA) as (co)-monomer. They compared both types of MGs towards their emulsion stabilization capability in a water/silicon-oil system. PNIPAM-*co*-MAA MGs formed exclusively o/w emulsions. For PNIPAM-*co*-VIM MGs they found an influence of particle concentration and oil phase fraction on the formed emulsion type. For small particle concentrations and high oil fractions the PEs were of w/o type. For low oil fractions o/w emulsions are formed. In between and for

higher particle concentrations they found the formation of double emulsions (o/w/o for intermediate and w/o/w for high particle concentration; w/o/w for intermediate oil fractions). They additionally tested a selection of edible oils (sunflower oil, soybean oil and corn oil) and found all of them to form w/o/w emulsions. The authors explain, that PNIPAM-*co*-VIM MGs display a delicate balance between hydrophilicity and lypophilictiy. Therefore, the MGs do not exhibit a preference for distinct droplet curvature. This results in a strong dependence of the emulsion type on the oil fraction and preparation parameters.

Haney *et al.* [134] synthesized Janus MGs from temperature sensitive poly(NIPAM) and pH sensitive poly(anhydride) by hydrolysis of two hemispheres upon each other. They showed that these hybrid particles respond asymmetrically to temperature and pH value. So far, the particles were only used to stabilize o/w emulsions. Still, these particles represent a step forward towards emulsions stabilized by particles with controllable hydrophobicity. Anisotropic responsive behavior in general might be used for switching different emulsion types one day.

Despite the important and promising recent progress, still PNIPAM based MGs might not be the ideal choice for w/o emulsion stabilization. It resembles an ideal starting point, because it is broadly studied and is very interesting due to its responsiveness. Nevertheless, due to its highly hydrophilic character NIPAM is not a suitable primary monomer for an ideal MG for w/o stabilization: Not all oil types are applicable and the chemical modification processes are often time consuming and complicated. For industrial applications such as in food industry, (industrial) catalysis or waste water treatment, the stabilizer manufacturing needs to be simple, reliable, cheap and upscalable. Therefore, a look on different other MG types and their modification is important and these MGs may provide suitable possible solutions in the future.

Jiang *et al.* [129] based their research on MGs with a monomer composition deviating from the NIPAM based standard. They used PDEAEMA based MGs and showed that these tolerate the use of toluene as the oil phase: They found that this type of MGs is able to stabilize w/o emulsions in their shrunken state (pH induced) at least for elevated oil fractions. This is one example of success in finding new and more suitable monomers for w/o emulsion stabilization.

However, the bandwidth of possible monomers for MGs, which are able to stabilize w/o emulsions, is much larger and there are different other approaches to create MGs with distinct and/or switchable hydrophobicity. Unfortunately, it seems that so far many potential candidates were not tested for emulsion stabilization yet: Already in

the year 2014, Bonham *et al.* [135] wrote a detailed review where they wrap up a large variety of reported synthesis methods for non-aqueous MGs. Most of the reported cases are using more hydrophobic monomeres and/or cross-linkers such as styrene and divinylbenzene. They pointed out that many of these MG synthesis approaches can be carried out in a variety of non-aqueous environments including many non-polar solvents and oils such as heptane, hexane and toluene. They even emphasized the possible application in emulsion stabilization. Still, these MGs did not attract high attention in this field so far. This may be attributed due to their disadvantage of the necessity of a non-green solvent such as toluene or acetonitrile for their synthesis.
Another fundamentally different approach to modify MGs for w/o emulsion stabilization, which reaches to the limit of the definition of a MG, is letting solid particles grow inside a parent MG. Watanabe *et al.* [130] proposed this rather radical approach and synthesized hydrophobized nanocomposite hydrogel microspheres from PNIPAM based BIS cross-linked MGs with fumaric acid as a co-monomer (poly(*N*-isopropyl acrylamide-*co*-fumaric acid) = NF). They used surfactant free emulsion polymerization to form either polystyrene (NF-S) or methyl-methacrylate spheres (NF-M) inside the parent MGs. These hybrids are very potent stabilizers for w/o emulsions and the authors showed the successful stabilization of w/o emulsions for an impressively large number oil types and w/o ratios. The stabilization may be caused by the mixture of stabilization by MGs with the stabilization by the incorporated solid particles, *i. e.* Pickering type stabilization.

Stabilization Assisted by Other Particle Types

Besides MG modification the mixing of MGs with other stabilizing particle types may provide new possibilities of w/o emulsion stabilization. However, mixing two or more particle types is a very broad topic with numerous influence factors and synergistic effects. In this case, not only the interaction between the liquids and the interaction between the liquids and the stabilizer is important but also the interaction of the stabilizing agents between each other comes into play. Recently, Zembyla *et al.* [136] gave a detailed review about w/o emulsions stabilized by combinations of surfactants, bio-polymers and/or particles. In summary, a variety of different combinations of soft matter from bio-polymers over proteins towards surfactants were already tested. It becomes obvious, that this field of research strongly lacks of generalized explanations, which is attributed to the enormous variety of soft stabilizers with specific interactions.

Here MGs may be helpful, because of their soft but defined structure. Combining well characterized MGs with well characterized other stabilizers like solid particles might help to elucidate the synergistic effects of co-stabilizers. A more application based motivation is to implement MGs as co-stabilizers to add responsiveness or change the mechanical properties of emulsion droplets. While the mixing of soft and often biological matter with other stabilizing species is a large but also a steadily growing field [32], studies of mixing MGs with other stabilizing species to obtain w/o emulsions are rather rare. Zembyla *et al.* [131] showed, that the combination of MGs with other particles even has a synergistic effect in stabilizing w/o emulsions when the forces between the MGs and the second stabilizer is attractive. They combined hydrophilic whey protein microgel particles (WPMs) with hydrophobic and oppositely charged polyphenol crystals. The polyphenol crystals (curcumin and quercetin based) exhibit a negative surface potential in the used soy bean oil while the WPMs show a positive ζ-potential in the water phase. By adding WPMs to the system, the synergistic interaction between WPMs and polyphenol nanocrystals increases the emulsion stability compared to emulsions that are formed with polyphenol crystals alone. This increase in stability is attributed to the electrostatic attraction between the different particle types: The WPMs act as a "colloidal glue" for the polyphenol crystals at the interface [105, 137, 138]. For larger particle concentration they observe even particle bridges between different droplets. Since WPMs are cheap and digestible, these findings pave the way to use WPMs as healthier and more efficient stabilizers in food-grade emulsions with an increased long-lastingness than the common use of fatty acid based surfactants.

MGs can also be applied as a secondary stabilizer with a high payload carrying potential. For example, Jiang *et al.* [129] used MGs at the interface of w/o emulsions tailored for interfacial catalysis. Their aim was to include MGs loaded with enzymes at the w/o interface to drag the enzymes towards the interface, and protect them in order to ensure their functionality. For this purpose they synthesized PDEAEMA MGs to encapsulate the enzyme for a safe and efficient transport towards the interface. Hydrophobic fumed silica as the primary stabilizing agent ensured the formation of a w/o emulsion. After emulsion preparation the hydrophilic MG and the hydrophobic silica coexist at the interface. This way, Jiang *et al.* [129] could not only achieve a significant increase in reaction speed and ensured the protection of the vulnerable enzyme. This way, they also enabled the application of simple and cost efficient separation strategies for product extraction such as membrane filtration or other

suitable techniques. Their study established a new strategy with very promising results, which may improve a large number of interfacial reactions.

2.3 Catalysis in Pickering Emulsions

Catalysis is a chemical process where a catalyst enables or facilitates the formation of a product from a substrate [139]. The structure of the catalyst remains in or returns to the initial state and it is not consumed during the reaction. Catalysis is a very important concept in the industrial production of chemicals due to reducing costs and saving resources. The proportion of products produced in chemical industry made by catalytic processes is about 85-90 % [139]. This makes catalysis a field with outstanding relevance for optimization. In particular, the interfacial catalysis in PEs gained a large amount of attention in the last decade.

2.3.1 Parameters for the Performance of Catalytic Reactions

To evaluate the performance of catalytic reactions multiple factors reflected by multiple parameters have to be considered [139]. A good performance is not only characterized by a high conversion but also by the amount of desired product (*i. e.* yield) and the preferably low amount of by-products (*i. e.* a high selectivity or a high n:iso ratio, *e. g.*, in case of the hydroformylation of alkanes). In addition, the deployed amount of catalyst (*i. e.* turnover number and turnover frequency), the needed amount of volume and time (*i. e.* space time yield) that led to a certain outcome are important factors to evaluate the reaction performance.
The conversion X is defined as the amount of converted substrate $n_{\text{substrate}}(t=0) - n_{\text{substrate}}(t)$ relative to the initial amount of substrate $n_{\text{substrate}}(t=0)$:

$$X(t) = \frac{n_{\text{substrate}}(t=0) - n_{\text{substrate}}(t)}{n_{\text{substrate}}(t=0)} \tag{2.18}$$

The yield Y is defined as the amount of the desired product $n_{\text{product}}(t)$ in relation to the initial amount of substrate:

$$Y(t) = \frac{n_{\text{product}}(t)}{n_{\text{substrate}}(t=0)} \tag{2.19}$$

The selectivity $S(t)$ is the ratio of desired product to the total amount of converted substrate and gives insight into the amount of by-products formed.

$$S(t) = \frac{n_{\text{product}}(t)}{n_{\text{substrate}}(t=0) - n_{\text{substrate}}(t)} \tag{2.20}$$

In case of the hydroformylation often the n:iso ratio is given. It resembles the ratio between the desired aldehyde to the amount of its unwanted isomers.
The space time yield STY takes in consideration the reaction time and reactor volume and is given in $\frac{\text{kg}}{\text{m}^3 \cdot \text{h}}$:

$$STY(t) = \frac{m_{\text{product}}(t)}{V_{\text{reactor}} \cdot t} \tag{2.21}$$

where $m_{\text{product}}(t)$ is the mass of desired product achieved and V_{reactor} is the reaction volume.
The amount of catalyst influences the reaction results and is reflected by the turnover number and the turnover frequency. The turnover number TON is defined by the amount of converted substrate $n_{\text{substrate}}(t=0) - n_{\text{substrate}}(t)$ in relation to the amount of catalyst used n_{catalyst}:

$$TON(t) = \frac{n_{\text{substrate}}(t=0) - n_{\text{substrate}}(t)}{n_{\text{catalyst}}} \tag{2.22}$$

The turnover frequency TOF is defined by the amount of converted substrate in relation to the amount of catalyst used per time. It is the TON per time:

$$TOF(t) = \frac{TON}{t} = \frac{n_{\text{substrate}}(t=0) - n_{\text{substrate}}(t)}{n_{\text{catalyst}} \cdot t} \tag{2.23}$$

A high TON or TOF indicates an efficient use of the present catalyst, but does not consider selectivity.

2.3.2 Earlier Studies on Pickering Emulsions as Reaction Environments

Because the interfacial catalysis in PEs is quite new field of research, with early works dating only back about 10 years ago, the documented cases of it are very disjointed. In addition, the approaches and ideas of these studies are coming from different fields of

research. Some aim at the design and development of the particles, some focus more on the emulsion structure and other address the reaction performance and catalyst choice. However, the main intentions in almost all cases are to drag the catalyst towards at the interface and protect it there [140]. Another aim is to enable the application of energy-efficient product separation strategies, while retaining the catalyst in the system [141]. In most studies, the overall target is a combination of both with a focus in one or the other direction.

Different reviews on the topic of catalysis in PEs brought order into these diverging approaches. Titus *et al.* [140] suggested to categorize the reported cases into Pickering assisted catalysis (PAC) and Pickering interfacial catalysis (PIC) and other authors adapted this categorization [13, 142, 143]. In their definition, PAC describes the case when particles are only added for the stabilization of the PE to enable the catalysis by an additional homogeneous catalyst. Examples for this are often found for bio-catalytic reactions where the enzyme (catalyst) is present in the aqueous phase while other particles, often silica, ensure the PE stability [38, 39, 144–151]. PIC describes emulsions where the particles act as both, the stabilizer and the catalyst. Most often this is realized by anchoring a catalytic active Pd layer on a support particle of colloidal size such as silica or titania [146, 152–157]. The reaction then takes place exclusively at the particle surface that is protruding into the substrate containing phase. In their recent review, Rodriguez and Binks [13] updated the review of Titus *et al.* and delivered an almost complete list of documented cases of catalysis in PEs in their supporting material and summarize each study by the used liquids, the particle type, the catalyst, the emulsion type and the catalyzed reaction.

Other reviews focused on other aspects of this topic. In the most recent review about catalysis in PEs by Ni *et al.* [143], the authors compared the reaction performance of different catalyzed reactions in PEs with those in the corresponding traditional bi-phasic catalysis and listed the most important studies with the best reaction performance in order of the underlying reaction mechanism. They found that overall the performance in PEs is superior to that of the bi-phasic system in terms of yield, selectivity and TOF. The reason for that is the larger interfacial contact area of PEs in comparison to non-stabilized bi-phasic systems. In addition to the previous authors, Chang *et al.* [142] also summarized advances in reactor engineering and collected those publications which tried to realize a continuous reaction cycle. Looking at these publications it becomes obvious that the implementation of PEs in continuous reaction columns is in a very early state. Most of the reactors used in these publications are not much more than a

state of the art demonstrations in rather rudimentary glass column reactors on laboratory scale [146, 147, 158–161] (with the exceptions of the works of Heyse *et al.* [38, 162] and Vis *et al.*[163] which used more elaborate reactor designs). Nonetheless, these first trials demonstrate the great potential, which this application has in the future and imply, that better and application tailored reactor designs will be able to amplify the advantages of catalysis in PEs further [164]. This includes not only the yield and selectivity or other parameters for the performance of the catalytic reaction itself but also the advantages that PEs have in terms of product separation and catalyst retention. An underrated field of research in this context is the membrane filtration of PEs which is enabled by the inherent high stability of the PEs (see section 2.3.4).
Table 2.2 summarizes all publications that investigated interfacial catalysis in PEs in alphabetical order of the name of the chemical reaction and distinguishes if at least one of the authors demonstrated already recycling and/or implemented a continuous reaction process for each reaction.

Table 2.2: Collection of publications documenting the interfacial catalysis in PEs classified if catalyst recycling or a continuous reaction process was realized, yet. It gives an overview about the impact of a specific type of catalysis in the last decade. *Tao *et al.* [165] implemented a continuous flow reactor, but with remain times of more than 100 h. The table was adapted from the book *Integrated Chemical Processes in Liquid Multiphase Systems* [36].

Reaction	Reference	recycled batch	continuous process
Acetylization	[166–168]	✓	-
Acylation	[160]	✓	-
Alkylation	[169]	✓	-
Carboligation	[34]	-	-
(Photocatalytic) Degradation	[170, 171]	-	-
Dehydration	[169, 172]	✓	-
Epoxidation	[173–178]	✓	-
(Trans-)Esterification	[38, 129, 144, 147–150, 162, 179–187]	✓	✓
Hydrodeoxygenation	[152, 153, 188, 189]	✓	-
Hydroformylation	[58, 72, 165, 190, 191]	✓	(✓)*
Hydrogenation	[154, 155, 157, 192–200]	✓	-
Hydrolyisis	[145, 150, 201–208]	✓	-
Knoevenagel condensation	[209–212]	✓	-
Oxidation	[213, 214]	-	-
Reduction	[27, 159, 176, 215, 216]	✓	-
other	[146, 217–219]	✓	✓

2.3.3 Hydroformylation of Long-chained Olefins

The term *hydroformylation* describes a catalytic reaction of olefins with carbon monoxide and hydrogen. Its primary products are aldehydes. Hydroformylation has a very high impact for industry [220], delivering products with an increasing consumption each year [221]. The hydroformylation process was invented by Otto Roehlen by accident during experiments with the Fischer-Tropsch synthesis in the year 1938 [222]. Since then huge developments of this novel reaction mechanism followed. Today, it is known that nearly all alkenes [223] and a multitude of other substrates are suitable for hydroformylation such as allyl alcohol [224] or methyl methacrylate [225]. In industry most of the hydroformylation reactions are carried out in one-phase systems (see BASF-oxo process, Exxon process, Shell process, Union Carbide process) [221, 226]. The Ruhrchemie/Rhone-Poulenc process was the first hydroformylation process where the catalyst is present in a second aqueous phase [227, 228]. It is used for the hydroformylation of propene to butanal and exhibits a remarkebly low catalyst loss.
More recent developments of new multi-phase approaches are not ready for the industrial scale implementation, yet, but show success at least on a laboratory up to mini-plant scale. The approaches here may be divided into the application of thermomorphic systems (TMS), micellar systems (MS) and PEs [141].
TMS rely on the miscibility gap between the substrate and one or multiple solvents. These systems are based on the idea of using a catalyst that is soluble in the solvent but not in the substrate-phase. The reaction is then carried out at temperatures and mixing ratios (and pressures) where the system is present as one phase [141, 229]. This drastically improves the catalyst substrate contact. For product separation, the temperature is decreased to induce phase separation of the liquid for an easy product extraction and catalyst retention in the solvent phase [230, 231]. A core challenge for the application of TMS is finding green but suitable solvents [232–234].
In MS, the addition of surfactants to a system that contains polar and nonpolar solvents leads to a drastic decrease of the surface tension between the liquids [141]. At different temperatures and surfactant concentrations various phase compositions occur. In analogy to the TMS, a suitable temperature and surfactant concentration leads to a macroscopic one phase system, which is in detail a micro-emulsion state [235, 236]. In this one phase state, the catalyst/substrate contact is highly increased, which results in a good reaction performance with high yield and satisfactory selectivity. A key challenge for the MS is the complex and temperature sensitive behavior of the system

as well as the choice of a suitable surfactant [237] and an ideal amount and type of catalyst [238, 239]. Both, TMS and MS face the problem that the ideal operating point of these systems is not only highly temperature sensitive but also changes, because the reaction distorts the molecular composition continuously.
The hydroformylation in a PE takes place at the interface of the droplets while the catalyst is kept in the aqueous phase and the substrate is located in or constitutes the oil-phase. Although it is also possible to perform the hydroformylation of alkenes in an o/w emulsion [72, 191], the w/o type is preferred. In this case, the product phase constitutes the continuous phase which enables an easier extraction of it without the necessity to break the emulsion. The choice of the particle type and the resulting emulsion structure are essential for the reaction results. Zhao *et al.* [190] and Tao *et al.* [165] used expensive and elaborate mesoporous silica particles, hydrophobized them and applied them as stabilizers for PEs. They could show that the mesoporous particles with their superior particle surface area outperform solid spheres of the same size and with the same surface treatment. Unfortunately, their mesoporous nanosized silica spheres are very expensive because their production is quite elaborate and was not realized in industrial scale production, yet. For instance, the cost of 1 g untreated mesoporous silica beads is more than 200 € (scientific standard)[240]. In comparison, the cost of fumed silica varies from about 40 € per 100 g as scientific standard [241] down to 5 € for 10 kg bags for industrial applications. Thus, mesoporous silica beads are about 500 to 400000 times more expensive. Stehl *et al.* [72, 191] realized the hydroformylation of 1-dodecene in PEs stabilized by particles that are cheaper and available in larger amounts such as fumed silica and Halloysite nanotubes. Even though these first applications were very promising, a detailed model of the process remains open. For example it remained unclear where exactly the reaction takes place - in between the particles or also on the surface of the particles protruding into the substrate phase. Also, drawing a connection between droplet area, *i. e.*, emulsion structure, and reaction results is a necessary step to enable the comparison of different PE systems [58].
In this work exemplary the hydroformylation of 1-dodecene with the water-soluble catalyst Rhodium-Sulfoxantphos (Rh-SX) is studied. Hydrogen and CO are needed as synthesis gases to deliver the stoichiometrically necessary molecules for the hydroformylation reaction (Figure 2.9 A). Rh-SX is a bi-dentate ligand metal catalyst complex [242, 243]. The ligand Sulfoxantphos (SX) is a hydrophilic derivate of Xantphos, which is proven being very effective for hydroformylation in various

applications, and makes the catalyst complex water-soluble but oil-insoluble. This water solubility enables the application of the elaborate multiphase approaches that were discussed above with the aim to reduce the catalyst loss.

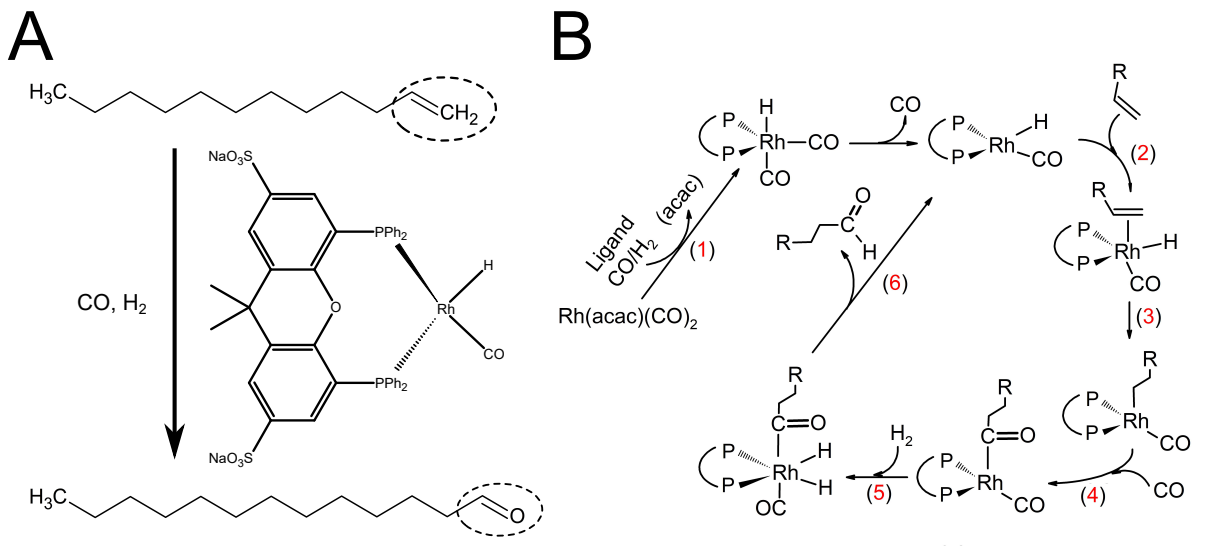

Figure 2.9: (A) Scheme of the hydroformylation of 1-dodecene *via* the water-soluble catalyst Rhodium-Sulfoxantphos (Rh-SX) and with carbon-monoxide and hydrogen as synthesis gases. The desired product is the aldehyde tridecanal. (B) Detailed step-wise depiction of the hydroformylation reaction including the preparation of the catalyst from the precursor Rh(acac). The scheme was taken from the Ph. D.-Thesis of Dmitrij Stehl [191] where it was adapted from Kiedorf *et al.* [244].

The reaction process cycle is depicted in Figure 2.9 B. Prior to the reaction, the catalyst Rh-SX is prepared from the precursor (acetylacetonato)dicarbonylrhodium(I) (Rh-(acac)$(CO)_2$) with the ligand SX *via* a ligand exchange (step 1) [245]. In step 2, the actual hydroformylation reaction cycle begins [242]: The alkene coordinates with the catalyst. In step 3, the hydrogen is inserted into the alkene and forms an alkyl species [246]. In step 4, CO is inserted into the alkyl species [247] followed by step 5 where H_2 is absorbed and inserted into the acyl species. In the last step 6, the aldehyde is released which closes the cycle.

2.3.4 Membrane Filtration of Pickering Emulsions

The membrane filtration of PEs is a convenient technical solution to separate the droplet phase from the continuous phase. This is important for systems where a water soluble catalyst is enclosed in the water droplets of a w/o PE. PEs are suitable systems for membrane filtration due to their inherent high stability. Membrane filtration avoids the necessity of other energy inefficient product separation strategies such as breaking the emulsions. Suitable membrane types come from the field of ultra filtration and the organic solvent nanofiltration and offer high membrane fluxes at low applied pressures [36]. With membrane filtration the concentration of the dispersed phase can be increased up to 80 % [248]. Kempin *et al.* could show that the membrane filtration of PEs is a very robust process. It is not impaired by important process parameters such as temperature [41] and offers the application of a large variety of solvent types [36]. It is also applicable for a large variety of PE properties irrespective of particle type [40], particle concentration [40], dispersed phase fraction [52] and droplet size distribution [52].

3 Experimental Section

3.1 Material

Water with $\rho = 18.2\,\mathrm{M\Omega{\cdot}cm}$ at 25 °C was used from a Milli-Q purification system (Merck KGaA, Darmstadt, Germany). Ludox TM40 colloidal silica spheres, Ethanol (>99%), 1-dodecene (>96%), Fluorescein sodium salt, nile red, polyethylenimine (PEI), dimethyloctadecyl[3-(trimethoxysilyl)propyl]ammonium chloride (60% in methanol), *N*-isopropylacrylamide (NIPAM), *N*,*N*'-Methylenbisacrylamid (BIS), and dodecene (>96%) were purchased from Sigma-Aldrich (Merck KGaA, Germany). 2,2'-azobis-2-methyl-propanimidamide dihydrochloride (AAPH) was purchased from Cayman Chemical Company (Cayman Chemical, USA). Octadecyltrimethoxysilane (97%) was purchased from ABCR (ABCR GmbH, Karlsruhe, Germany) and ammonia (25 % in water) was purchased from Acros Organics (Thermo Fisher Scientific, Belgium). The precursor (acetylacetonato)dicarbonylrhodium(I) (Rh-(acac)$(CO)_2$) was purchased from Umicore (Umicore AG & Co. KG, Germany) and the water soluble ligand Sulfoxantphos was obtained by Molisa (Molisa GmbH, Germany) where it was synthesized by the procedure of Goedheijt *et al.* [249]. Argon 5.0 obtained from Linde (Linde GmbH, Pullach, Germany) was used for purging the sample and a syngas mixture of CO(purity 1.6):H_2 (purity 3.0) = 1:1 was used.

3.2 Silica Particle Preparation

The used SNs are obtained from two origins, commercially purchased and self synthesized. Ludox TM40 are the largest commercially available SNs of the Ludox series and have a size of about 30 nm. These particles were used as purchased after 10 days of dialysis (100 ml against 50 l). Larger SNs were self made with tailored size. These SNs

were synthesized using the well-known sol-gel approach, called Stöber process [87]. Different particle sizes were achieved by increasing the particle size of the core particles according to a protocol described by van Blaaderen *et al.* [250]. Diameters of 50 nm, 100 nm or 200 nm were aimed. The particle surface was modified by silanization using the same silanes as Zhao *et al.* [190] but with a different procedure and concentration. Negatively charged hydrophobic SNs were obtained using octadecyltrimethoxysilane. The negative charge results from residual hydroxy groups at the silica surface [251]. To obtain positively charged hydrophobic SNs the same amount of dimethyloctadecyl[3-(trimethoxysilyl)propyl]ammonium chloride was used, which represents a silane with a similar hydrophobic chain length while simultaneously inducing a positive charge. For silanization, an amount of silane corresponding to roughly 2 silane molecules per nm^2 of particle surface was added. The reaction was then performed in ethanol at 20 °C with 200 rpm for 1 hour and an additional hour at 60 °C. After the reaction, the solvent was completely removed by evaporation under vacuum and approximately 1.5 g white powder was obtained which was redispersed in a desired solvent by ultrasonication. The sample names describe the particle origin or aimed particle diameters and the silane used for modification. The modified Ludox particles are denoted as LC18n+ or LC18n-, with respect to their surface modification. The self made, smaller oppositely charged SNs with an aimed diameter of 50 nm are denoted as 50C18n+ or 50C18n-, respectively. The larger positively charged SNs with an aimed diameter of 100 nm and 200 nm are denoted as 100C18n+ and 200C18n+, respectively. For the untreated SNs the notation 'pristine' is used.

3.3 Microgel Synthesis

The MGs were synthesized using a common and broadly studied recipe *via* precipitation polymerization reaction [106, 107, 252–254]. The monomer *N*-isopropylacrylamide (NIPAM) and the cross-linker *N*,*N*'-Methylenbisacrylamid (BIS) were dissolved in 120 ml water. The solution was degassed in a glass reactor under constant stirring (1000 RPM) and constant nitrogen flow through the solution for at least 1 hour at 80 °C. While the sum of NIPAM and BIS molecules was kept constant at 0.02 mol, their ratio to each other was varied to achieve different cross-linking densities. The cross-linker content is given as the molecular fraction of BIS to the total amount NIPAM and BIS molecules. Three different MG types were produced: lower cross-linked MG_L

(2.5 mol% BIS), medium cross-linked MG_M (5 mol% BIS) and higher cross-linked MG_H (7.5 mol% BIS). The reaction was initiated by adding 33.5 mg 2,2'-azobis-2-methyl-propanimidamide dihydrochloride (AAPH, starter) in 1 ml water *via* a syringe and then carried out for 90 min at 80 °C and 1000 RPM. The obtained MGs were cleaned by dialysis for at least 10 days (10 cycles, 120 ml dispersion against 50 l water in total), dried by lyophilization and stored at -20 °C.

3.4 ζ-Potential Measurements

The ζ-potential of particles gives hints about their surface charge and their electrostatic interaction. It was determined for all used particle systems.
Counter-ions assemble around every type of charged interface in a liquid environment such as the plane interface of a planar substrate or the convex interface of a spherical (or non-spherical) colloidal particle. This assembly of negatively and positively charged counter- and co-ions is described by the term *electrical double layer* [42]. Early descriptions of Helmholtz assumed that for every charge at the interface a corresponding counterion adsorbs at the interface to compensate the charge [255, 256]. In this Helmholtz-model the surface potential decreases linearly in analogue to the situation in a parallel-plate capacitor. An alternative description of the situation from Gouy and Chapman includes the loose and entropy rooted diffuse layer around the interface resulting from the thermal motion of the ions [257, 258]. They described the potential *via* an exponential decay. For large distances away from the interface the surface potential decreases asymptotical to zero. Stern combined the advantages of both models to the Gouy-Chapman-Stern model which describes the potential as a linear decrease for small distances but adopts the idea of a diffuse layers and with that the asymptotical decrease in potential for larger distances from the interface.
The ζ-potential is defined as the electric potential at the slipping plane where the loosely bound ions of the ion cloud in the diffuse double layer around a charged interface start to flow. In case of colloidal particles the ζ-potential describes the electric potential at the edge of the ion cloud. The ζ-potential is an indicator for the particle charge and provides important estimations about electrostatic interaction between likely charged as well as oppositely charged interfaces.
The most common way to determine the ζ-potential of colloidal particles is the calculation from the electrophoretic mobility of the particles measured during electrophoresis

in an outer electric field (Figure 3.1).

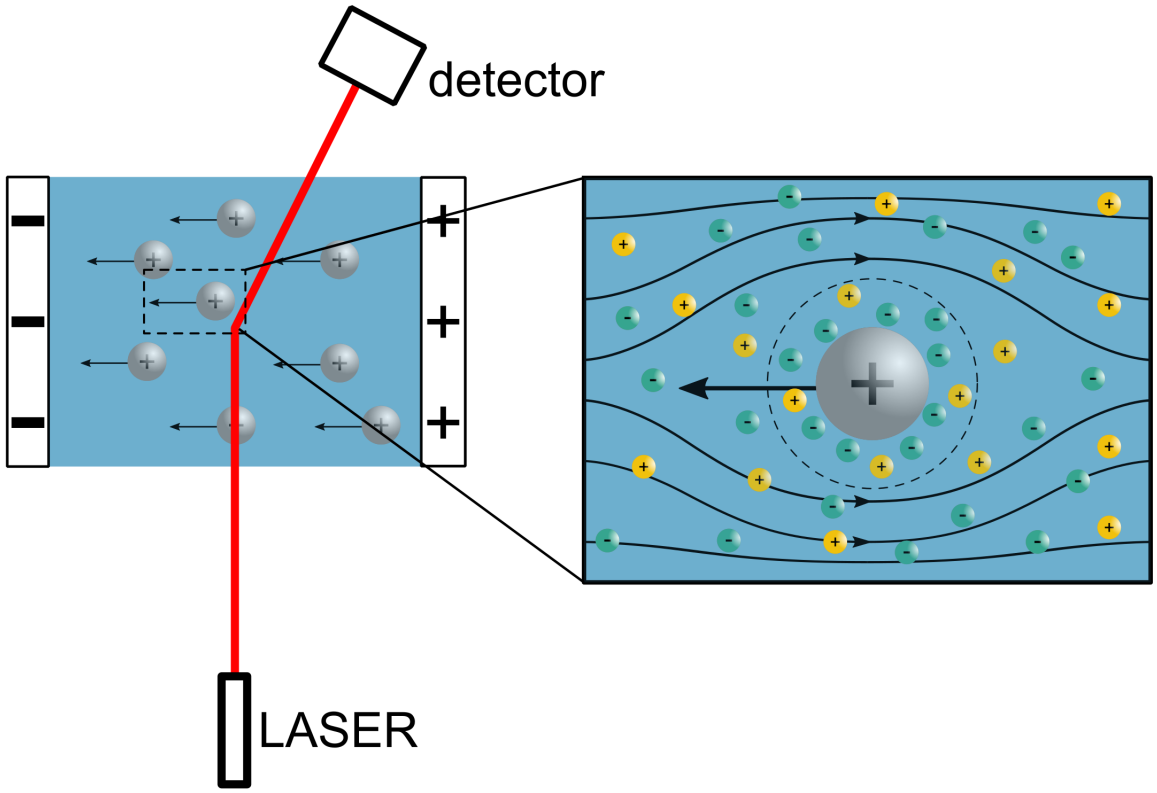

Figure 3.1: Measurement of the ζ-potential of colloidal particles: The ζ-potential is the electrostatic potential at the slipping plane of the ion cloud. It is measured by quantification of the velocity of the particles in an outer electric field.

The electrophoretic mobility μ_e is defined as follows [259]:

$$\mu_e = \frac{|\vec{v}|}{\left|\vec{E}\right|} \tag{3.24}$$

where $\vec{v}$ is the constant drift velocity of the particles in the electric field with the local electric field strength $\vec{E}$. The electrophoretic mobility depends linearly of the ζ-potential ζ:

$$\mu_e = \frac{\epsilon_r \epsilon_0}{\eta} \zeta f(\kappa a) \tag{3.25}$$

with ϵ_0 the electric constant, η the viscosity and ϵ_r the relative permittivity of the solvent and $f(\kappa\alpha)$ the Henry-function. The Henry-function itself is a function of the

particle diameter a and the Debye-Hückel parameter κ which is the reciprocal Debye-length and is a measure of the extent of the particles surface potential into the bulk. If the Debye-length κ^{-1} is very small compared to the particle diameter a, the term κa is approximately ∞ ($\kappa a \rightarrow \infty$) and the Henry-function returns 1 ($f(\kappa a) \rightarrow 1$). This approximation corresponds to a high ionic strength and/or a large particle size and eq. (3.25) becomes Smoluchowski's equation:

$$\mu_{\mathrm{e}} = \frac{\epsilon_{\mathrm{r}}\epsilon_0}{\eta}\zeta \tag{3.26}$$

For small spherical particles and a low ionic strength the term κa is approximately 0 ($\kappa a \rightarrow 0$) and the Henry function returns 2/3 ($f(\kappa a) \rightarrow 2/3$). With this approximation eq. (3.25) becomes Hückel's equation:

$$\mu_{\mathrm{e}} = \frac{2\epsilon_{\mathrm{r}}\epsilon_0}{3\eta}\zeta \tag{3.27}$$

Before every ζ-potential measurement the sample cell was purged with ethanol and water. The sample cell was tested prior to use and after the measurements with a standard provided by the manufacturer of the instrument. The ζ-potential of the SNs was determined at particle concentrations of 0.02 wt% using a Malvern Zetasizer Nano (Malvern Panalytical, UK) in ethanol. For the measurements of the interaction between the SNs and SX, different vials with ethanol containing equal particle concentration were prepared and different catalyst concentrations were added to each vial. After 10 minutes in the ultrasonic bath the ζ-potentials of the mixtures were measured. The ζ-potentials of the MGs were measured in water at a concentration of 0.006 wt%. The resulting ζ-potentials are calculated using Hückel's approximation. This may be or not be suitable, but since the focus does not lay on a prediction of the exact ζ-potential but on a comparison between different particle systems no approximation is interfering with the resulting scientific statements.

3.5 Contact Angle Determination

The hydrophobicity of the particles was estimated by evaluating the contact angle of a water droplet on a deposited layer of the respective particles on a silicon wafer. The procedure is depicted in Figure 3.2.

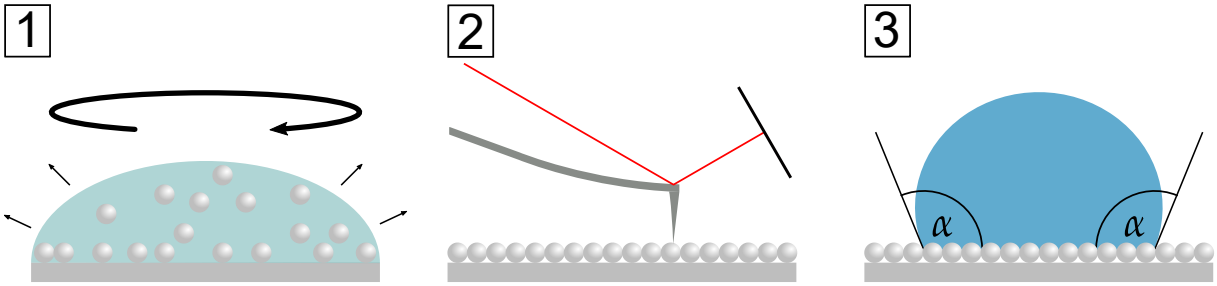

Figure 3.2: Steps for the determination of the contact angle of the SNs. (1) the particles are spin coated on a pre-cleaned silicon wafer in a suitable solvent (ethanol or water).(2) The particle layer is investigated afterwards with AFM and the roughness of the surface is measured. (3) A water drop is deposited on the particle layer and the three-phase contact angle is determined by drop shape analysis.

Spin Coating The deposition of the particle layer was carried out by spin coating (Figure 3.2 (1)). Prior to use, the silicon wafers were etched in a piranha solution (H_2O_2:H_2SO_4, 3:1) for 30 min. For the negatively charged particles the wafers were coated with 0.01 wt% solution of PEI first. The particle suspension containing 1 wt% particles was then deposited on a wafer (300 μl on 25 mm $\times$ 25 mm) until the silicon wafer was fully covered with the liquid. After a waiting time of 2 min the wafer was rotated with 1000 rpm for 2 more minutes using the spin coater Model WS-400B-6NPP-LITE by Lawel Technology Cooperation.

Atomic Force Microscopy Atomic Force Microscopy (AFM) works *via* a laser that is focused on a micron sized cantilever (Figure 3.2 (2)). When the cantilever with its tip approaches the interface, it is bent leading to a change of the deflection of the laser beam. This deflection is measured and transferred into a height value. By tapping at the surface in a 2D grid the topology of the surface is measurable. The obtained particle layer on the wafers were examined in detail with a JPK Nanowizard II Atomic Force Microscope (JPK, Germany). An AC160TS cantilever (Olympus, Japan) was used in intermittent contact mode to scan the surface. The surface roughness was determined on at least three different places with a size of 2 µm x 2 µm and the average was taken as a value and the standard deviation as a hint for the measurement error.

Drop Shape Analysis The wettability of the particle layer was measured by evaluation of the contact angle of a water droplet deposited on the particle layer (Figure 3.2 (3)). These sessile drop measurements were carried out with a OCA 15 (dataphysics, Germany) dropshape analyzer (DSA) with a drop volume of 3.5 µl using the Young-Laplace fitting method. The contact angle was measured for 1 min carrying out a measurement every second. From an average of at least five different drops the average value and standard deviation as an indicator for the error was calculated.

3.6 Transmission Electron Microscopy and Particle Size Evaluation

Transmission Electron Microscopy (TEM) was used to determine the particle size and shape of the SNs. In TEM, an electron beam is focused onto a grid with the sample. The shadow of the particles is made visible on a screen. It utilizes the smaller wavelength of the electrons in comparison to that of photons in the visible spectrum to enable the resolution of smaller structures. For the particle size distribution measurements, a drop (8 µl) from a particle suspension in ethanol was put on a Cu TEM grid with carbon film using a microliter pipette. The particle concentration was 0.027 wt% for the smaller SNs (LC18n+, 50C18n+/-), 0.1 wt% for 100C18n+ and 0.2 wt% for 200C18n+. The ethanol was allowed to evaporate from the TEM grid until it was completely dry. The samples were then examined with a FEI CM 20 ST transmission electron microscope. The size distribution and the Sauter mean diameter of the SNs were determined as shown in Figure 3.3. The TEM micrographs were thresholded in black and white contrast and automatically analyzed with ImageJ. From the area for each SN in pixels the radius of the SNs in pixels and then with the scale in nanometers was calculated. The Sauter mean diameter was calculated using eq. (2.4). To ensure representativeness at least 10 TEM images containing at least 350 particles were included in the analysis.

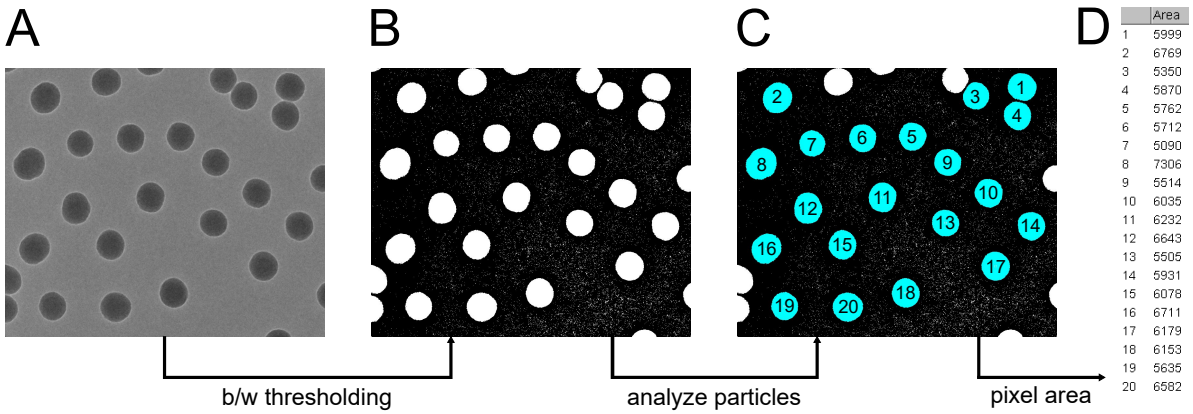

Figure 3.3: Particle size determination from TEM images: From the TEM micrographs (A) a black/white converted image (B) was created using the software ImageJ. (C) shows the SNs detected by the program, excluding the particles to close to the edges. The pixel area of the particles in (C) as data as shown in (D). Using this data, the Sauter mean diameter of the particles can be calculated.

3.7 Dispersion Density Determination

The density of the dispersions were measured with a DM40 densitometer from Mettler Toledo at 20 °C. The instrument is based on a flexural resonator, which determines the solution mass in a fixed volume by measuring the mass induced shift in resonance frequency. Its precision is given as 0.001 $\frac{g}{cm^3}$ by the manufacturer. The instruments reliability was checked after every measurement with a pure water sample. The average particle density was determined from the measurement of the total density of the dispersions with a known particle concentration. It is calculated from the slope of a linear fit from the reciprocal total dispersion density over the particle mass fraction. For more information see Section 4.1.1.

3.8 Dynamic Light Scattering

The size and the VPT behavior of the MGs were examined with Dynamic Light Scattering (DLS). DLS is a common technique to determine the size of colloidal particles in dispersions. For more detailed information see the book *Dynamic Light Scattering* [260]. The resulting value is the hydrodynamic radius/diameter (r_H/d_H). The principle setup is depicted in Figure 3.4.

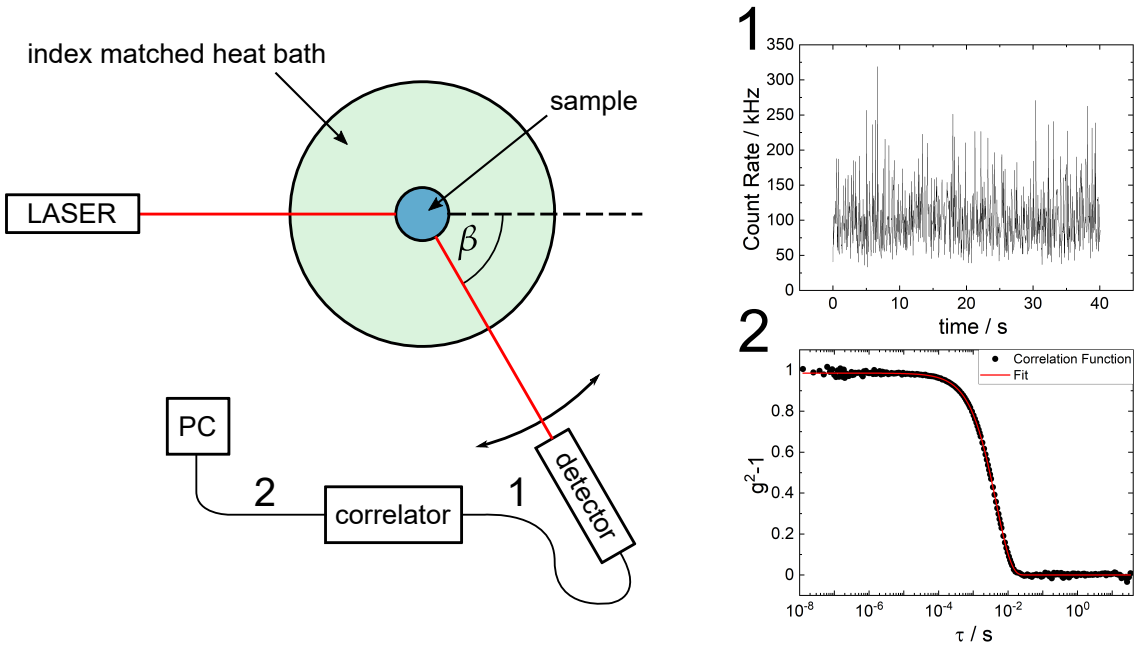

Figure 3.4: DLS setup and data. A DLS setup consists of a laser source that is directed into the sample. The scattered light is collected with a detector that is movable around the angle β around the sample. The signal (1) is transferred to the correlator which is producing the autocorrelation function (2) and sends it to the PC.

A DLS setup is based on a laser that is directed into the sampled. A detector that can be moved circularly around the sample collects the scattered light. The system is adjustable in temperature *via* an index matched heat bath. The resulting signal for a sample that contains colloidal particles at a certain angle α is fluctuating over time due to the movement of the particles in the sample. In detail, the movement of the particles leads to a fluctuation in the relative distance of the particles to each other. This

fluctuation of the distance of the scattering centers causes the time fluctuation of the interference pattern that is caught by the detector (Figure 3.4 (1)). In other words, the fluctuation of the signal over the time contains information about the diffusion speed of the particles. It is evaluated *via* the calculation of the autocorrelation function:

$$g^2(\tau) = \frac{\langle I(\vec{q},t)I(\vec{q},t+\tau)\rangle}{\langle I(\vec{q},t)\rangle^2} \tag{3.28}$$

where τ is the correlation time, $I(\vec{q},t)$ is the measured intensity of the scattered light and $\vec{q}$ is the scattering vector, which is defined as:

$$|\vec{q}| = \frac{4\pi n}{\lambda}\sin\left(\frac{\beta}{2}\right) \tag{3.29}$$

where n is the refractive index, λ is the wavelength of the laser and β the measurement angle. The mathematical calculation described by eq. (3.28) is realized electronically in the correlator. An example of an autocorrelation function is shown in Figure 3.4. The autocorrelation function measures the degree of similarity of the signal with itself with a time difference of τ. A value in the autocorrelation function close to 1 indicates high correlation and close to 0 no correlation. For short correlation times τ the particles had not enough time to move and the signal is very correlated. This correlation vanishes for large τ. The second-order correlation function $g^2(\tau)$ is related to the first-order correlation function of the electric field $g^1(\tau)$ *via* the Siegert relation:

$$g^2(\tau) = 1 + k\left|g^1(\tau)\right|^2 \tag{3.30}$$

where k is a coherence factor, depending on the instrumentation optics and laser beam. For a sample of monodisperse particles following Brownian motion $g^1(\tau)$ is described by an exponential decay:

$$g^1(\tau) = \exp -\Gamma\tau \tag{3.31}$$

with the decay rate $\Gamma = D\,|\vec{q}|^2$. A method to evaluate the signal of polydisperse samples is the *cumulant analysis*. It approximates $g^1(\tau)$ as follows:

$$g^1(\tau) = \exp\left(-\bar{\Gamma}\left(\tau - \frac{\mu_2}{2!}\tau^2 + \frac{\mu_3}{3!}\tau^3 + ...\right)\right) \tag{3.32}$$

where $\bar{\Gamma}$ is the average decay rate which is proportional to the average diffusion coefficient $\bar{D}$ of the particle ensemble. By fitting eq. (3.32) to the measured correlation functions for all measured angles one obtains $\bar{\Gamma}$ for each angle. The average diffusion

constant $\bar{D}$ is obtained from the slope in the Γ over $|\vec{q}|^2$. The diffusion coefficient is related to the hydrodynamic radius r_{H} *via* the Stokes-Einstein equation:

$$r_{\mathrm{H}} = \frac{k_{\mathrm{B}}T}{6\pi\eta D} \tag{3.33}$$

k_{B} as Boltzmann's constant, T the temperature and η as the solvent viscosity.

The hydrodynamic diameter of a diluted MG in water suspension (0.006 wt%) was measured using a commercially available DLS setup by LS-Instruments (Switzerland). The correlation function for at least 9 different angles was measured and fit using eq. (3.32).

3.9 Interfacial Tension Measurements

Interfacial Tension Measurements using Du Noüy Ring Method The interfacial tension between the catalyst solution (Rh-SX) and the oil phase was measured using a K11 tensiometer by Krüss (Germany) equipped with a platin/iridium Du Noüy ring. For the calculation of the interfacial tension the oscillating lamella technique and the related theory by Huh and Mason was applied [261]. Before the measurement the system was equilibrated for 30 min. The final value was taken from the average of at least 5 measurement cycles.

Interfacial Adsorption Characterization The interfacial activity of the MGs was measured *via* Pendant Drop Tensiometry with a drop shape analyser OCA 20 (DataPhysics, Germany) measuring an inverse oil drop on a hook shaped tip (0.01 wt% in the water phase, oil drop size 9 µl).

3.10 Emulsion Preparation

The PEs were prepared by dispersing the desired amount of SNs in their preferred phase. Prior to emulsification, the hydrophobic SNs were dispersed in the oil and

eventually used catalyst, dye and/or MGs in the water-phase, separately. The respective amounts of both phases were weighed in a vial and emulsificated with an Ultra Turrax (IKA, Germany) equipped with a S25N-10G dispersing unit at 20 kRPM for 5 minutes. If not stated otherwise the emulsion preparation was carried out at room temperature. In those cases were the preparation temperature was varied, the lower temperature of 8 °C was realized with an unsaturated ice bath and the higher temperature of 50 °C was realized with a closed loop heat controlled water bath. Prior to mixing, the water/oil mixture was equilibrated at the respective temperature for 10 minutes.

3.11 Fluorescence Microscopy and Droplet Size Determination

After preparation the emulsions were, unless stated otherwise, investigated within less than 1 hour *via* microscopy using a Axio Imager A1 (Zeiss, Germany), a combination of a transmissive light microscope and a (reflective) fluorescence microscope.
Fluorescence microscopy was carried out to examine the present emulsion type, i. e. w/o or o/w. For this purpose, the water phase was dyed prior to emulsification with water soluble but oil insoluble fluorescein sodium salt (Uranine) at a concentration of $5.32 \cdot 10^{-3}$ mmol·L^{-1}. Afterwards, the images were colored green using ImageJ for better readability.
The light microscopy images were used to determine the Sauter mean diameter of the droplets. For this purpose, the images were analyzed with an image analysis software (SOPAT GmbH, Germany) which automatically calculates the droplet size distribution from the recognized droplets and among other characterizing moments, the Sauter mean diameter.

3.12 Cryo-Scanning Electron Microscopy

Cryo-Scanning Electron Microscopy (cryo-SEM) is one of the rare methods to directly image the SNs situated at the interface of the emulsions. Cryo-SEM is based on the rapid freezing of an emulsion and subsequent electron microscopy. The measurements

for this thesis were conducted at the university of Leeds. The samples were secured into a cryo shuttle by use of a freezing rivet and submerged into slushed nitrogen. The sample was then transferred under vacuum into a Quorum PP3010 cryo preparation chamber which was under high vacuum and pre-cooled to -140 °C. The samples were fractured using a cooled knife. Prior to imaging, an Iridium coating was sputtered onto the samples and it was transferred into a Thermo scientific Helios G4 CX DualBeam (Focused ion beam scanning electron microscope; FIB-SEM) operating at 1 or 2 kV and 0.1 nA. The FIB-SEM is fitted with a cold stage (-140 °C) and cold finger (-175 °C).

3.13 Sedimentation Analysis

W/o emulsions tend to sediment down to the bottom of the vial, leaving behind a clear oil phase completely deprived of water droplets. This leads to a characteristic intensity profile along the height of the vial. By gentle shaking, the initial dispersed state is reversible (Fig. 3.5 A). After PE preparation the emulsions were equilibrated to room temperature for 1 hour. Then, the sedimentation behavior was quantified by monitoring the height of the white turbid droplet containing phase relative to the total liquid height (PE fraction) over time by taking pictures with a Nikon (Japan) D7200 equipped with a TAMRON (Japan) SP 90 mm F/2.8 macro lens every 10 seconds. Afterwards, the intensity profile was extracted by image analysis for every picture. The height position of the liquid/air interface and the turbid-clear-transition was evaluated by a low degree polynomial fit around the respective maximum/edge for every obtained intensity profile using an algorithm written in Python (Fig 3.5 B).

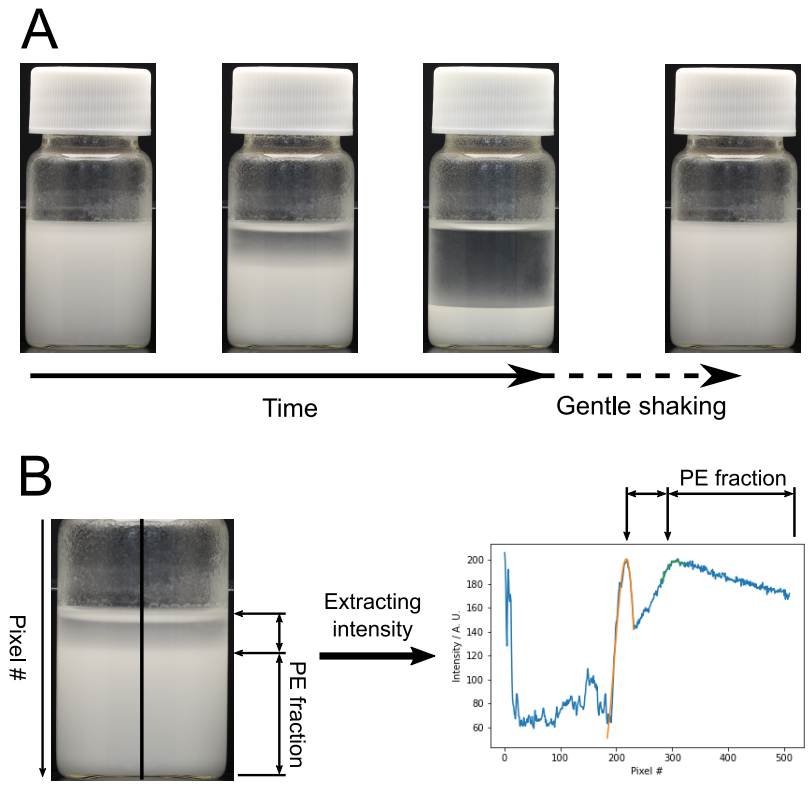

Figure 3.5: (A) The water droplets of a w/o emulsion has the tendency to sediment towards the bottom of the vial. PE droplets are usually stable enough to not break during the sedimentation and will form a sedimented high concentrated bottom phase. Gentle shaking is sufficient to redisperse the emulsion. (B) In order to study the emulsions sedimentation behavior, the time dependent PE fraction is evaluated from the vertical intensity profile extracted from pictures taken by a camera every 10 seconds.

3.14 Reaction Procedure and Result Evaluation

The hydroformylation was carried out in w/o PEs stabilized by SNs. The reaction result was and the PEs were filtrated by membrane filtration afterwards. While for the investigation of the PEs a smaller batch with a total volume of 12.55 mL, a larger batch with a total volume of 39.58 mL was used for the reaction to simulate a more application-oriented approach. For the reaction, the water phase was fixed to 25 wt% with respect to the liquid phase ($\approx$ 20 vol%) using 8 g water and 24 g 1-dodecene. While preparing the PEs for the catalysis additional steps were carried out to prevent

the contact between the oxygen sensitive Rh-catalyst and air. First, the vessel used for the PE preparation was flushed with argon, then the particle/1-dodecene suspension was added and the vessel was flushed again with argon. The catalyst solution was introduced using a syringe and the emulsion process was started immediately under constant argon stream above the vessel. After homogenization, the vessel was closed, shaken carefully and the emulsion was poured into the prepared and argon flushed reactor.

Catalyst Preparation For the hydroformylation catalyst, 38.5 mg (0.15 mmol, 1 eq.) of the precursor $Rh(acac)(CO)_2$ and 466.9 mg (0.6 mmol, 4 eq.) of the ligand SX were evacuated three times and flushed with argon by using the Schlenk technique. 6 g of degassed water were added and the catalyst solution was stirred (700 rpm) for at least 12 h at room temperature.

Catalytic Reaction For the hydroformylation reaction in the batch reactor, the PEs were prepared according to the description above. After PE preparation the emulsion was transferred into the batch reactor immediately. Syngas (1:1) with a pressure of 15 bar and a temperature of 100 °C was applied increasing both simultaneously from atmospheric pressure and room temperature. During heating and cooling the emulsion was stirred at 300 rpm while during the reaction over a duration of 20 hours the PE was stirred at 1200 rpm. The composition of the product phase was determined by gas chromatography after the reaction.

Evaluation of the Reaction with Gas Chromatography A sample of 30 - 60 µL (1-2 drops) was taken from the batch at room temperature after the reaction. The sample was then diluted in isopropanol and the internal standard nonan was added. The composition of the sample was determined *via* the gas chromatography setup GC2010plus by Shimadzu from the height of the different maxima. For the measurement, the gas chromatography column Restek RTX5-MS (30 mm x 0.25 mm x 0.25 µm) was used.

Emulsion Filtration Filtration experiments were conducted at room temperature in a solvent resistant stirred cell (XFUF04701 by Merck KGaA, Darmstadt, Germany) with an active membrane area of 13.2 cm^2. An organic solvent nanofiltration membrane

with a molecular weight cut-off (MWCO) of 900 Da was used (oNF-3, BORSIG Membrane Technology GmbH, Gladbeck, Germany). According to the manufacturers instructions, membrane samples were soaked in pure 1-dodecene for at least 2 hours prior to use for preconditioning. The membrane samples were then washed with pure 1-dodecene at a constant pressure of p = 4 bar for t = 90 min and the mass of permeate was measured with a balance and the weight was recorded using a LabVIEW program. The flux was then calculated from the actual recorded permeate mass m, time t, solvent density ρ_s and effective membrane area A_{eff}, according to eq. (3.34):

$$J = \frac{\Delta m}{\rho_s A_{eff} \Delta t} \tag{3.34}$$

The flux was then normalized with respect to the pure 1-dodecene flux from membrane pre-treatment. Applying 4 bars and stirring the emulsion at 500 rpm half of the continuous phase was extracted while recording the flux, *i. e.*, the phase fraction increased from 25 wt% to 40 wt%. For a more detailed view of the used setup see Kempin *et al.*[40]

4 Particle Characterization

This chapter summarizes the results for the characterization of the particles which were applied in the following chapters. Two fundamentally different particle types are presented: Solid SNs that were hydrophobized and adjusted in charge and soft hydrophilic MGs. The inorganic SNs were aimed to be a well-defined model-system with mono-disperse size distributions and a hydrophobic surface modification. For information about their preparation see Section 3.2. In this chapter their geometry, density, charge and hydrophobicity is discussed.
The MGs were prepared using a very common and broadly studied recipe. For detailed information about their preparation see Section 3.3. In this chapter, they are characterized regarding their size and charge, swellability, interfacial adsorption kinetics and their resistance against mechanical stress under stirring. Besides the unpublished data, parts of this chapter were published already in publications of the author in *Physical Chemistry Chemical Physics* (2021) [58], in *Soft Matter* (2021) [132] and in *Nanomaterials* (2022) [262]. The reproduced part happens with permission of the Royal Society of Chemistry (RSC) and the Multidisciplinary Digital Publishing Institute (MDPI), respectively.

4.1 Silica Nanosphere Characterization

This section provides the results and discussion of the SN characterization. The SNs are characterized regarding their density, geometry, hydrophobicity and charge to provide a sound foundation for further analysis in their application in the following chapters. The methods for this are image processing of TEM images, density measurements, AFM, sessile drop contact angle analysis and ζ-potential measurements. The notation for the SNs includes the aimed size and the modification. The aimed sizes are for all SNs close to the actual value. The particle type LC18n+ is an exception of this notation

because these stem from commercially available SNs (LudoxTM40) that were surface modified.

4.1.1 Size, Density and Specific Cross-Section

For a system of SNs the single particle density and Sauter mean diameter of the particles are the parameters that are defining the specific interface of the particles (eq. (2.5) and (2.7)). For the determination of the Sauter mean diameter of the particles, TEM images of a dried particle layer were taken and than analyzed. The results are shown in Figure 4.1. The TEM images show that all applied silica particle systems are approximately consisting of spherical particles with a quite narrow size distribution. The Sauter mean diameter of the SNs was calculated from the particle size distribution with eq. (2.4). Figure 4.1 A - C shows the comparison between the SNs with an aimed diameter of 50 nm with and without surface modification. The actual diameter of the SNs lays slightly below the aimed diameter at around 46.3 nm. Both applied procedures of surface modification (described in Section 3.2) do not change the size of the SNs noticeably and the measured differences in their Sauter mean diameter are covered by the uncertainty of the measurement. Figure 4.1 D - F shows the data for the other particle systems with smaller and larger sizes. Using SN systems that differ in size but are similar in any other property allows the investigation of size dependent effects.

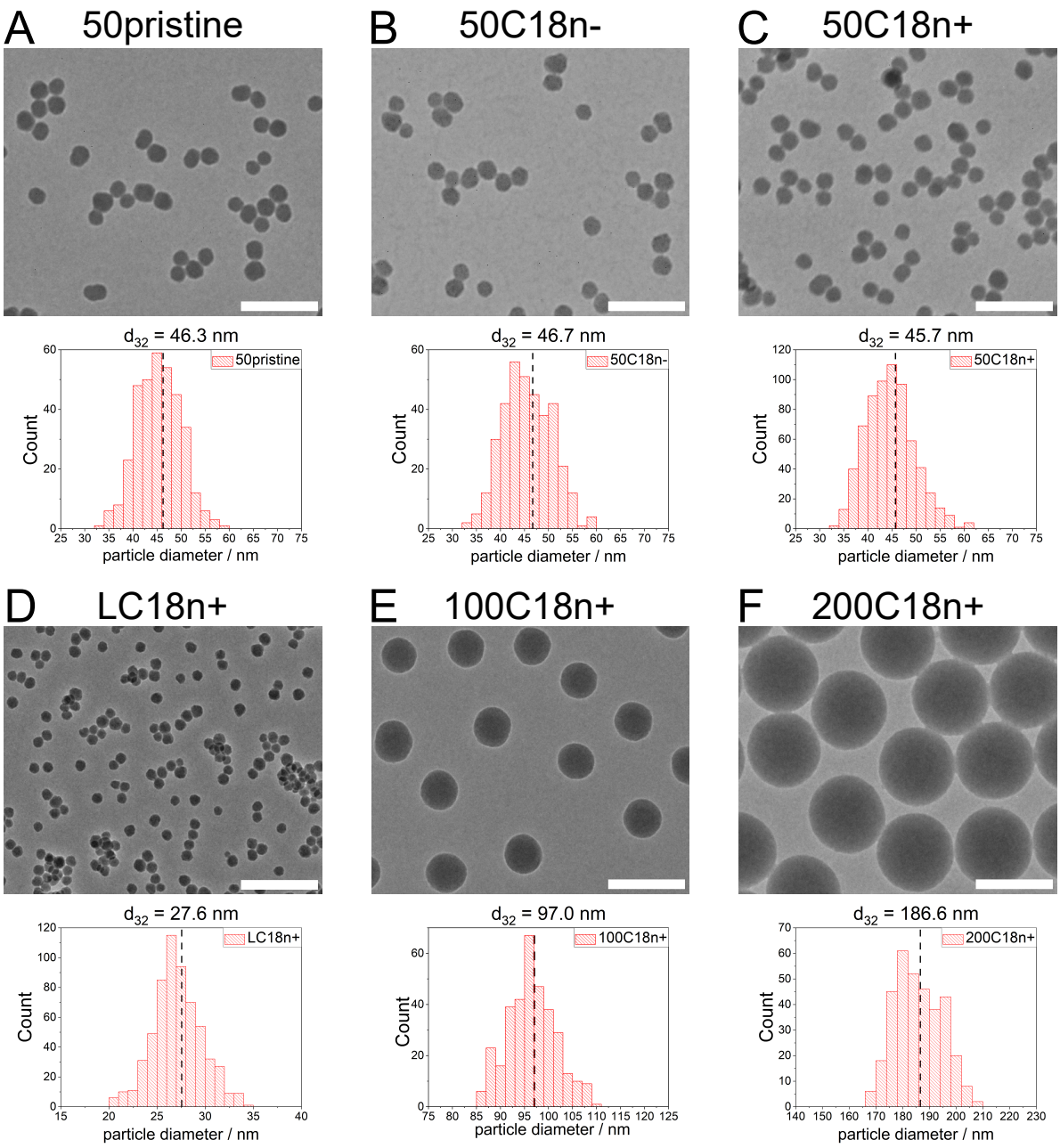

Figure 4.1: TEM image analysis for the size determination of the used SNs. The figure shows a selected TEM image and the evaluated size histogram for (A) pristine (50pristine), (B) negatively charged (50C18n-) and (C) positively charged (50C18n+) hydrophobic SNs with an aimed diameter of 50 nm. The actual Sauter mean diameter is measured to about 46.3 nm. Further, the figure shows TEM images and size histograms for hydrophobic and positively charged SNs with other sizes such as (D) modified commercial SNs (from LudoxTM40, LC18n+), (E) SNs with intended diameter of around 100 nm (100C18n+) and (F) SNs with intended diameter of 200 nm (200C18n+). The white scale bars represent 200 nm.

The single particle density of the SNs was calculated from measurements of the density of the total dispersion in a densitometer. The idea was inspired by studies that measured single particle densities in micro-fluidic devices [263, 264]. The following calculations are in analogue to that of a molecular binary solution without excess volume [265–267]. The total dispersion density $\rho_{d,tot}$ of a dispersion containing solid nanospheres that are not swellable by the solvent depends only on the density of the solvent ρ_s, the average single particle density ρ_p and the particle mass fraction x_p which is defined by:

$$x_p = \frac{m_p}{m_{d,tot}} \tag{4.35}$$

where m_p is the total mass of the particles and $m_{d,tot}$ the total dispersion mass. In analogy the solvent fraction x_s is defined as:

$$x_s = \frac{m_s}{m_{d,tot}} \tag{4.36}$$

where m_s is the mass of the solvent. The relation between x_p and x_s is:

$$x_p + x_s = \frac{m_p + m_s}{m_{d,tot}} = 1 \tag{4.37}$$

The assumption that the particles are not swellable by the solvent leads to an expression for the total dispersion volume $V_{d,tot}$:

$$V_{d,tot} = V_p + V_s \tag{4.38}$$

The average single particle density ρ_p is defined as:

$$\rho_p = \frac{m_p}{V_p} \tag{4.39}$$

The density of the solvent is defined as:

$$\rho_s = \frac{m_s}{V_s} \tag{4.40}$$

The total dispersion density can be expressed as the following:

$$\rho_{d,tot} = \frac{m_{d,tot}}{V_{d,tot}} = \frac{m_p + m_s}{V_{d,tot}} = \frac{V_p\rho_p + V_s\rho_s}{V_{d,tot}} = \frac{V_p\rho_p + \left(V_{d,tot} - V_p\right)\rho_s}{V_{d,tot}} \tag{4.41}$$

$$= \frac{V_p\left(\rho_p - \rho_s\right)}{V_{d,tot}} + \rho_s = \frac{\frac{m_p}{\rho_p}\left(\rho_p - \rho_s\right)}{\frac{m_{d,tot}}{\rho_{d,tot}}} + \rho_s = \frac{x_p\left(\rho_p - \rho_s\right)}{\rho_p}\rho_{d,tot} + \rho_s \tag{4.42}$$

Rearrangement of this expression leads to:

$$\rho_s = \rho_{d,tot} - \frac{x_p \left(\rho_p - \rho_s\right)}{\rho_p} \rho_{d,tot} \tag{4.43}$$

From this, a new expression for $\rho_{d,tot}$ is obtained only depending from ρ_p, ρ_s and x_p:

$$\rho_{d,tot} = \frac{\rho_s}{1 - \frac{\rho_p - \rho_s}{\rho_p} x_p} \tag{4.44}$$

The reciprocal dispersion density $\rho_{d,tot}^{-1}$ linearly depends on the particle mass fraction x_p:

$$\frac{1}{\rho_{d,tot}} = \frac{1}{\rho_s} - \underbrace{\frac{\rho_p - \rho_s}{\rho_p \rho_s}}_{m_\rho} x_p \tag{4.45}$$

This enables the determination of the average single particle density from the slope of the reciprocal dispersion density over the particle mass fraction m_ρ if the solvent density is known.

Figure 4.2 shows the measured data with a linear approximation and the resulting single particle density values for the different systems. The average single particle density ρ_p of the different silica particle systems was evaluated from the slope m_ρ of the reciprocal total dispersion density $\rho_{d,tot}^{-1}$ against the particle weight fraction x_p (eq. (4.45)). The data reveal that the common assumption that the density of silica is similar to the density of a natural SiO_2 crystal ($\rho(SiO_2) \approx 2.2 - 2.7\,g{\cdot}cm^{-3}$) (Skinner and Appleman [268]) is often an illegitimate approximation and will lead to larger errors in the calculation of the potentially covered interface. The presented results are in good agreement with the conclusion by Kimoto *et al.* [269] who measured the average single particle density with an aerosol particle mass analyzer. The measurements show that the determination of the average particle density is a pivotal step for a complete particle characterization.
From the measured single particle density and their Sauter mean diameter, the specific cross-section and the specific surface of the particles are calculated using eq. (2.5) and eq. (2.7), respectively. The results are displayed in Table 4.1 which summarizes the most important particle values at the end of this chapter. The uncertainty in the single particle density is considered as the main contribution to the error in the geometrical area values. Nonetheless, the standard deviation of the size distribution of the SNs was also taken in consideration for the calculation of the error.

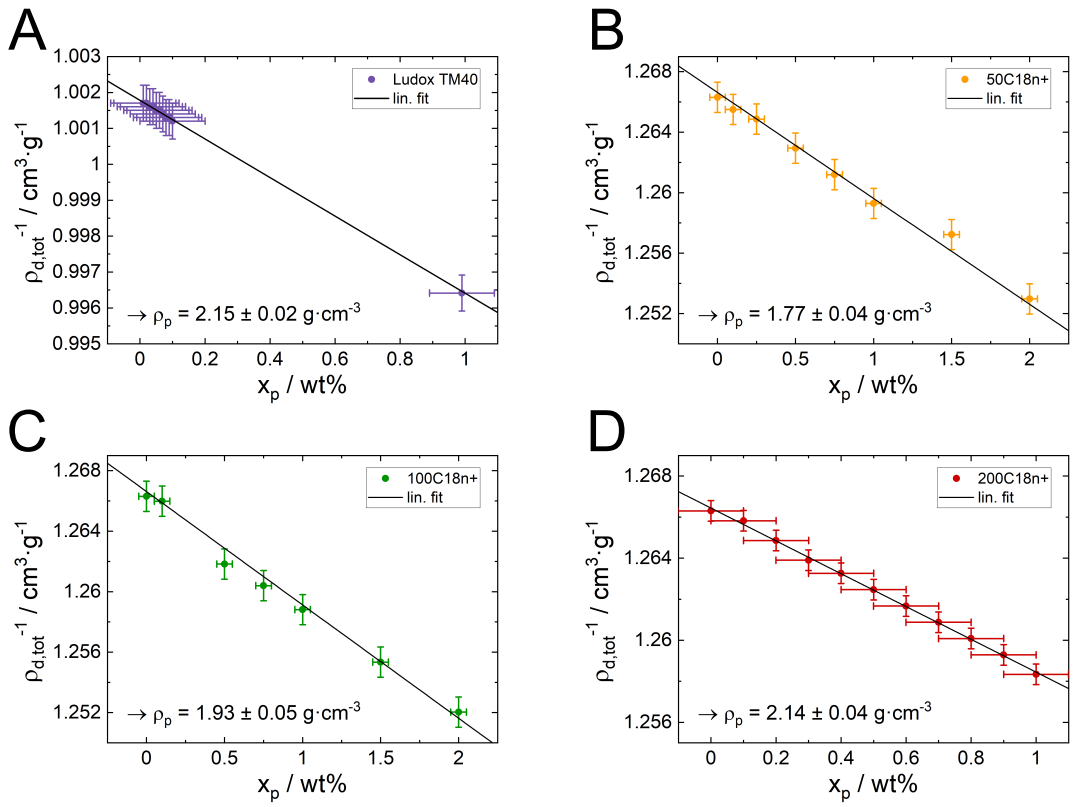

Figure 4.2: Determination of the single particle density ρ_p from the reciprocal total dispersion density $\rho_{d,tot}^{-1}$ over the particle weight fraction x_p. (A) The smaller Ludox TM40 were measured before surface modification in water. (B) 50C18n+ (C) 100C18n+ and (D) 200C18n+ were measured after surface modification in ethanol. The single particle density of the particle systems was calculated from the slope of the curves (eq. (4.45)).

4.1.2 Hydrophobicity Determination by Contact Angle Evaluation

The contact angle of the SNs against water is a measure of their hydrophilicity/hydrophobicity and is beside the phase composition of system a major influence factor that determines the final PE type. The pristine SNs were surface modified with the aim to hydrophobize them. This hydrophobization can be proven by the evaluation of the contact angle of a water droplet on a deposited particle layer on a silicon wafer. The deposited particle layer needs to be sufficient close and the roughness between compared particle types should be reasonably low. Figure 4.3 shows the water droplets

on a deposited particle layer, the respective AFM images and the values for the contact angle and the roughness. The pristine particles are hydrophilic and exhibit a very low contact angle significantly below 90 °. The surface modification of the particles turns them hydrophobic with a contact angle slightly above 90 °. All surface modified particles have a similar wettability regardless of their size and final ζ-potential. The contact angle of the other particles is given in the summary table (Table 4.1). The data show that the surface modification works and results in similar particle wettability for irrespective of the particle size and charge.

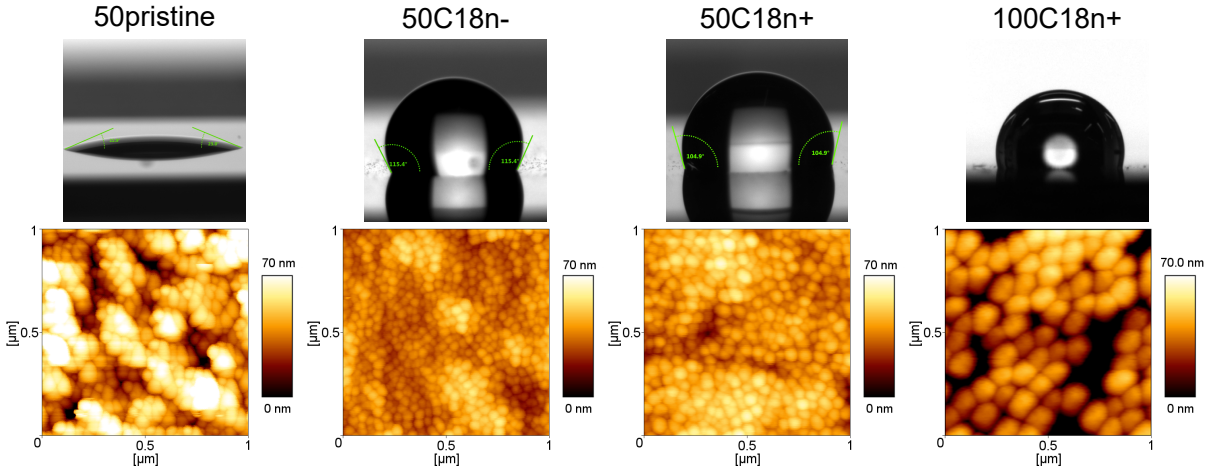

	50pristine	50C18n-	50C18n+	100C18n+
Contact angle / °	24 ± 4	113 ± 3	107 ± 4	105 ± 3
RMS Roughness / nm	18 ± 3	13 ± 4	17 ± 4	29 ± 8

Figure 4.3: First row: 3.5 µl water droplets deposited on top of wafers spin coated with unmodified and selected modified SNs. Pristine particles are hydrophilic (low contact angle), the modified particles are similarly hydrophobic (high contact angle of around 110 °). Second row: AFM images of the particle layers used for the contact angle determination. Table: Determined values for the contact angle and the RMS roughness of the deposited particle layer.

4.1.3 ζ-Potential

The ζ-potential of the SNs reflects the strength and sign of their surface charge. The intention of the surface modification of the SNs was to achieve hydrophobic but neg-

atively or positively charged particle systems in order to test charge specific effects while enabling the stabilization of w/o emulsions. Figure 4.4 shows the measured ζ-potentials for the SN particle systems. The absolute value for the charge of the 50pristine particles of -63 mV is higher than those of the modified negative particles of around -50 mV. This indicates that the surface modification occupies and neutralizes some of the charged surface groups. The charge of the negatively charged particles and that of the positively charged particles is similar in their absolute value regardless of their size. The data show that the resulting SNs are suitable as a model system to test and quantify the influence of certain parameters like the influence of the charge sign.

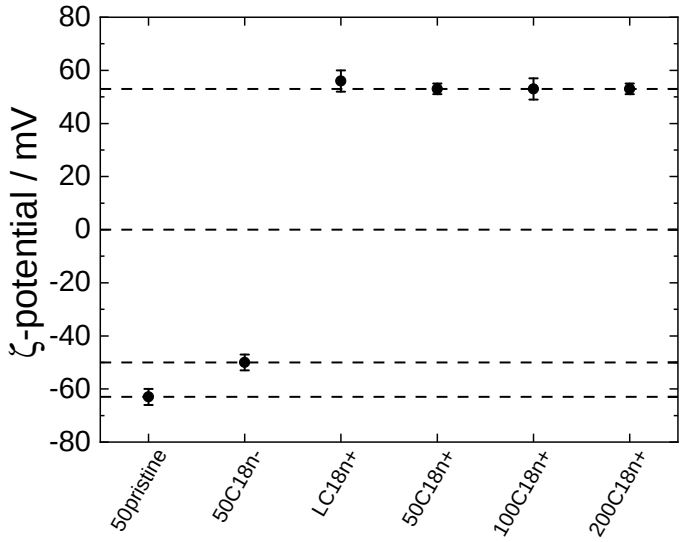

Figure 4.4: Overview of the measured ζ-potentials for the different unmodified and surface modified SNs. The potentials of the negatively charged hydrophobic modified SNs (50C18n-) and the positively charged hydrophobic SNs (LC18n+, 50C18n+, 100C18n+) exhibit similar absolute values.

4.2 Microgel Characterization

Besides solid SNs, soft polymeric MGs are used to stabilize emulsions. Their single particle properties are less easy to characterize because their shape and size differ between

the dry state and their state in dispersion as well as their bulk state and their adsorbed state. Their deformability is a challenge to address in the following. Three increasingly more cross-linked MGs are presented: a lower cross-linked (MG_L, 2.5 % BIS), a medium cross-linked (MG_M, 5 % BIS) and the stronger cross-linked (MG_S, 7.5 % BIS). Their size is characterized by DLS and their charge is determined *via* ζ-potential measurements. In addition, their adsorption kinetics at the o/w interface is characterized by drop shape analysis and their durability against stirring was tested. A summary of their properties is given in Table 4.1.

4.2.1 Size and Charge

The size of the MGs was measured with DLS. The resulting value, the hydrodynamic diameter, is a value for the particle size in bulk water. The measured values for the first heating (shrinking) and subsequent cooling (swelling) cycle are shown in Figure 4.5. The MGs show a typical VPT. By increasing the temperature above 32 °C, the MGs shrink in size from between 600 nm and 800 nm at low temperatures to a diameter between 250 nm and 320 nm at high temperatures. This process is reversible by cooling down the MG dispersion. The swelling and shrinking cycles were repeated at least 4 times and the measured diameters at 20 °C and 50 °C were averaged, respectively. From these averaged values, the swelling parameter q was calculated using eq. (2.17). The resulting values are presented in the lower part of Table 4.1. The swelling parameter q decreases with increasing cross-linking density. This reflects the decreasing ability to change the particles shape and is an indicator for their stiffness.

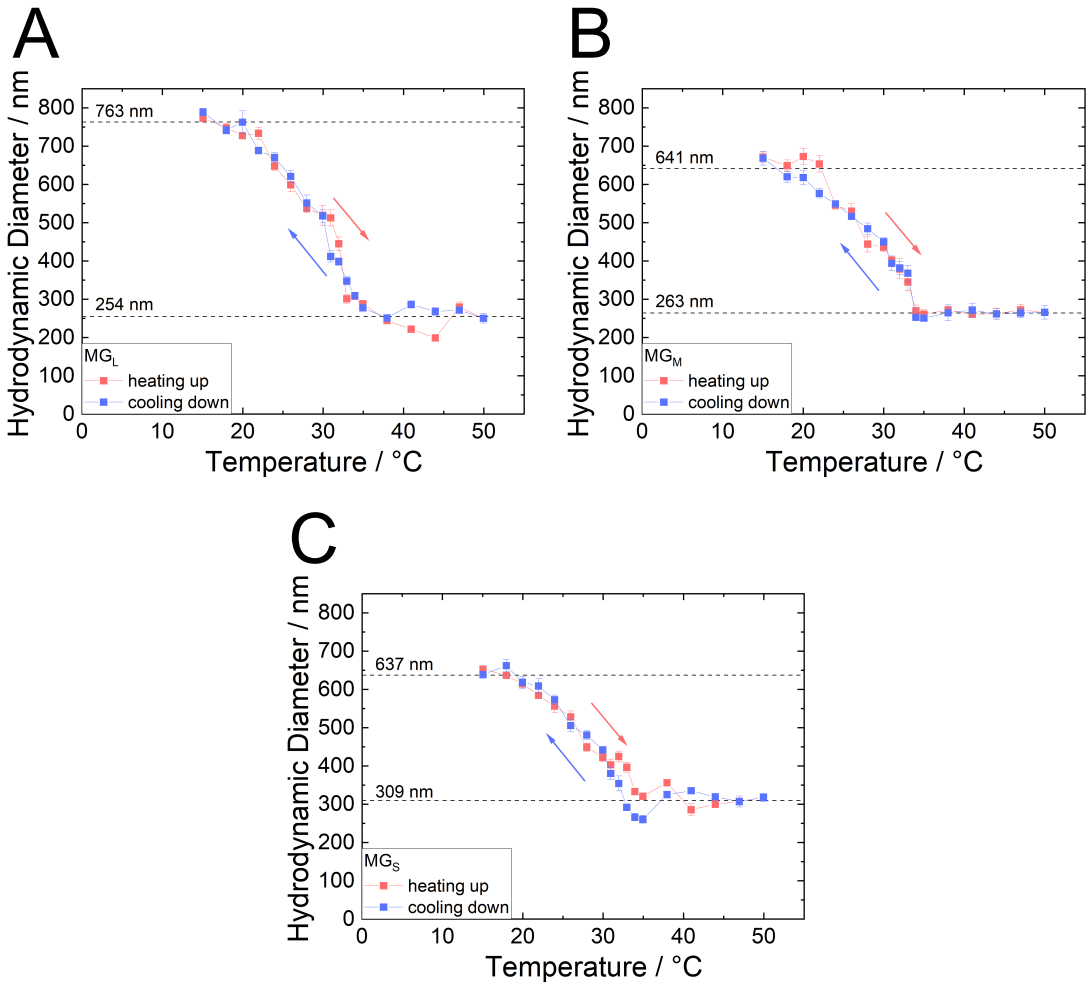

Figure 4.5: Measured hydrodynamic diameter of (A) the lower cross-linked MG_L, (B) the medium cross-linked MG_M and (C) the stronger cross-linked MG_S during the first heating and cooling cycle. All three MGs show a typical VPT. From room temperature to an elevated temperature of 50 °C the MGs shrink to less than half of their initial diameter. This process is reversible.

The charge of the MGs was measured in form of their ζ-potential using a zeta-sizer. The results are plotted in Figure 4.6. The ζ-potential of the MGs behaves inverse to their current size. During the shrinking of the MGs in size their ζ-potential increases (red curves) due to the compression of roughly the same amount of charged groups on a smaller volume. This process is reversible with the subsequent swelling of the MGs (blue curves). The increase of the ζ-potential with shrinking is more pronounced for

the lower cross-linked MGs because also their swelling ratio is significantly higher.

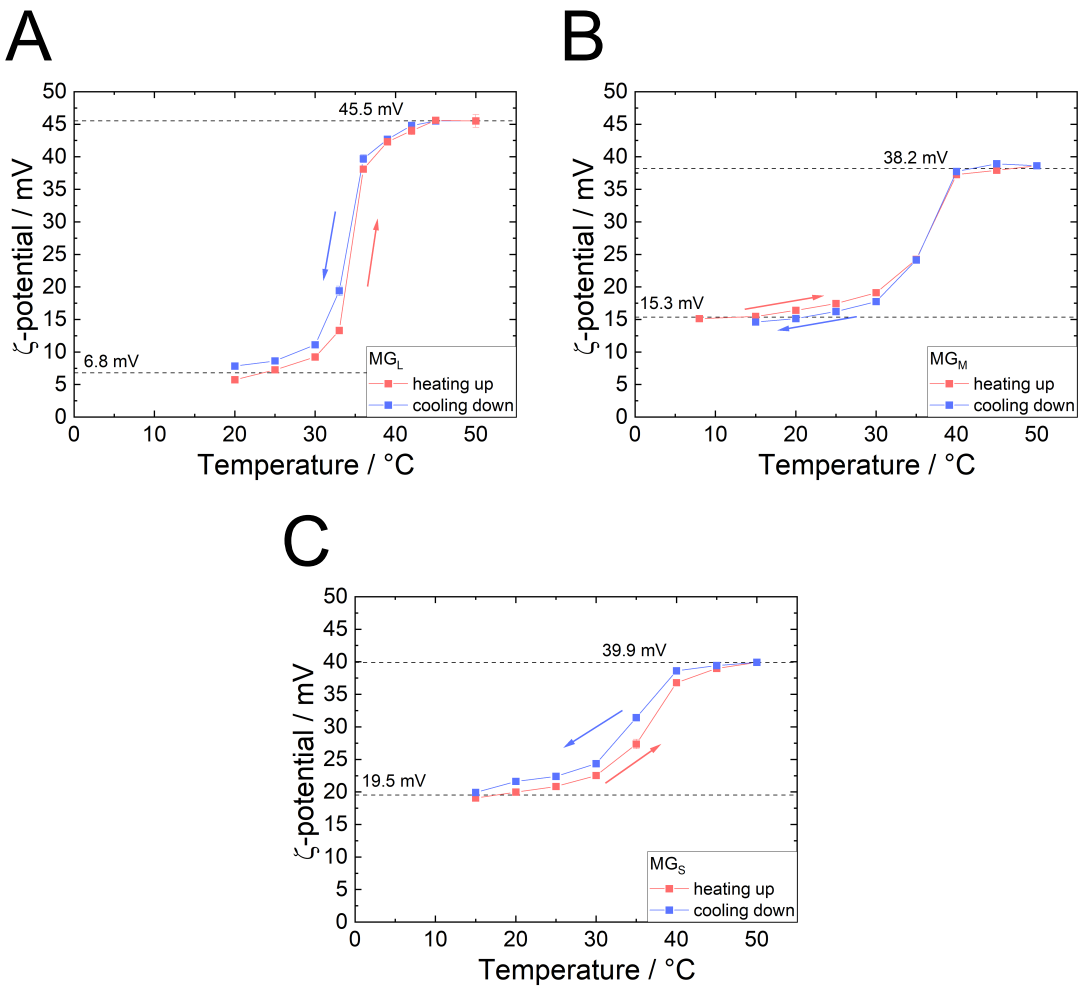

Figure 4.6: Measured ζ-potential for (A) the lower cross-linked MG_L, (B) the medium coss-linked MG_M and (C) the stronger cross-linked MG_S during the first heating and cooling cycle. All three MGs show an increase of their ζ-potential during their VPT. This process is reversible and more pronounced for higher swelling ratios of the MGs, *i. e.* a lower cross-linker content.

4.2.2 Interfacial Adsorption

In contrast to the SNs, the contact angle of the MGs against water could not be determined exactly, because the water droplet swell the MG layer on the waver and this way

slowly spread over the surface within several seconds. Nonetheless, the initial contact angle was well below 40 °. This indicates that MGs are hydrophilic but still surface active which is well known in literature [108]. MGs are able to adsorb spontaneously and irreversibly at the water-oil interface. With their adsorption the interfacial tension decreases. The initial adsorption process is slow because a necessary inter-digitation network is slowly forming with the accumulation of more and more MGs. After the initial slow decrease of the surface tension the decrease accelerates at first but runs into a saturation at around 18 $mN \cdot m^{-1}$, irrespectively of the MGs cross-linker content. The time with which the interfacial tension decreases depends on the mass-flow of the MGs towards the interface and the coverage potential of the respective MG type. The MGs with the lowest cross-linker content decreases the interfacial tension faster than the other two because the MGs can deform more severely and are this way able to cover more interface with the same present amount of MGs [119]. It is possible to accelerate the adsorption kinetics with ultra-sonication. More details are found in the bachelor-thesis of Luca Mirau [270].

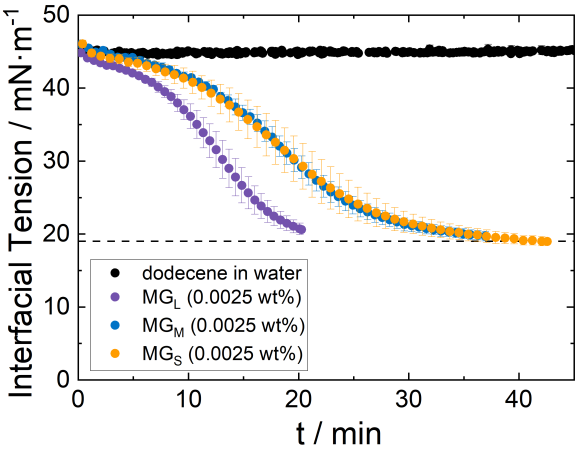

Figure 4.7: Interfacial tension of a dodecene drop in water or in aqueous dispersion containing the different cross-linked MGs, respectively. All three MG types decrease the interfacial tension over time and end up at the same final interfacial tension value of 18 $mN \cdot m^{-1}$. The lower cross-linked MG decreases the interfacial tension faster because they deform significantly more. The data were measured by Luca Mirau [270].

4.2.3 Durability under Stirring

The idea of preparing MG stabilized emulsions using the high energy input rotor-stator mixer Ultra Turrax raised the concern that the MGs may be destroyed by the heavy stirring. To test the integrity of MGs after stirring, dispersions of the moderate cross-linked MG_M were spin coated on a bare silicon wafer after treatment with the Ultra Turrax. The MGs on the wafer were then scanned with AFM. Figure 4.8 shows photographs of the resulting dispersions and AFM images of the scanned MGs. The conditions were chosen similar to the case of emulsion preparation (20 kRPM, 5 minutes) at two different temperatures at 8 °C (swollen MG) and 50 °C (shrunken MG). No damage of the MGs is observable when comparing the untreated dispersion (Figure 4.8 A) with the suspensions stirred at 8 °C (Figure 4.8 B) and at 50 °C (Figure 4.8 C). Heavy foaming occurred during the treatment of the MG suspension at 8 °C while only a small amount of foam formed when stirring at 50 °C which instantly collapses and MGs attache in low amounts to the stirrer.

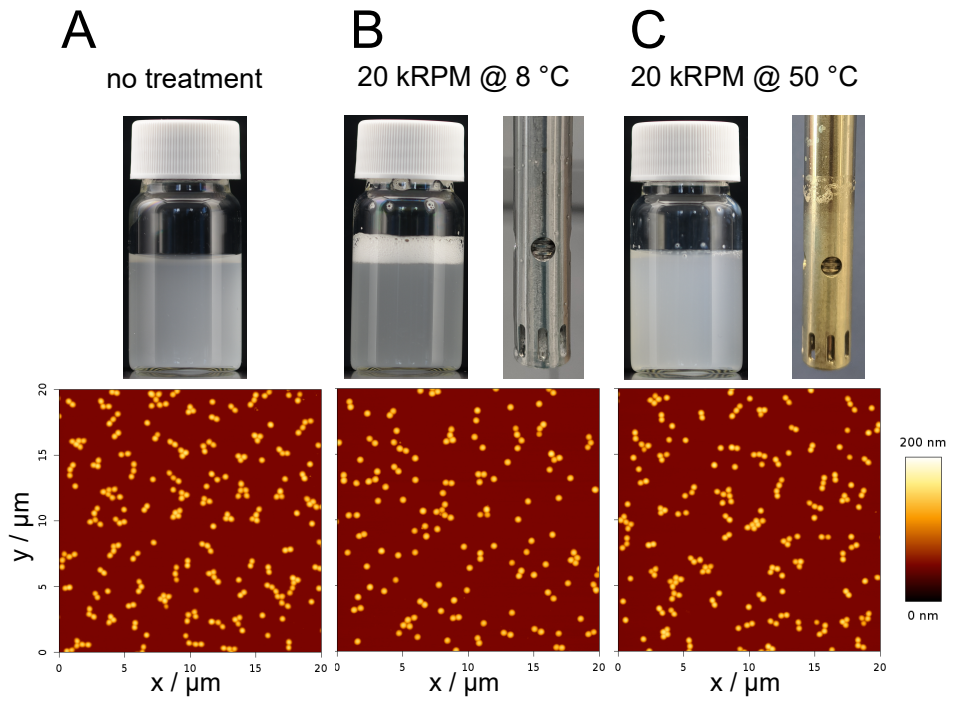

Figure 4.8: Durability test of MG_M against stirring with the Ultra Turrax homogenizer: MG dispersions were stirred (5 min, 20 kRPM) at 8 °C and 50 °C, respectively and compared to a sample with no treatment. Heavy foaming occurred during the preparation at 8 °C while only a low amount of instantly collapsing foam was seen during stirring at 50 °C. In both cases the stirrer tip stayed clean. At 50 °C, only a low amount of aggregated MG accumulated on that spot on the stirrer where the unstable foam instantly collapsed. The corresponding AFM pictures taken from a spin coated particle layer (selection out of at least 4 scanned spots out of 2 prepared samples) show no damage to the MGs.

4.3 Summary of the Particle Characterization

Table 4.1 shows the summarized properties of the SN particle systems and the summarized properties of the MGs. The data for the SNs show clearly how similar the systems are. It is possible to find two corresponding modified particle systems that differ only one of their main characteristics such as size, charge and ζ-potential. This makes them

ideal model systems for testing the influence of these properties on the PE composition, the interaction with a catalyst and the catalysis. The data for the MGs show the size and charge (ζ-potential) for the three different MG types: MG_L (low cross-linked, 2.5% BIS), MG_M (medium cross-linked, 5% BIS) and MG_S (stronger cross-linked, 7.5% BIS).
In all cases, the SNs are significantly smaller than the used MGs. Since, except the pristine and 50C18n- particles, both particles, SNs and MGs, are positively charged they repel each other in the bulk as well as at the interface. They also exhibit very different wettability. The SNs are very hydrophobic with a contact angle well above 90 ° while the MGs are very hydrophilic (initial contact angle well below 90 °), forming very stable dispersions in water.
The gathered data for the SNs as well as for the MGs will be used and their influence on PEs will be discussed in the following chapters.

Table 4.1: Overview of the evaluated properties of all particles. The upper part of the table shows the properties of the SNs. The lower part sums up the characterization of the MGs. [a] measured for the positively charged version of the same batch. [b] measured for the pristine version of the same batch. [c] averaged over the values for at least 8 swelling and deswelling curves.

	50pristine	50C18n-	LC18n+	50C18n+	100C18n+	200C18n+
d_{32} / nm	46.3 ± 5	46.7 ± 5	27.6 ± 3	45.7 ± 5	97.0 ± 5	186.6 ± 9
ρ_p / g·cm^{-3}	1.77 ± 0.04[a]	1.77 ± 0.04[a]	2.15 ± 0.02[b]	1.77 ± 0.04	1.93 ± 0.05	2.14 ± 0.04
$a_\varnothing$ / m^2·g	18.2 ± 0.4[a]	18.2 ± 0.4[a]	25.3 ± 2.7[b]	18.2 ± 0.4	8.0 ± 0.2	3.8 ± 0.2
a_O / m^2 ·g	72.7 ± 1.5[a]	72.7 ± 1.5[a]	101.0 ± 10.7[b]	72.7 ± 1.5	32.0 ± 0.5	15 ± 0.8
ζ-potential / mV	-63 ± 3	-50 ± 3	$+56 \pm 4$	$+53 \pm 2$	$+53 \pm 4$	$+53 \pm 2$
CA / $^\circ$	24 ± 4	113 ± 3	106 ± 8	107 ± 4	105 ± 3	102 ± 7

	MG_L		MG_M		MG_S	
	20 °C	50 °C	20 °C	50 °C	20 °C	50 °C
d_H [c] / nm	736 ± 21	272 ± 34	616 ± 25	269 ± 35	611 ± 9	351 ± 3
q	19.9 ± 7.7		12.1 ± 4.9		5.3 ± 0.3	
ζ-potential / mV	$+5.7 \pm 1$	$+45.5 \pm 2$	$+15.3 \pm 2$	$+38.2 \pm 2$	$+19.9 \pm 2$	$+39.9 \pm 2$

5 Role of Catalytic Active Interfaces in Interfacial Catalysis

This chapter describes how to determine catalytic active interfaces in PEs and shows an evaluation of the resulting consequences for interfacial catalysis. The main content is taken from the authors publication in *Physical Chemistry Chemical Physics* (2021) [58] with permission of the RSC.

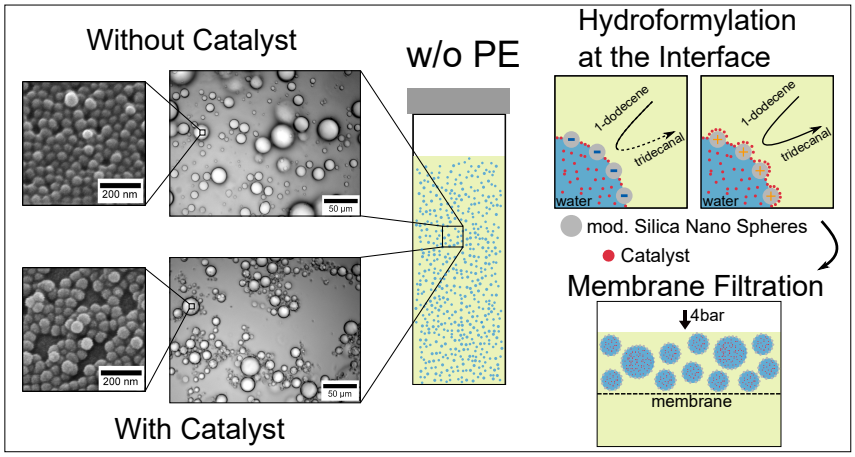

Abstract

PEs are used as reaction environment in biphasic catalysis for the hydroformylation of 1-dodecene into tridecanal using the catalyst rhodium (Rh)-sulfoxantphos (SX). This chapter connects knowledge about particle catalyst interaction and PE structure with reaction results. It quantifies the efficiency of the catalytic performance of the catalyst localized in the voids between the particles (liquid-liquid interface) and catalyst adsorbed on the particles surface (liquid-solid interface) by a new numerical approach.

First, it is ensured that the overall packing density and geometry at the droplet interface and the size of the water droplets of the resulting w/o PEs are predictable. Second, it is shown that approximately all particles assemble at the droplet surface after emulsion preparation and neither the packing parameter nor the droplet size change with particle surface charge or size when the total particle cross-section is kept constant. Third, studies on the influence of the catalyst on the emulsion structure reveal that irrespectively of the particles charge the surface active and negatively charged catalyst Rh-SX reduces the PEs droplet size significantly and decreases the particle packing parameter from s = 0.91 (hexagonal packing in 2D) to s = 0.69 (shattered structure). In this latter case, large voids of free w/o interface form and become covered with catalyst. With profound knowledge about the PE structure the reaction efficiency of liquid-liquid vs. solid-liquid interfaces are quantified. By excluding any other influence factors, it is shown that the activity of the catalyst is the same at the fluid and solid interface and the performance of the reaction is explained by the geometry of the system. After the reaction, the catalyst retention *via* membrane filtration is shown to be successfully applicable without damaging the emulsions. This enables the continuous recovery of the catalyst, *i. e.*, the most expensive compound in PE-based catalytic reactions, being a crucial criterion for industrial applications.

5.1 Introduction

In this chapter, the influence of the PE structure on the catalysis and catalyst recovery is investigated on the basis of the hydroformylation of the long chained olefin 1-dodecene into the aldehyde tridecanal. This reaction is catalyzed *via* the water soluble catalyst complex rhodium-sulfoxantphos (Rh-SX) in varied PE environment. Earlier studies on this system dealt with the general feasibility of the hydroformylation in PEs and their filtration for liquid-liquid separation and thus catalyst recovery after the reaction [23, 37, 71, 72, 165, 190, 191]. In this context Stehl *et al.* [72] showed that a positive surface charge on the surface of Halloysite nanotubes is more beneficial for the product yield than a negative one. Zhao *et al.* [190] and Tao *et al.* [165] used positively charged SNs and compared them to positively charged mesopourous SNs and speculated that the porosity facilitates mass transport through the particle layer. They found that the adsorption of the negatively charged catalyst onto the positively charged particles is beneficial for the reaction. Results from these earlier works imply that on the one hand

the surface occupation by the particles provides the desired high stability, but on the other hand it hinders the interfacial contact between oil and water and therefore hinders the mass transfer.
An often underestimated challenge when comparing results by various authors for finding an adequate model system and also for developing analytical models for the desired catalytic process is the low comparability between different particle systems and the lack of quantitative parameters describing those. So far, the particles of different studies and also within the same study vary in a whole bunch of parameters. Therefore, the prediction and identification of dominant properties influencing the reaction behavior is very difficult or even impossible and deducing conceptual conclusions becomes often speculative. Differences in particle shape, size and hydrophobicity may lead to a varied water/oil droplet size, may affect the fraction of SNs being able to adsorb at the interface or may also affect the particles packing geometry and density at the droplet surface. Both, the droplet size and the packing condition, may influence the mass transfer and with that the reaction outcome such as yield and conversion rate as well as the stability and liquid-liquid separation for catalyst recovery. A deeper physico-chemical understanding of the system is needed for improving the catalytic and general process performance in PEs beyond trial and error or fine tuning approaches. Therefore, for the exact prediction of reaction and separation outcomes for future PE formulations it is essential to understand the effect of different particle properties as well as their interaction with the catalyst on the PE structure and subsequently on the reaction and separation performance in detail.
In summary, this chapter addresses the following questions: I) Where are the catalyst molecules located during the reaction process and II) Does the PE morphology influence the catalyst efficiency? In order to answer these questions, model system PEs are designed from the nano-sized particle properties to microscopic PE structure. First, the effect of the tailored particle properties and catalyst on the resulting PE structure is determined. Second, the impact of several parameters on the reaction are considered. The w/o emulsion type is used because it allows the retention of the water soluble catalyst in the water droplets in the system. Finally, the surface coverage and its impact on the reaction results are determined and discussed in detail. This includes the discussion on the effect of particle size and particle surface charge. In addition to this and in order to find further explanations for the earlier found increase in reaction performance for positively charged SNs, the particle/catalyst interaction was investigated. In view of the envisaged continuous PE reaction process, the influence of particle properties on

membrane filtration is finally studied.

5.2 Results

The results in the following show the characterization of the prepared PEs and their performance during interfacial catalysis and membrane filtration with a thorough analysis of the role of the different interface types. For a detailed characterization of the particles see Chapter 4.

5.2.1 Emulsion Characterization

The SNs that were characterized in Chapter 4 are used for emulsion stabilization. In the following, the ability of the particles to stabilize PEs is explored. Figure 5.1 A shows photographs of emulsions with different particles 12 hours after preparation. The emulsion with untreated 50pristine particles is unstable and breaks within a few hours into the initial two phase system. The turbidity of the bottom phase (water) corresponds to the turbidity of the initial particle suspension and no emulsion droplets were identified under the microscope. The PEs stabilized by the modified particles sediment and form the white phase at the bottom of the flask. Light microscopy after 12 hours (Figure 5.1 B) shows, that the droplets stay intact. This stability was observed even after months and beyond. A fluorescein dyed version of each emulsion was investigated additionally by fluorescence microscopy, which confirms the water in oil type (w/o) of the PEs (Figure 5.1 B).

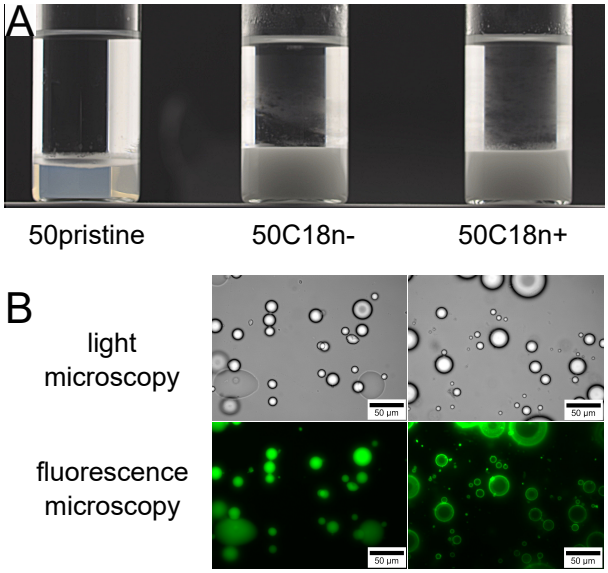

Figure 5.1: (A) Photographs of water/dodecene PEs formed with three different particle systems (0.5 wt%) with a water fraction of 25 wt% (20 vol%) after 12 hours. While the hydrophobized SNs are able to form stable PEs the pristine SNs are not able to stabilize lasting emulsions. (B) Related microscopy images for fluorescein dyed samples show intact droplets and fluorescence microscopy images prove the w/o type for the non-pristine particles.

The effect of water and particle fractions on the packing geometry of the 2D self assembly of the SNs at the water/oil interface was studied for the positively charged SNs 50C18n+ and 100C18n+ systematically by microscopy (Figure 5.2).

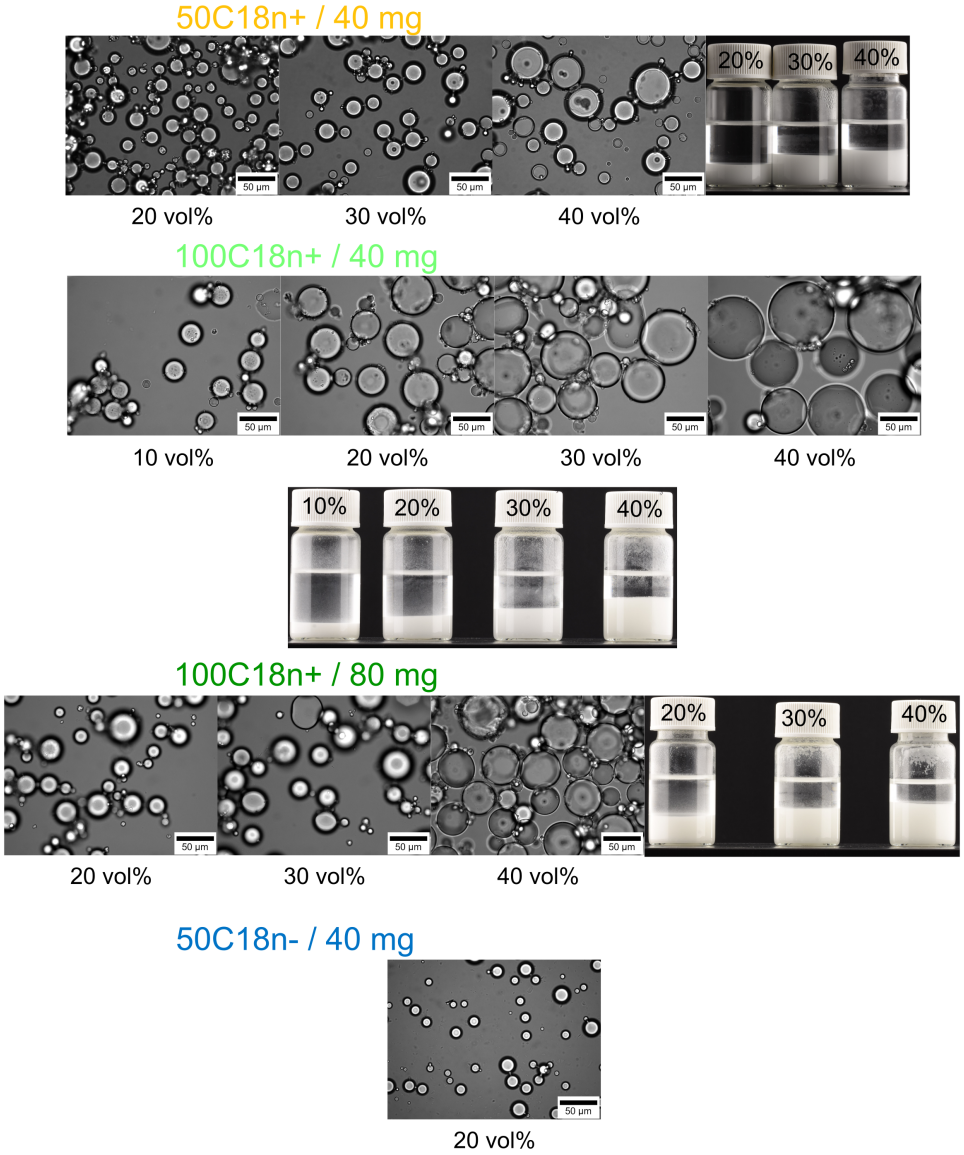

Figure 5.2: Selection of microscopy images of the prepared PEs with different SNs and different water fractions with the corresponding photographs of the PEs. At least 15 of these images of each sample containing in total 400 to 800 droplets were used for the determination of the Sauter mean droplet diameter in dependence of the water fraction. The photographs show the sedimentation of the PEs after a few hours. The droplets themselves stay intact.

The resulting Sauter mean droplet diameters (d_{PE}) are shown in Figure 5.4. d_{PE} of the droplets increases linearly with the water fraction. Measurements after approximately 2 months show that for the 40 mg 100C18n+ sample with 40 vol% water con-

tent the Sauter mean diameter increased from 72.4 µm to 80.6 µm. For higher particle concentration or lower water content the differences were negligible. For water contents above 50 vol% the PE structure changes fundamentally (Figure 5.3): A bimodal droplet size distribution is observed consisting of very large ($\gtrsim$ 180 µm) and very small droplets ($\lesssim$ 15 µm).

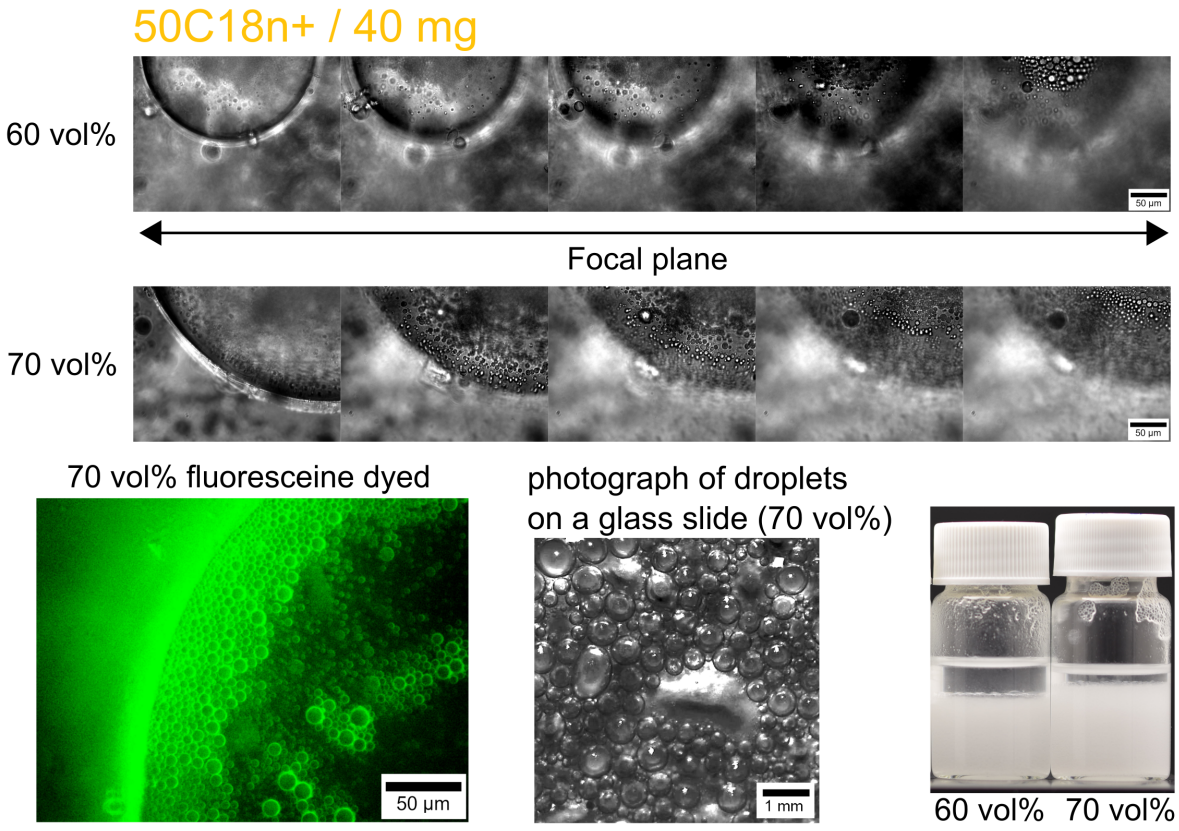

Figure 5.3: The structure of PEs with a water fraction above 50 vol% deviate fundamentally from PEs with water fractions below 50 vol%. Top: Micrographs of PEs prepared with water fractions of 60 vol% and 70 vol%. Very large and very small droplets are observed. When moving the focal plane of the microscope towards the bottom of the larger droplet the smaller droplets become visible. The small droplets occur only inside the large droplets but not in the continuous phase outside the droplet. Bottom: The fluorescein dyed version of the 70 vol% PE indicates that the smaller droplets are water droplets in agreement with the small droplets in the large droplets. A photograph of the droplets spread on a glass slide shows the scale of the larger droplets. The photographs on the right show the macroscopic PEs.

The solid lines represent linear fits to the data. They are used to calculate the packing parameter s. The dashed lines result from a calculation assuming a hexagonal packing using eq. (2.12). This allows the prediction of PE droplet sizes when knowing the specific particle cross-section $a_{\oslash}$, the input particle weight $m_{\mathrm{p,tot}}$, the total PE mass $m_{\mathrm{PE,tot}}$, the total PE volume $V_{\mathrm{PE,tot}}$, the used water fraction f_w and assuming a 2D hexagonal packing (packing parameter $s \approx 0.907$). The linear fits (solid lines) agree very well with these completely independent predictions.

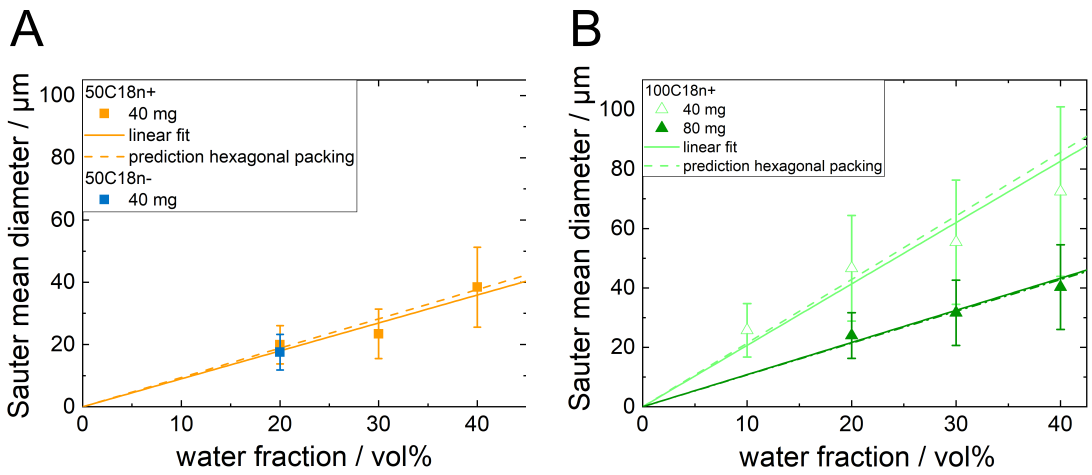

Figure 5.4: Sauter mean diameter d_{PE} for water/dodecene PEs at constant volume of 12.55 mL. Every point was calculated from 400 to 800 measured droplets. The error bars represent the standard deviation of each droplet size distribution. The Sauter mean diameter scales roughly linearly with the water fraction. The solid line represents a linear fit. The dashed lines were calculated using eq. (2.12) with the determined particle properties. The packing parameter was set to s = 0.907 assuming a hexagonal packing. The completely independent predictions agree well with the linear fits.

The conformation of the SNs at the water-oil-interface was studied by in-situ cryo-SEM of selected samples. The micrographs in Figure 5.5 show dense packing of the SNs at the w/o interface. The micrographs reveal two kinds of structures on the droplet surface: a relief-like structure of missing SNs in Figure 5.5 B and the SNs occupying the interface in other regions in Figure 5.5 C. The structure in panel A results most presumably from the sample preparation process in which some SNs broke away during freezing and cutting. In both cases, a hexagonal like structure can be recognized.

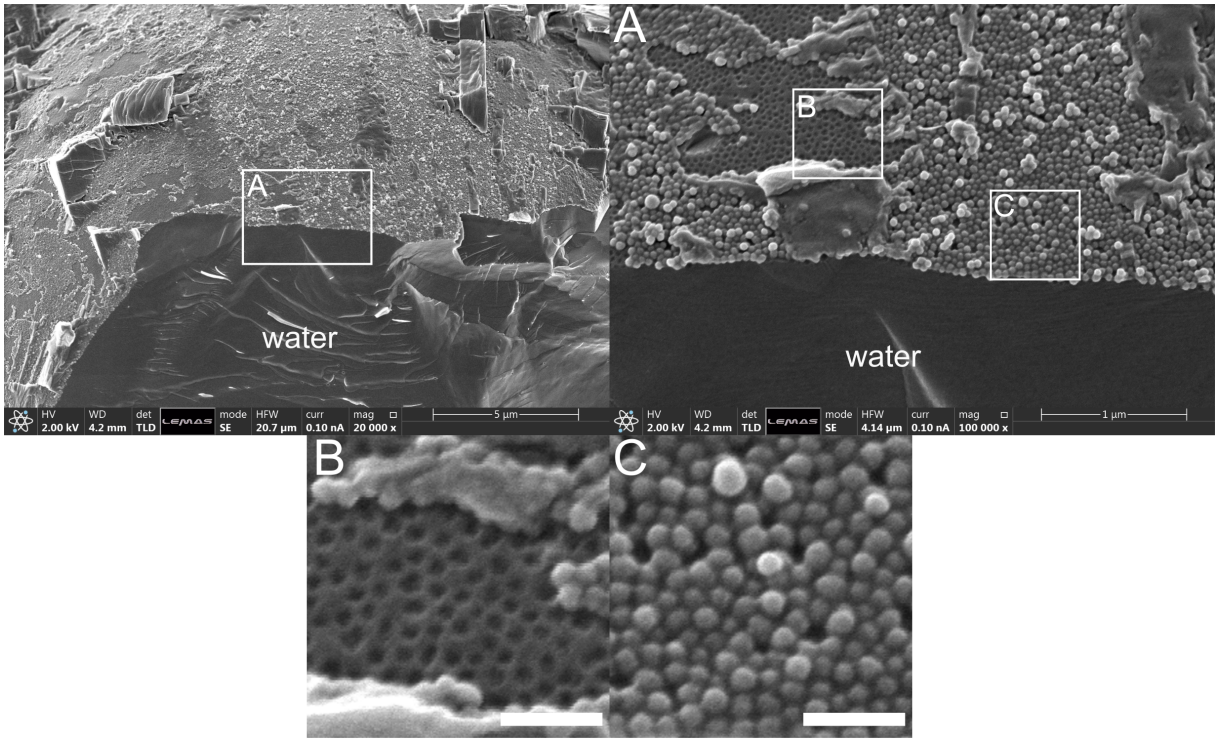

Figure 5.5: Cryo-SEM images of water/dodecene PEs with particle concentration $c_p = 0.5$ wt% and water fraction 20 vol% using 50C18n+ particles. The SNs form a structure similar to the 2D hexagonal close packing. This is well recognizable in the areas where some SNs broke away in the preparation process and left gaps behind (B). The length of the white bars in (B) and (C) corresponds to 200 nm. The images were taken about one week after emulsification.

5.2.2 Localization of the Catalyst

In this section, the influence of the catalyst on the emulsion structure is quantified. Stehl *et al.* [72] determined the surface tension of the ligand-water-solution (SX) against air and compared it to the catalyst-solution (RH-SX). The determined values for both substances are similar so that it was stated that the physical interfacial behavior of the catalyst system is dominated by the ligand SX. Thus, for investigating the physical properties of the catalyst system it is sufficient to only use the cheaper SX instead of the expensive catalyst complex. In this work, the surface tension of an aqueous SX solution was measured against dodecene using the Du Noüy ring method (Figure 5.6). The curves follow a typical trend for a classical surfactant. In the inter-

val between 10^{-4} mol·L^{-1} and 10^{-2} mol·L^{-1} the surface tension decreases by about 20 mN·m^{-1} from slightly above 40 mN·m^{-1} to slightly above 20 mN·m^{-1}. From this, the required space for one SX molecule was estimated to a_{SX} = 0.96 nm^2 using Gibbs equation [271].

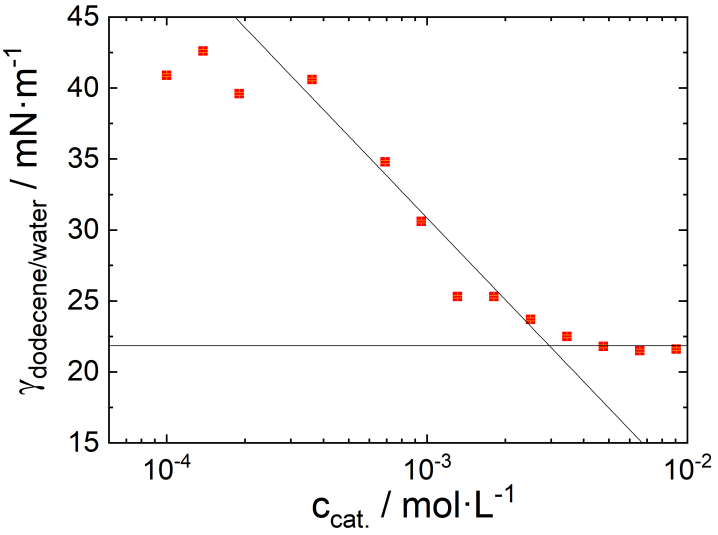

Figure 5.6: Measured surface tension γ for a SX solution in water at the water/oil interface using Du Noüy ring method. γ decreases with increasing SX concentration until it reaches a plateau (vertical line) at $3 \cdot 10^{-3}$ mol/L To get a value for the occupied space of a single SX molecule the Gibbs equation was fit to the data. The required space for a single molecule was estimated to a_{SX} = 0.96 nm^2. During the reaction, the concentration of the ligand in the water phase of the PE is ∼0.075 mol·L^{-1}.

The ligand-particle interaction was quantified by measurements of the particles the ζ-potential in ethanol with increasing ligand concentration. The particles are not dispersible in water and the ligand is not soluble in oil. Although these measurements do not represent the reaction environment, they reveal a general trend of the behavior of the ligands adsorption onto the particles. Figure 5.7 shows the measured ζ-potential for the particle-SX-complexes as a function of the ligand amount per particle area k_N. The concentration of SX was normalized with respect to the total surface of the added SNs, which was calculated from particle size (TEM) and density data (Table 4.1). The potentials of both initially positively charged particles 100C18n+ and 50C18n+ show a

decrease with increasing k_N, *i. e.* SX, and even change sign at about 2-6 molecules per nm^2. The curves of both positively charged particles nearly overlay each other. The potentials of the negatively charged SNs do not change with the catalyst concentration.

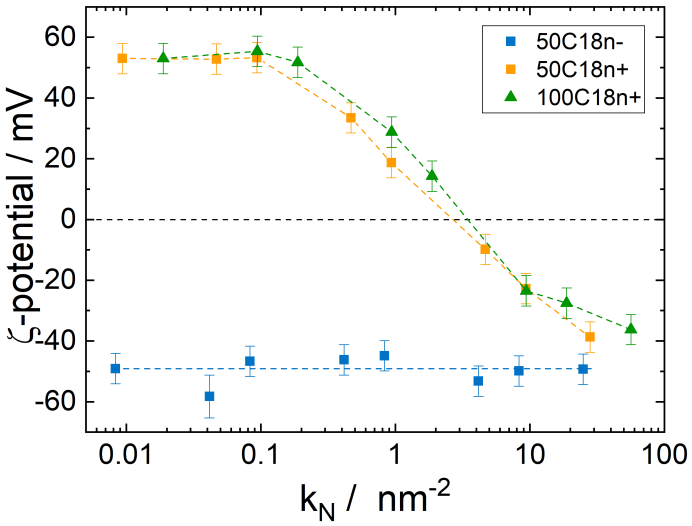

Figure 5.7: ζ-potential as a function of the concentration of SX per particle area (k_N). The ligand SX decreases the ζ-potential for both positively charged particle types while the ζ-potential of the negatively charged SNs is not influenced by the presence of SX.

Both, the surface activity of the ligand SX and its ability to adsorb onto the positively charged SNs are presumed to affect the PEs structure. For further investigations, PEs were prepared with and without SX to compare the droplet sizes. Different PEs with a constant water fraction of 20 vol %, a constant total volume and a constant amount of SX were produced (Figure 5.8). The particle concentrations were varied and their droplet size distributions were determined. The results for the measured Sauter mean diameters are shown in Figure 5.9.

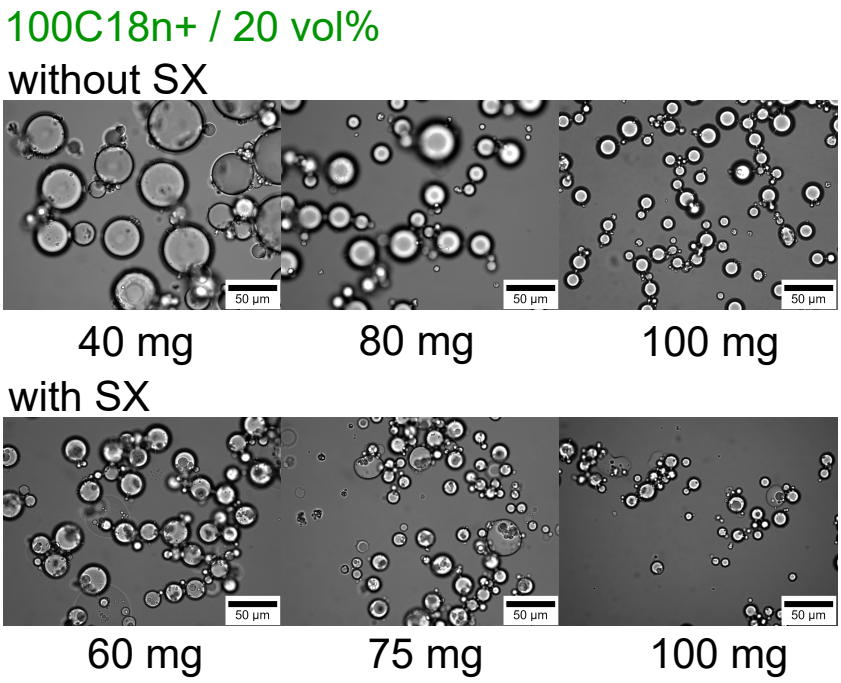

Figure 5.8: Micrographs of PEs prepared with and without the ligand SX in dependence of the particle concentration. PE total volume 12.55 ml, 20 vol % water fraction and 0.015 mol $\cdot$ L^{-1} $\approx$ 147 mg SX.

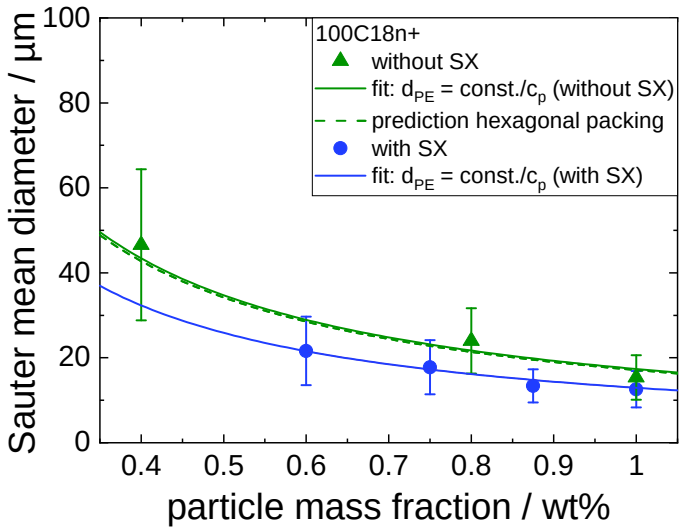

Figure 5.9: Sauter mean diameters for PEs produced with different 100C18n+ particle concentrations with SX (0.015 mol·L^{-1} $\approx$ 147 mg) and without SX for a water fraction of 20 vol% and 1-dodecene as continuous phase. The error bars represent the standard deviation of each droplet size distribution. The dashed line was calculated using eq. (2.12) with the determined particle properties above and setting s = 0.907. The solid lines represent a non linear fit with the form $d_{\mathrm{PE}} = \frac{\mathrm{const.}}{c_{\mathrm{p}}}$ (according to eq. (2.12)). The packing parameters were calculated from the fits to s = 0.92 $\pm$ 0.05 (without SX) and s = 0.69 $\pm$ 0.01 (with SX).

In both cases (with and without SX), the curves follow a trend reciprocal to the added particle mass as predicted by eq. (2.12). The predicted values calculated from experimental particle properties (Table 4.1) are shown as a dashed line. The calculated values are in perfect agreement with the $d_{\mathrm{PE}} = \frac{\mathrm{const.}}{c_{\mathrm{p}}}$ fit. The addition of SX leads to a reduction of the droplet size and by fitting eq. (2.12) a decrease of the packing parameter from s= 0.92 $\pm$ 0.05 to s = 0.69 $\pm$ 0.01 was determined. The effect of SX reducing the droplet size was seen irrespectively of size and charge (Figure 5.10).

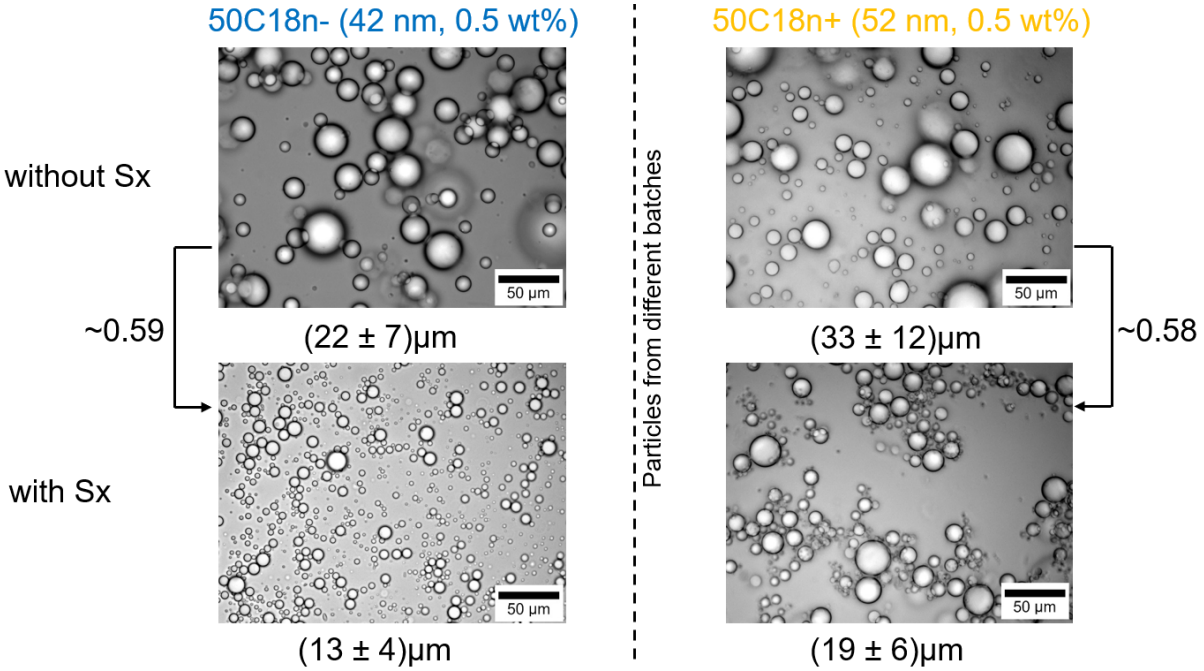

Figure 5.10: Micrographs and droplet size measurements with a slightly smaller sized particle batch of 50C18n- particles ($d_{32} = 41.5\,\text{nm}$) and a batch of slightly larger 50C18n+ modified particles ($d_{32} = 52.4\,\text{nm}$) than the SNs presented in the rest of Chapter 4 and Table 4.1. The emulsions that were prepared with a concentration of 0.5 wt% and a water fraction of $f_w = 20\,\text{vol\%}$ show also the effect of a decrease in coverage parameter. The Sauter mean droplet diameter for the negatively charged 50C18n- particles decreased with the addition of SX from $d_{32} = 22\,\mu\text{m}$ to $d_{32} = 13\,\mu\text{m}$ and for the positively charged 50C18n+ particles from $d_{32} = 33\,\mu\text{m}$ to $d_{32} = 19\,\mu\text{m}$. This represents a decrease in both cases of roughly 40 % $c_{SX} = 0.015\,\text{mol}\cdot\text{L}^{-1} \approx 147\,\text{mg}$.

These findings raise the question whether the presence of catalyst modifies the particle arrangement at the droplet surface. For answering this, cryo-SEM images were recorded of PEs containing SX one week after preparation (Figure 5.11). Comparing these new images for PEs containing SX with the images of PEs without SX (Figure 5.5) a more shattered surface occupation structure of the SNs is observed for both particle systems 50C18n+ and 50C18n-. Voids can be found between the particles in the form of smooth areas in the particle formed relief in (A) and (C) as well as in the visible particle layer in (B) and (D) between the SNs.

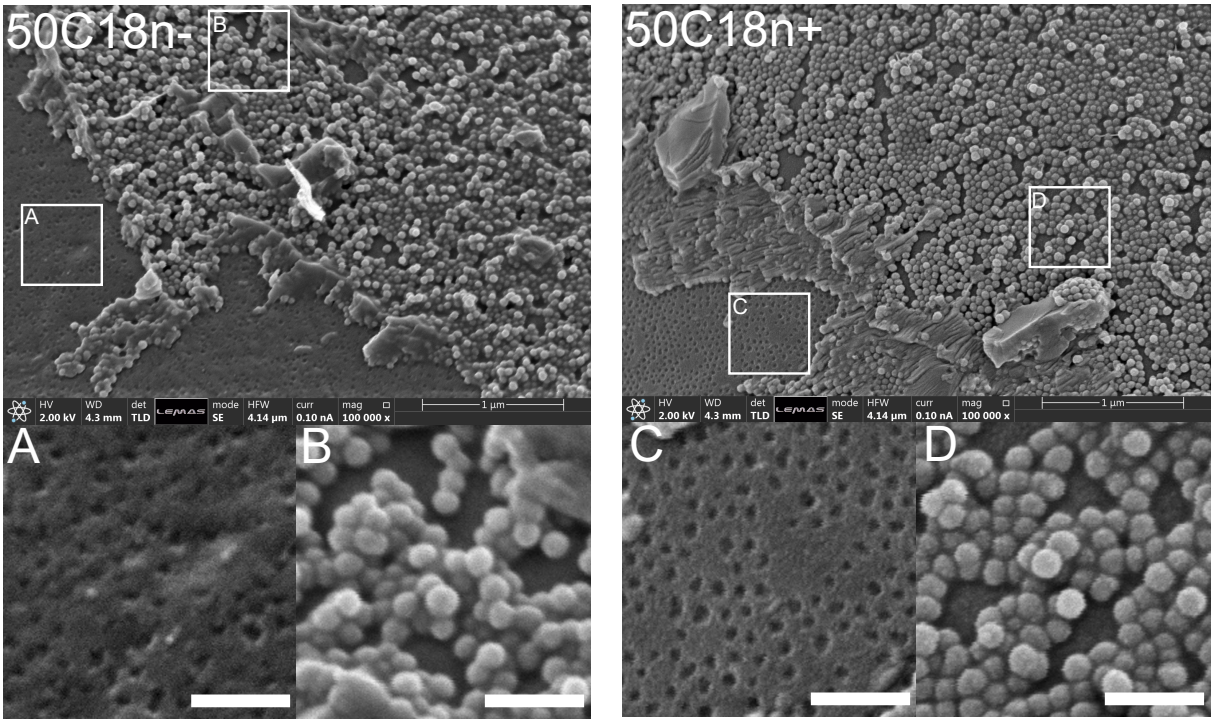

Figure 5.11: Cryo-SEM images of PEs produced with 50C18n- (left) and 50C18n+ (right) (water fraction 20 vol%, particle mass fraction 0.5wt%) in presence of SX (0.015 $\frac{\text{mol}}{\text{L}}$) . In both cases the addition of SX results in numerous voids in the structure. This effect can be seen in the areas where SNs broke away and the relief was scanned (A) and (C) as well as in the particle structure present on the droplets surface (B) and (D). SX has molecular size and is invisible in the SEM picture. The images were taken roughly one week after emulsification. The white bars in (A) - (D) represent 200 nm.

5.2.3 Hydroformylation of 1-Dodecene

In the next step, the hydroformylation of 1-dodecene was studied in PE environment in a batch reactor. The PEs total volume was increased by a factor of approximately 4 to 24 g oil and 8 g aqueous catalyst solution. Compared to the 50C18n+/- system twice the mass fraction of 100C18n+ particles was used to achieve a similar droplet diameter in the reactive system. This minimizes the influence of the droplet size and curvature on the reaction yield. The space time yield is shown in Figure 5.12 A. Other related reaction results are summarized in Table 5.1.

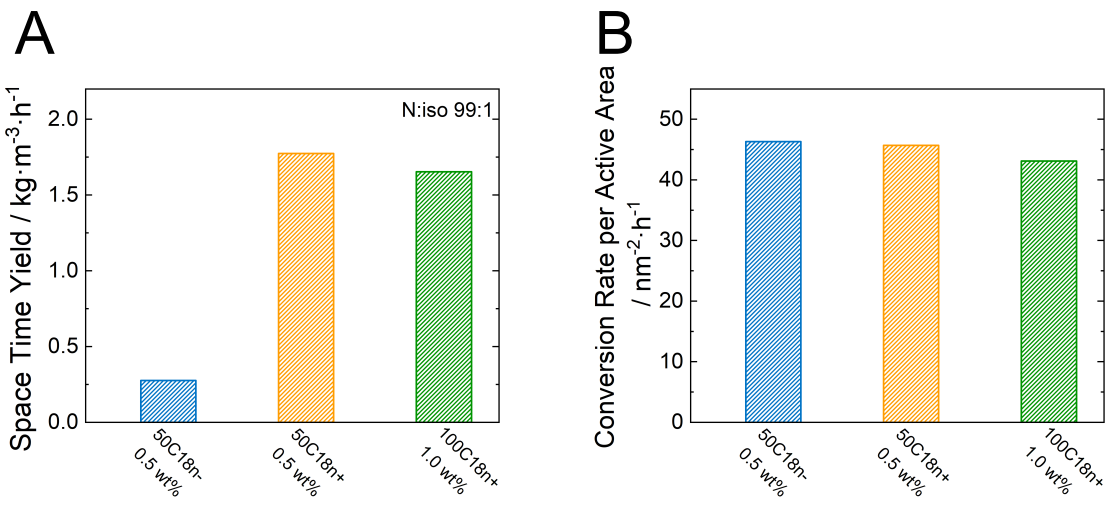

Figure 5.12: (A) Reaction results for the space time yield using a larger batch with 32 g in total for the whole PE after 20h. Reaction conditions: metal:ligand = 1:4, amount of catalyst: $146 \cdot 10^{-3}$ mmol , S/C = 960, amount of SNs 160 mg 50C18n+/- and 320 mg 100C18n+, water fraction 20 vol% (B) Conversion rate per active area (CRAA) calculated using eq. (2.14) for PEs with 50C18n- and eq. (2.16) for PEs with 50C18n+ and 100C18n+.

Table 5.1: Reaction related parameters. * calculated with eq. (2.14) using s = 0.69 ** calculated with eq. (2.16)

	50C18n- (0.5 wt%)	50C18n+ (0.5 wt%)	100C18n+ (1 wt%)
conversion / %	1.4	7.6	6.3
selectivity / %	64	78	87
TON	13.7	72.4	60.4
conv. rate per total void area / $\frac{1}{nm^2 h}$ *	46.3	-	-
conv. rate per total oil contact area / $\frac{1}{nm^2 h}$ **	-	45.7	43.1

The space time yield for positively charged particles is significantly higher than for negatively charged ones. Moreover, it was found that the particle size has no impact

on the space time yield when the difference in particle size is compensated by the mass fraction. Nevertheless, the PEs containing 100C18n+ particles were identified to be less stable. After the reaction, a thin layer of excess water ($\lessapprox$ 5 vol%) was found denoting that at least some of the droplets broke during the reaction. This was not the case for the PEs stabilized with the 50C18n+/- spheres. When knowing the packing parameter in a catalyst containing system to change from $s \approx 0.91$ to $s = 0.69$ (Figure 5.9) the conversion rate per active (CRAA) area can be calculated. From the ζ-potential measurements in the presence of SX, it was assumed that for the negatively charged SNs the reaction exclusively takes place in the voids between the SNs at the oil /water interface. Therefore, the conversion in number of molecules achieved was divided by the total void area. The total void area can be calculated using eq. (2.14).
In case of the positively charged 50C18n+ and 100C18n+ particles, the reaction takes place at both the w/o interface and the particle surface. Therefore, the achieved conversion per active area requires the inclusion of the particle surface protruding into the oil phase. This total active area includes the particle-oil contact area and the total void area and is calculated by eq. (2.16).
The difference between the total void area and the total substrate contact area are illustrated schematically in Figure 2.6. The determined values for the conversion per active surface are very similar for all three samples around 45 $nm^{-2}\,h^{-1}$ with only a difference of about 7 % (Figure 5.12B or Table 5.1).

5.2.4 Membrane Filtration

In this section, the potential of catalyst recovery *via* membrane filtration of the PEs after reaction is elaborated. For this, the PEs are transferred into the corresponding equipment. Under constant stirring and applied pressure of 4 bars, the organic phase (consisting of 1-dodecene and the products from the hydroformylation reaction) was filtered through the membrane while the particle stabilized dispersed phase droplets containing the valuable catalyst were retained by the organic solvent nanofiltration membrane. A stable flux was reached after only a few minutes and stayed constant until the filtration was stopped after 50 wt% of the organic phase had permeated. Figure 5.13 A shows the measured flux normalized with respect to the flux of pure 1-dodecene from the membrane pretreatment.

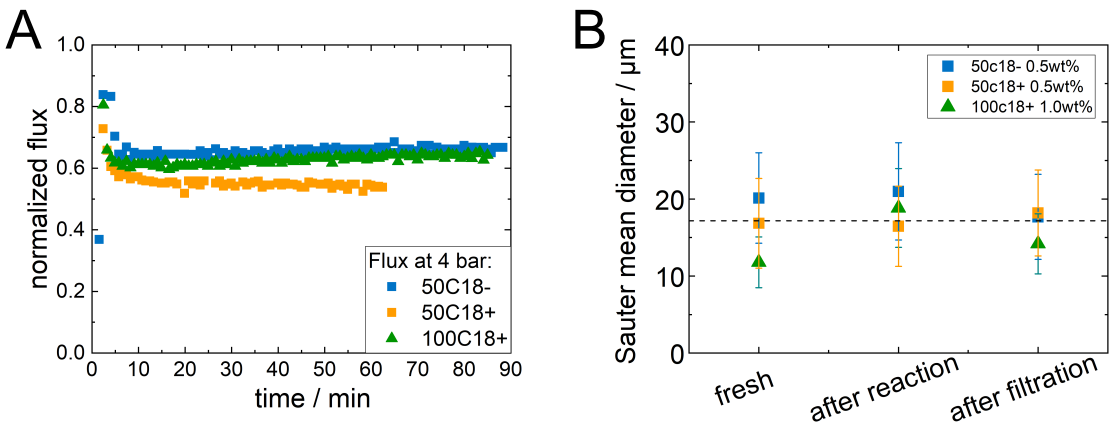

Figure 5.13: (A) Normalized Flux during filtration experiments for catalyst retention. (B) Droplet size before and after the reaction as well as after the filtration. It was proven that the PEs stayed intact over the whole process and the droplet size did not change.

The SNs surface charge seems to play a minor role if any at all. The normalized flux curves are similar to each other with no significant deviation. The slight deviation for 50C18n+ may be explained by small inherent differences in different membranes used [40]. The droplet size was measured of the freshly prepared emulsion, after the reaction and after filtration of 50 wt% of the product phase (Figure 5.13B and Figure 5.13). The results show that the Sauter mean diameter is preserved after each step. This stability of the PEs enables continuous reaction processes with droplet recycling *via* membrane filtration. Again, the charge and size are found to have no influence on the Sauter mean diameters of the recycled emulsion droplets.

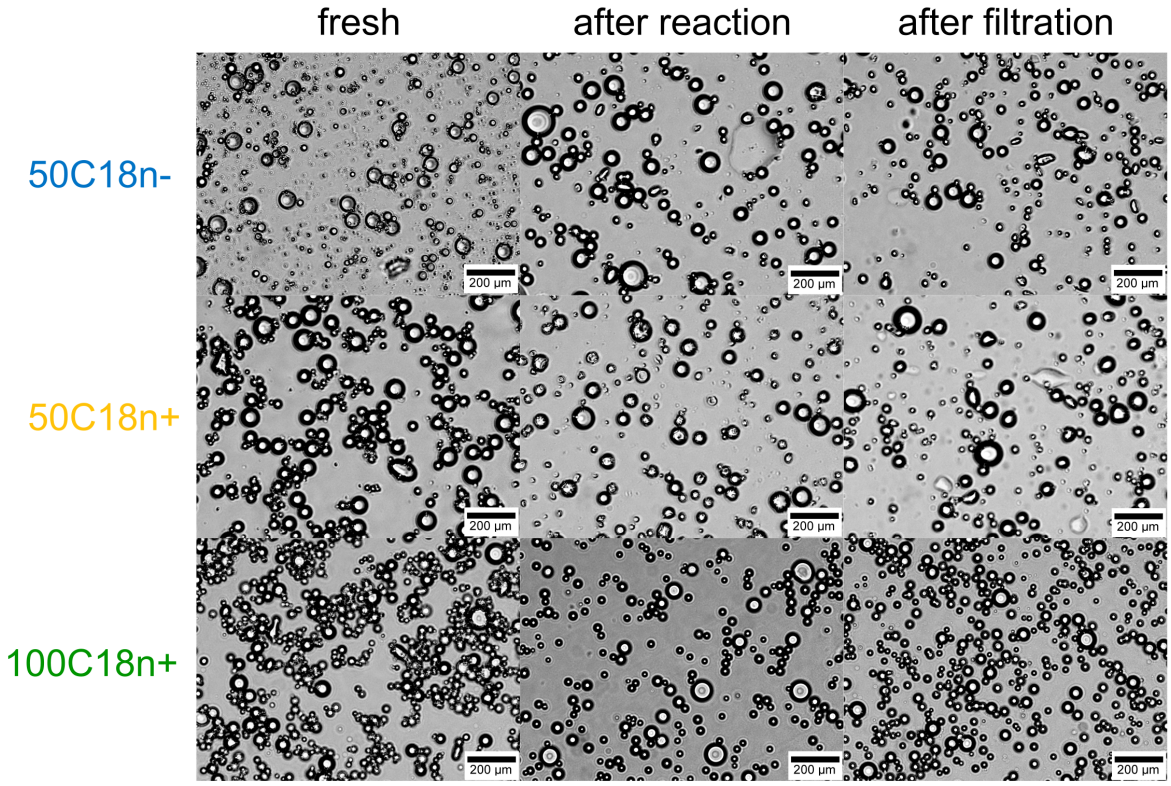

Figure 5.14: Micrographs of PEs used for the reaction. The droplet sizes were determined before and after the reaction as well as after the filtration. For the droplet size determination more than 15 images were used.

5.3 Discussion

5.3.1 Structure of the Applied PEs

Modified and comparable SNs varying in size (50 & 100 nm in diameter) and charge (+/-) were successfully produced and characterized in terms of their particle parameters. The characterized parameters are particle charge, size, shape, density, and specific particle cross-section. The samples 50C18n- and 50C18n+ have very similar size but an opposing surface charge. The samples 50C18n+ and 100C18n+ have quite the same surface charge but vary significantly in size.

The SNs were used to produce very stable PEs of w/o type. The droplet size in dependence of the water fraction was shown to follow eq. (2.12) proving that the

droplet size can be easily predicted by the given total emulsion volume and the determined particle cross-section under the assumption of a hexagonal packing. The other way around, the particle packing at the droplet interface can be determined for known droplet sizes. The validity of the model assumptions is proven by the very good agreement of the predictions and the experimental data points. The first assumption states that nearly all SNs adsorb at the droplet interface. The second stating hexagonal packing of the particles at the w/o interface is the most probable ordering at the droplet surface. These are important observations because insights into the surface ordering of the SNs in a PE system are generally difficult to resolve experimentally: light microscopy methods are limited to the regime beyond the micrometer scale. Scattering and reflectometry techniques heavily rely on complex models with many parameters and their interpretation becomes vague when dealing with multiple interfaces at once. Even rare and elaborate imaging methods like cryo-SEM only show the frozen state and neglect the dynamics of the system in-situ. Anyhow, cryo-SEM is up to now by far the best approach to investigate the ordering of nm-sized solid particles at liquid interfaces [272]. The images obtained by cryo-SEM for selected emulsions confirm the results above. In these images (Figure 5.5), a very dense particle monolayer corresponding to a hexagonal packing is observed. The surface charge of the particles seems not to be strong enough to separate the particles so that the free space between the particles is limited to the very small voids caused by hexagonal packing. At first glance this seems contradicting to the high ζ-potential of around $|\zeta| \approx 50mV$ (Table 4.1). However, the ζ-potential is measured in ethanol, a polar solvent. In non-polar solvents such as dodecene, in which the particles are dispersed before PE preparation, colloidal particles are less charged due to the high energetic costs for charge stabilization [273]. This might enable the formation of the dense hexagonal packing. All in all, the measurements show, that with a simple model and the knowledge of the necessary parameters a good estimation of the droplet diameter is valid.

In the following, the influence of the catalyst on the emulsion structure is discussed. The space for one SX molecule at the water/dodecene interface was estimated to $a_{SX} = 0.96\,nm^2$ using Gibbs law. This corresponds to a density of roughly one molecule per nm^2 present at the water/dodecene interface. By using a metal to ligand ratio of 1:4 means that in the reaction on average one active molecule of catalyst is found every $4\,nm^2$ in the void area. While the catalyst is adsorbed to the interface minimizing its free energy, it is attracted by the SNs positive surface charge electrostatically. The ζ-

potential measurements confirm the strong attraction between the negatively charged SX molecules and the positively charged SNs but not with the negatively charged ones. The charge reversal of the particle-SX-complex with increasing SX concentration is explained by adsorption of SX onto the particle surface. This adsorption is solely dependent on the total particle surface: the curves for 50C18n+ and 100C18n+ show strong coincidence after normalizing the SX concentration with respect to the total particle surface. Since the diameter of several 10's of nm is much larger than the molecular size of a catalyst the curvature seems to have no impact here.

The surface activity of SX was found to modify the structure of the PEs by introducing large voids into the packing of the SNs leading to a shattered internal structure (Figure 5.11 and Figure 5.15 A).

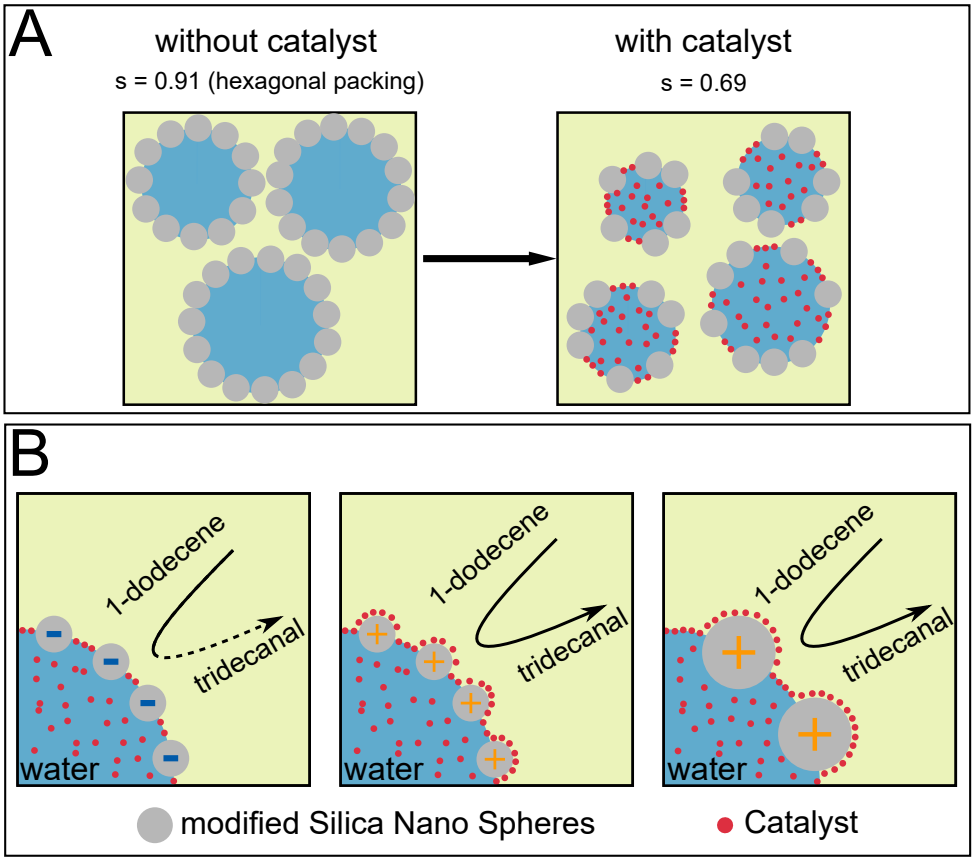

Figure 5.15: Illustration of the proposed model. (A) The catalyst molecules are able to decrease the packing parameter of the SNs at the droplet interface. (B) The negatively charged and surfactant-like catalyst molecules adsorb onto the positively charged SNs but not on the negatively charged ones. This results in a strong increase in reaction yield for the systems containing positively charged SNs. Catalyst molecules on the particle surface seem to dominate the reaction process in the present system but reaction takes place in a similarly effective manner at both surfaces, the voids and the particle surfaces.

This explains the smaller droplet sizes found for PEs prepared with SX. Additionally, this is why the droplet diameter cannot be predicted by eq. (2.12) when assuming a hexagonal packing of the SNs at the droplet surface. Interestingly, the droplet size values for PEs with SX remain proportional to the reciprocal particle concentration (Figure 5.9).

5.3.2 Hydroformylation of 1-Dodecene

The interaction between the catalyst and the SNs has a prominent impact on the reaction performance. In all investigated PEs the dense particle layer at the o/w interface hinders the mass transport to the catalyst, explaining the overall slow reaction rates. Nevertheless, the data allow some important conclusions. While the particle charge has no pronounced impact on the PE structure, a difference in yield was measured for the oppositely charged particles 50C18n+ and 50C18n- (Figure 4.1 A). The yield for 50C18n+ is up to 550% higher than for 50C18n- even though the determined droplet size for all PEs was very similar during the whole process (Figure 5.13 B). The only measured difference between both systems is the ability of 50C18n+ to attract and immobilize the catalyst molecules. The immobilization of the catalyst on the particles surface enhances thus the reaction yield for the positively charged particles (Figure 5.15 A and Table 5.1).

In summary, in case of 50C18n+ and 100C18n+ the particle oil interface is catalytically active which is not the case for 50C18n-. At this point, only the deep knowledge of the interfacial adsorption behavior of the SX molecules, the packing parameter and the PEs stability during the process enables more detailed insights, as demonstrated in the following.
The calculation of the conversion rates per active area is only possible when s and $A_{\emptyset,tot}$ are known, the PE is stable and nearly all SNs are located at the interface. In this way calculated conversion rates are normalized with respect to the total area of individual active interface (taking the convex particle oil interface into account for 50C18n+ and 100C18n+) and are very similar to each other (Figure 5.12 B). This leads to the conclusion that any interface where the catalyst is present is equally contributing to the total conversion. The other way around, this also implies that the SX concentration at the particle oil interface and in the void area between the SNs is similar (≈ 1 per nm^2).
The SX to particle surface ratio in the reaction was 43 molecules per nm^2. If only the particle area in contact with the substrate phase is taken into account, the value corresponds to 86 molecules per nm^2. Subtracting the amount of catalyst at the o/w interface still leads to the assumption that most of the catalyst molecules rather remain in the ”bulk” of the droplets than participating in the reaction. A turn over frequency (TOF_{int}) for only the catalyst molecules at the active interface is calculated

using eq (5.46):

$$\mathrm{TOF_{int}} = \mathrm{CRAA} \cdot a_{\mathrm{SX}} \cdot f_{\mathrm{l:m}} \tag{5.46}$$

$f_{\mathrm{l:m}}$ is the ligand to metal fraction. The resulting value of around $\mathrm{TOF_{int}} \approx 180\,h^{-1}$ is considered as highly speculative but is also the only number independent from the PE structure describing the efficiency of the catalyst. For future formulations the used amount of catalyst needs to be adjusted to its adsorption properties towards the interface (particle surface and void interface). Here, 1 SX molecule per $\mathrm{nm^2}$ is the ideal case, corresponding to the area per molecule of the catalyst. However, in reality this is hardly possible because of equilibration of SX molecules in the bulk and adsorbed at the interface.
Even though the internal sizing parameters differ, the reaction yield from the PEs stabilized by 50C18n+ and 100C18n+ (only 7 % lower for 100C18n+) is similar as shown in Figure 5.12 B. In the particle rich areas at the patchy droplet interface the single void size between the 100C18n+ particles in a 2D hexagonal layer is approximately $380\,\mathrm{nm^2}$ while for 50C18n+ it is only $84\,\mathrm{nm^2}$. This means, that the size of single voids between the SNs does not play a dominant role. Furthermore, the dynamics of the flux of substrate towards the voids is not a determining factor either.

5.3.3 Membrane Filtration

Regarding the results for the filtration process, the dense particle layer at the w/o interface seems very beneficial for the droplet and catalyst retention. After a few minutes a constant flux is achieved and the PEs droplet size did not change significantly during the filtration process. At least 50 % of the oil phase could be removed without difficulties and a clear permeate with no water breakthrough was obtained. Neither the particle surface charge nor the particle size has a significant influence on the filtration performance. The experience obtained shows, that using membrane filtration for droplet and catalyst retention in PEs is very robust and therefore very promising.

5.4 Conclusion

This chapter presents a detailed physico-chemical analysis of w/o PEs from the nano-sized particle level to the micrometer-sized domains of the emulsion structure. Special attention is drawn to the surface-active catalysts influence on the PE structure and its location during the reaction process. SNs with almost identical hydrophobicity, shape and value of the ζ-potential but with targeted opposite charges or difference in size respectively are successfully synthesized (see Chapter 4). This approach allows studying the effect of one separated particle feature while other influencing factors could be excluded. Reliable quantitative prediction of the droplet size in PEs is possible using a simple model which requires basic information about the particle properties such as size and density. The predictions for the droplet diameter agreed even quantitatively perfectly with the independently measured droplet diameters proving the validity of all assumptions made. The packing parameter of the investigated system corresponds to a hexagonal 2D lattice. Neither the size nor the charge of the SNs has an influence on the packing parameter. The coverage parameter reduces (from s = 0.91 to s = 0.69) after adding the catalyst to the PE. This did not diminish the PE stability. This stability is proven and utilized when using the PEs as a reaction environment and the subsequent performance of a membrane filtration for catalyst retention. The particle surface charge has a strong effect on the reaction yield while the particle size itself is not a determining factor. Obviously, the adsorption of the (negatively charged) catalyst onto the (positively charged) SNs favors the reaction. In addition to previous studies, it is shown that this increase in conversion is even quantitatively explained by the geometry of the system. In case of a positive surface charge of the SNs the particle-oil interface acts as an additional active surface and therefore the yield is increased. The other way around it is shown that the catalytic efficiency of both, the water-oil and the particle-oil interface, is roughly equal with a conversion of around 45 molecules per nm^2 and hour. This indicates that the amount of catalyst molecules at the oil-water interface is equal to the adsorbed catalyst molecules at the particles surface. The amount of ligand at the w/o interface is determined to be roughly 1 molecule per nm^2. So all in all the reaction takes place at the surface of the SNs as well as in the void area between the SNs. For future PE designs the active interface can be effectively increased in both ways, increasing the voids or increasing the particle surface indenting into the oil phase. But still the most important requirement should stay the verification of a sufficient PE stability. The successful membrane filtration (using oNF-3 membranes) of

the oil phase from the water droplet phase without damaging the emulsion proves this sufficient stability for the present system and demonstrates the possible application of a continuously operated catalytic process.

6 Water in Oil Emulsions Stabilized by Microgel and Silica Spheres

This chapter describes the formation of PEs simultaneously stabilized with hydrophobic solid SNs and hydrophilic, soft microgel with the aim to achieve water in non-polar oil emulsions. The MGs are not able to stabilize w/o on their own but the addition of SNs enables the w/o emulsion type. The results presented in this chapter are part of the publications of the author in *Soft Matter* (2021) [132] and in *Nanomaterials* (2022)[262]. The reproduced part happens with permission of the Royal Society of Chemistry and MDPI, respectively.

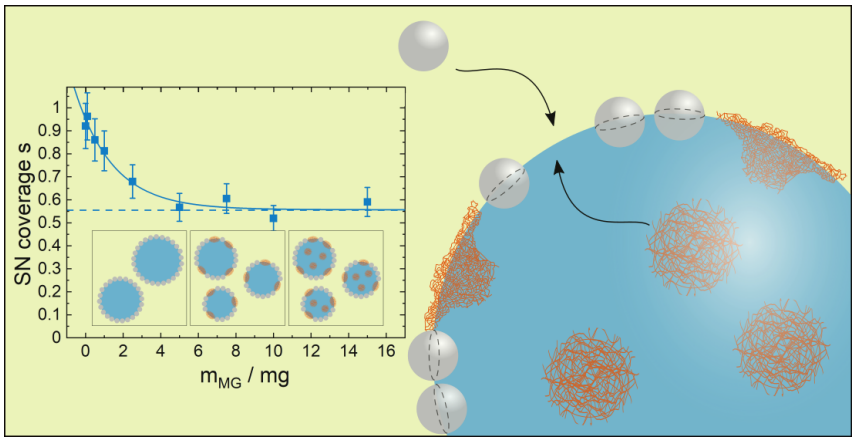

Abstract

MGs at the interface are able to increase the catalyst-substrate contact. However, a general drawback of MGs is that they do not stabilize w/o emulsions of non-polar oils. Simultaneous stabilization with solid hydrophobic nanoparticles and soft hydrophilic

MGs overcomes this problem. For a fundamental understanding of this synergistic effect the use of well defined particle systems is crucial. Therefore, the present chapter investigates the stabilization of water droplets in a highly non-polar oil phase using temperature responsive, soft and hydrophilic PNIPAM MGs and solid and hydrophobic SNs simultaneously. The size of the SNs is varied between around 30 nm and 100 nm and the softness of the MGs that have a size around 600 nm in the swollen state is varied by the variation of the cross-linking density. In a multi-scale approach the resulting emulsions are studied from the nanoscale particle properties over micro-scale droplet sizes to macroscopic observations. The synergy of the particles allows the stabilization of w/o emulsions, which was not possible with MGs alone, and offers a larger internal interface than the stabilization with SNs alone. Furthermore, the incorporation of hydrophilic MGs into a hydrophobic particle layer accelerates the emulsions sedimentation speed. Nevertheless, the droplets are still sufficiently protected against coalescence even in the sediment and can be redispersed by gentle shaking. Based on droplet size measurements and cryo-SEM studies a model is elaborated, which explains the found phenomena.

6.1 Introduction

The implementation of polymeric material at the interface of PEs is a possible solution to overcome the strict dependency of the catalytic active interface from the applied particle surface. An example is found in the field of bio-catalysis, where the application of MGs improved the catalyst-substrate contact significantly [129]. This usage of MGs as emulsion stabilizers may be expandable on other non bio-catalytic reactions. The problem is, that hydrogel particles in general and poly(N-isopropylacrylamide) (PNIPAM) MGs [108] in particular lack the ability to stabilize w/o type emulsions at all [130], especially, when a highly non-polar oil phase is used [26, 124] (see Chapter 2.2).
A promising strategy to overcome this problem is the use of a second species of particles to assist the stabilization. For example, Jiang *et al.* [129] quite recently demonstrated the use of silica particles to assist enzyme decorated Poly(2-(diethylamino)ethyl methacrylate)-based (pDEAEMA) MGs in the stabilization of w/o emulsions for catalysis. Still, the number of fundamental studies investigating the driving factors (*e. g.*, water fraction, particle mass ratio, *etc.*) and the particle-particle interaction at the interface of these multiple particle stabilized emulsions is very low, so this field lacks

significantly in understanding (see Chapter 2.2).
This understanding is only possible with well understood and sufficiently characterized particles. Therefore, this chapter investigates emulsions, which were simultaneously stabilized by two common and comparably well understood model particle systems (hydrophilic, soft PNIPAM MGs and hydrophobic, solid SNs) and aims for generalizable explanations to better understand the simultaneous stabilization. It investigates the influence of the solid/soft particle ratio, the maximum incorporation of MG at the interface and possible responsiveness of the soft MGs on the structure of the resulting w/o emulsions. In detail, it focuses on the influence of the simultaneous stabilization on the structure formation of the particles at the w/o interface, the resulting droplet diameter and the sedimentation behavior.
The use of likely charged stabilizers makes sure that the much smaller SNs do not adsorb into the larger MGs [274]. Emulsions were prepared with either one or both stabilizing agents. Hybrid SN/MG co-stabilized emulsions are formed from a two phase system where the two different particle types were separated initially. The hydrophobic SNs are present in the oil phase, while the hydrophilic MGs are present in the aqueous phase. During emulsification, the particles meet at the interface from opposite directions. The resulting emulsions are investigated by microscopy, droplet size analysis, cryo-SEM and sedimentation analysis and differences between simultaneously and single particle type stabilized emulsions are discussed.

6.2 Results

Emulsions with different soft/solid (MG/SN) particle ratios were prepared as described in Section 3.10 in Chapter 3. In the following, the total emulsion volume of 12.55 ml and the water volume fraction (f_w = 20 vol%) were kept constant. To analyze the influence of both, either the total stabilizer mass of MG and SN ($m_{MG} + m_{SN} = 20\,mg$ / $\sim$ 0.2 wt%) was kept constant and their ratio was varied or only the SN mass ($m_{SN} = 10\,mg$ / $\sim$ 0.1 wt%) was kept constant and the MG mass was increased.

6.2.1 MG Emulsions

Attempts to form emulsions with MGs (MG_M) only never resulted in the desired w/o type emulsion irrespective of preparation temperature and water volume fraction (Figure 6.1). Either they formed o/w emulsions or they were unstable. Attempts to form emulsions at 8 °C with 20 vol% water fraction resulted in a two phase system, which, at first glance, looks like the initial state (Figure 6.1 A). A closer look by microscopy of a drop from the lower aqueous phase reveals only few very small oil droplets (Figure 6.1 H). With a water fraction of 40 vol% (temperature at 8 °C) a pasty emulsion phase formed (Figure 6.1 C). After a few hours it creamed up and a lower turbid aqueous phase appeared. Fluorescence microscopy of a drop taken from this emulsion phase reveals oil droplets in water with very strong cohesion (Figure 6.1 I). At 8 °C, the stirrer looks clean (Figure 6.1 B). At a preparation temperature of 50 °C, no emulsions formed at all neither at 20 vol% nor at 40 vol% water fraction (Figure 6.1 D, F, J). In both cases, the stirrer was contaminated heavily by accumulated MGs afterwards (Figure 6.1 E, G).

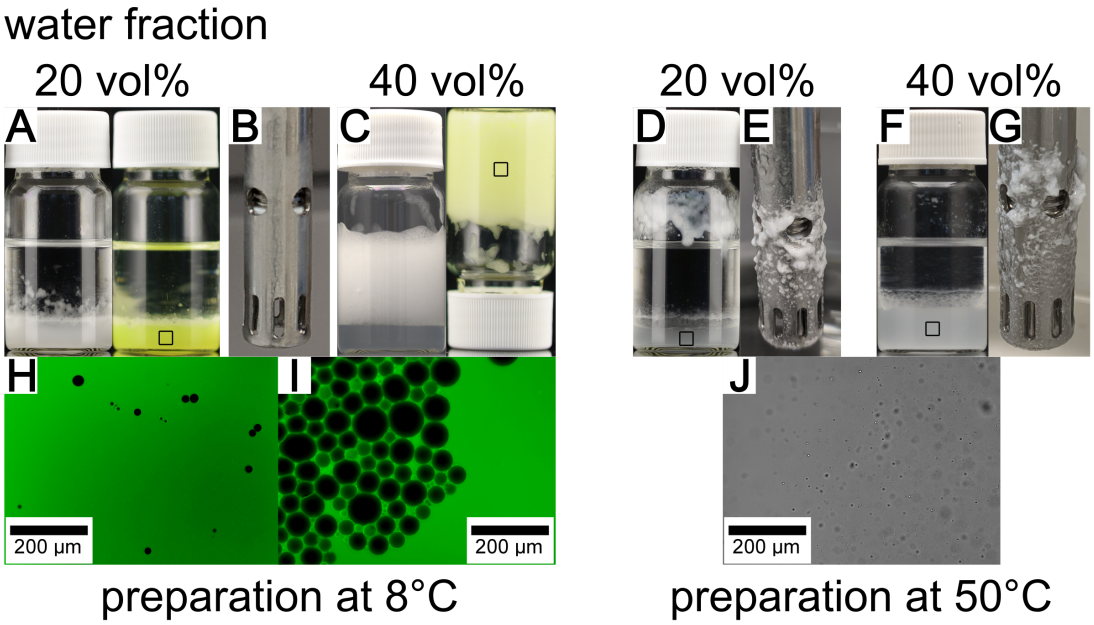

Figure 6.1: Attempts to form emulsions with MGs only ($m(MG_M)$ = 20 mg, V_{tot} =12.55 ml). Left: At 8 °C and a water fraction of 20 vol% only seldom oil droplets were observed in the water phase (fluorescence microscopy (H) with fluorescein dyed water phase of sample (A)). A pasty o/w emulsion phase was observed for a water fraction of 40 vol% (C). The photo of the sample without dye was taken ∼5 h after preparation; the photo with fluorescein shows a freshly prepared emulsion. The samples contain a high amount of droplets with strong cohesion (fluorescence microscopy (I) with fluorescein dyed water phase of sample (C)). Right: At 50 °C, no emulsions formed (D, F, J) with the exception of a thin layer of very large roughly millimeter scale droplets at the w/o interfacial region for a higher water fraction (F). In both cases, a significant amount of MGs accumulated at the stirrer (E, G), which was not the case at 8 °C (B).

6.2.2 Influence of SN/MG Ratio and Temperature

Attempts to form emulsions stabilized with only the hydrophobic SNs (LC18n+) or stabilized simultaneously by both solid and soft particles (with 20 vol% water volume fraction) resulted always in the desired w/o emulsions (Figure 6.2). All emulsions have the tendency to sediment and form a white sedimented phase after a few minutes. The droplets can easily be redispersed without damage by gentle shaking

(Figure 6.2 A, B). The emulsion formation consumed any free water present. None of the studied emulsions containing SNs showed residual water or any unexpected deviation in the macroscopic phase structure. Even without a detailed analysis, it is visible in the microscope images that droplet size increases with decreasing SN mass (Figure 6.2 A, B) for all samples. Neither a macroscopic nor a microscopic difference was found between the emulsions with MGs prepared at 8 °C and those prepared at 50 °C.

Figure 6.2 C shows the Sauter mean diameter of the droplets obtained from the image analysis. The drop size analysis shows a reciprocal behavior of the droplet size over SN mass for both, the emulsions with and without MGs. The measured mean droplet size of PEs prepared at 8 °C and those prepared at 50 °C are very similar. To describe the system models from classic PEs are applicable. For PEs in the case of limited coalescence and under the assumption that all particles adsorb at the interface, the droplet diameter is described by eq. (2.13). By using the SN specific parameters for $a_{\oslash}$ and $m_{\mathrm{p,tot}}$, the SN coverage (packing) parameter s describes the relative droplet surface covered by the SNs. By assuming different packing scenarios (s=0.25, 0.5, 0.75, 1) a set of droplet size curves can be predicted for orientation (gray dashed lines in Figure 6.2 C). By fitting eq. 2.13 to the data for the SN only stabilized emulsions, one obtains a packing parameter of $s(\mathrm{SNs_{only}})= 0.93\pm0.03$, which is close to the theoretical 2D hexagonal close packed (hcp) parameter of $s_{\mathrm{hcp}} \approx 0.907$. By fitting the data to the solid/soft simultaneously stabilized emulsions s(SNs/MGs)=0.56±0.02 was found. This includes the assumption that even in presence of MGs still nearly all solid particles adsorb at the interface.

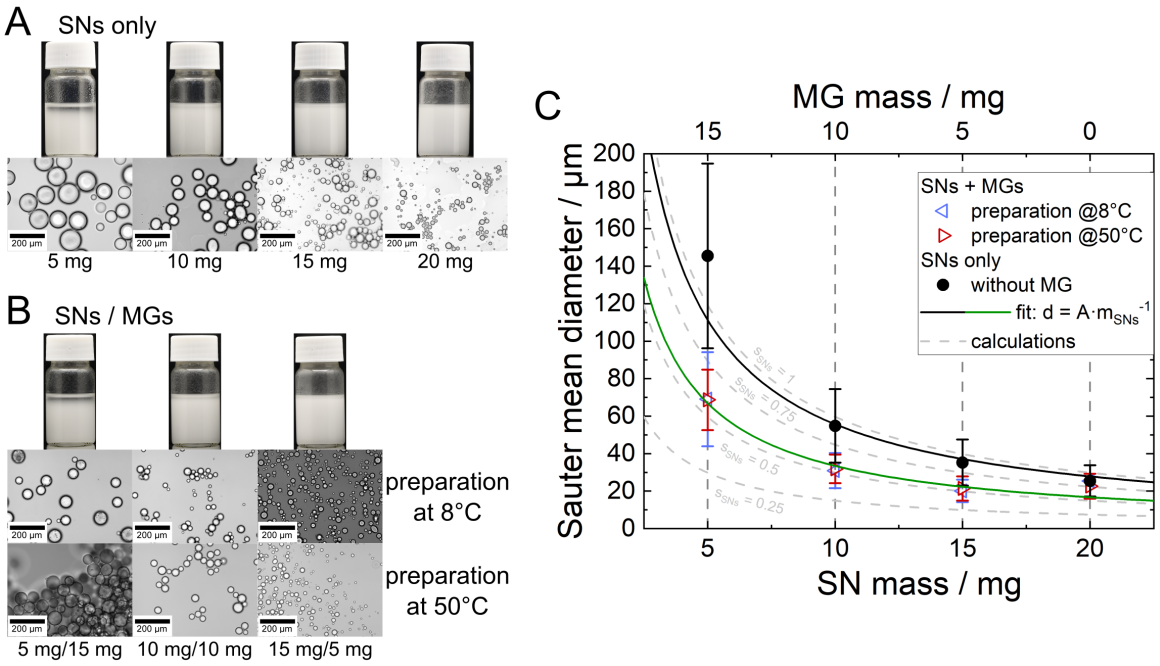

Figure 6.2: (A, B) Photographs and microscopy images of w/o emulsions stabilized by SNs only and simultaneously stabilized by SNs (LC18n+) and MGs (MG_M) prepared at 8 °C and 50 °C respectively but investigated at room temperature (V_{tot}=12.55 ml, f_w=20 vol%) in dependence on the solid particle content. The emulsions tend to sediment after a few minutes but can be redispersed by gentle shaking. (C) Sauter mean droplet diameter related to the microscopy images shown in (A, B) over the MG or SN mass. The error bars represent the standard deviation of the drop size distribution. Gray dashed lines represent calculations assuming different SN packing parameters s for orientation. The continuous black and green line are reciprocal fits using eq. (2.13) with s as the free parameter.

The nanoscopic structure formation on the water-oil-interface was investigated by cryo-SEM (Figure 6.3). The cryo-SEM images for the emulsion stabilized with SNs only (Figure 6.3 A - C) show spots where the particles are present and form a hexagonal close packed structure. On other spots the particles broke away during sample preparation. The results are in agreement on findings in the previous chapter.
The images taken from samples prepared with both, SNs and MGs (Figure 6.3 D - I), proof the simultaneous adsorption at the water-oil-interface. In both cases, the MGs adsorb at the interface and form a regular patterned (presumably hexagonal)

hyper-structure. The images with higher magnification for the sample prepared at 8 °C (Figure 6.3 E, F) show the MGs in between the SN layer, the residuals of which can only be detected in form of the relief structure (Figure 6.3 F). This offers a clear view on the MGs' structure formation. In the images with higher magnification for the sample prepared at 50 °C (Figure 6.3 H, I), the SN layer is intact and covers the whole droplet. It shows the SNs also decorating surface area of the MGs. In summary, the SNs arrange themselves around the MGs but also adsorb at their surface. Differences between the preparation at 8 °C and 50 °C are not evident, which is in agreement with the drop size distribution measurements. The interfacial structure formation looks in both cases very similar.

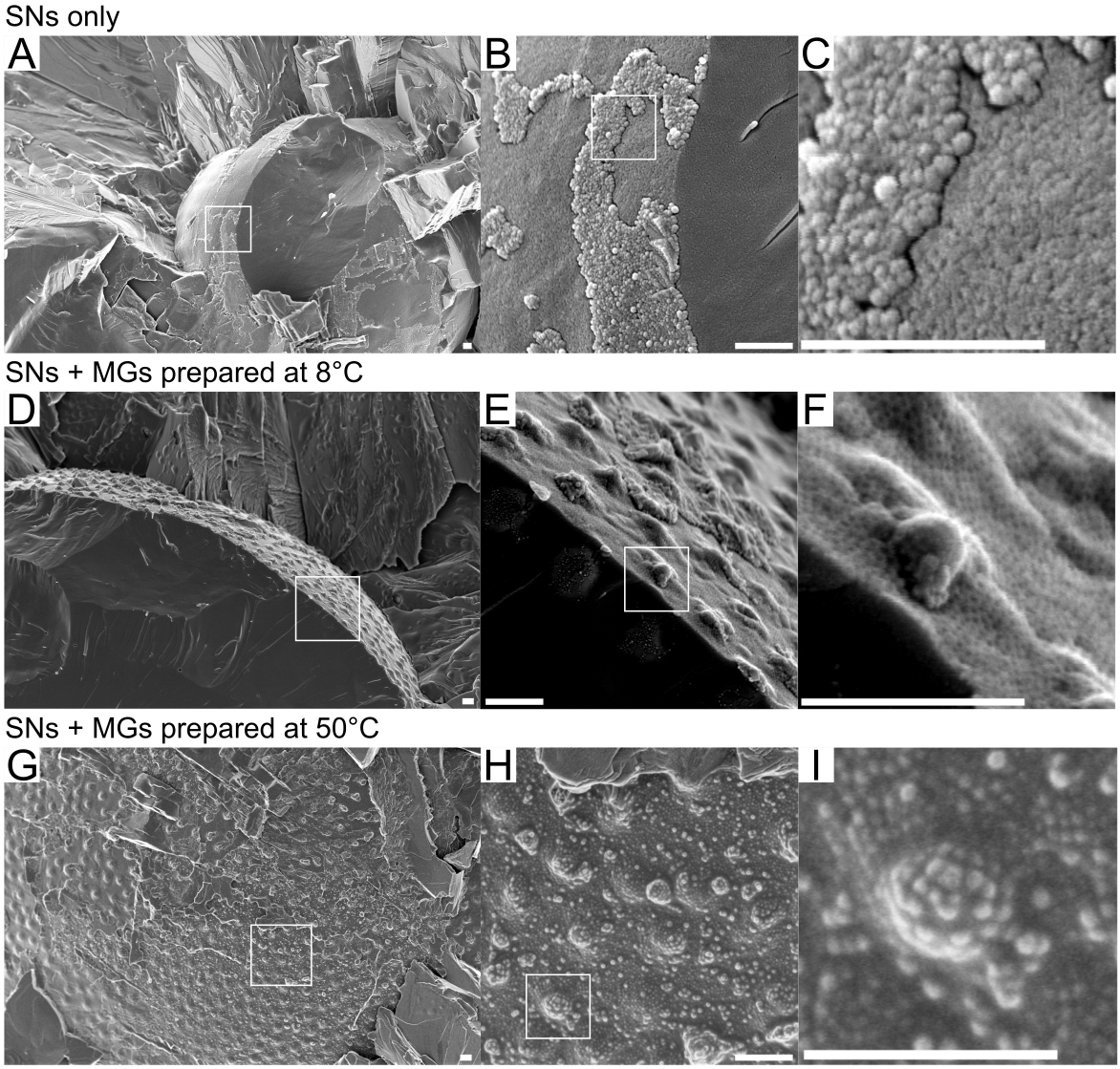

Figure 6.3: Cryo-SEM images from different emulsion types. A - C: SN (LC18n+) only stabilized emulsion (V_{tot}=12.55 ml, f_w = 20 vol%, m(SNs) = 20 mg). At the droplet interface spots are visible where the SNs form a crust-like structure with a close packing (presumably hcp). On other spots the particles are missing due to the breakage in the sample preparation. D - I: SNs (LC18n+)/MGs (MG_M) simultaneously stabilized emulsions prepared at 8 °C (D - F) or 50 °C (G - I), respectively, (V_{tot}=12.55 ml, f_w=20 vol%, m(SNs)=10 mg / m(MGs)=10 mg). In case of SN/MG emulsions prepared at 8 °C, the particles broke away and reveal a view on the MGs and left behind a relief-like structure. In case of SN/MG emulsions prepared at 50 °C, the particle layer remained on the interface. In both cases, the MGs form a regular patterned hyperstructure (presumably hexagonal but not close), while the particles assemble around the MGs but also adsorb at their surface. The white bars represent 500 nm.

6.2.3 Influence of MG Content, Stiffness and Particle Size

To test the capacity of the interface to take up and incorporate MG, emulsions were formed with a constant amount of SNs (10 mg) while increasing the present amount of MGs. With that the total amount of stabilizer material increases. With the exception of highest concentration of the lowest cross-linked MGs, w/o emulsions formed, clearly seen by the tendency of the emulsions to sediment. As shown in in Figure 6.4 A - C, the increasing amount of present MGs reduces the Sauter mean droplet diameter for all three different MG types.

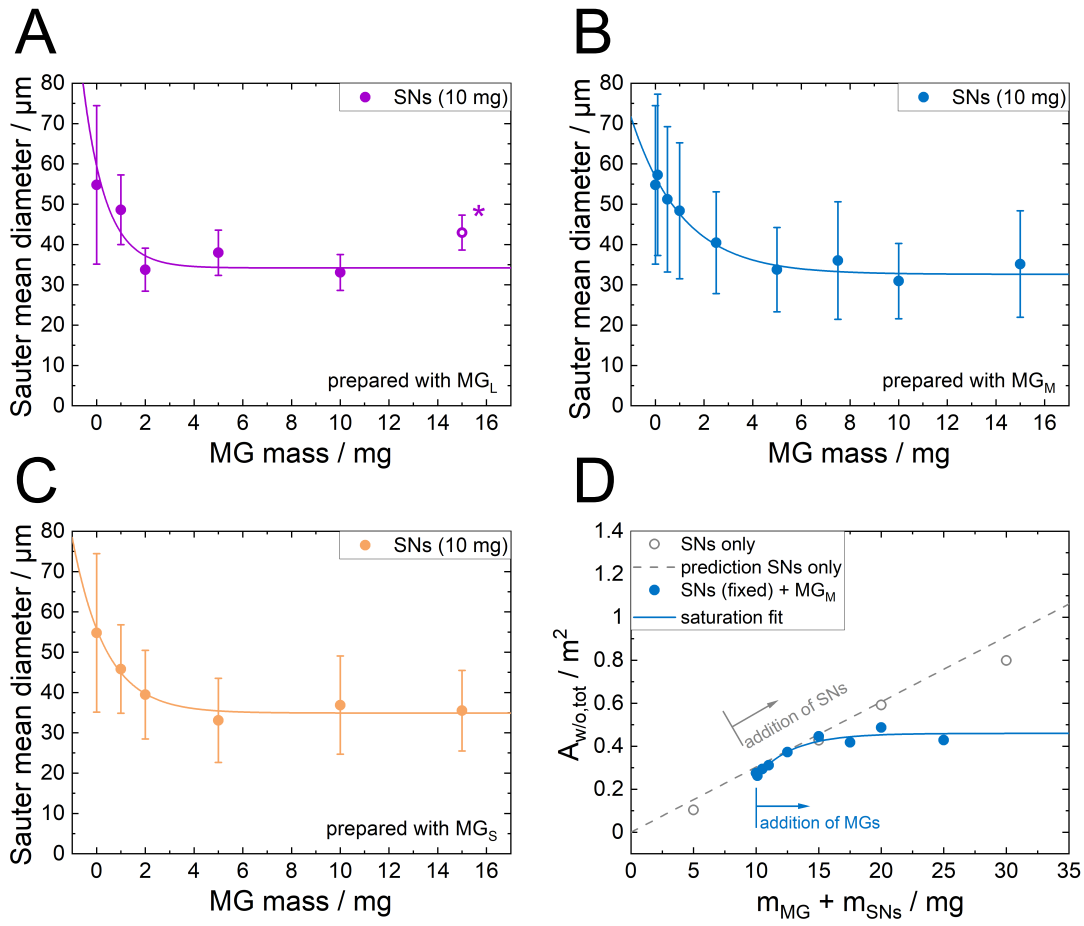

Figure 6.4: Sauter mean diameter for emulsions ($V_{PE,tot}$=12.55 ml, 20 vol%) formed with a constant amount of SNs (10 mg, LC18n+) and an increasing amount of MGs with a lower (A), medium (B) or higher (C) cross-linker content. The emulsion formation with the highest amount of present MG with the lowest cross-linker content lead to the formation of a double emulsion with oil droplets inside the water phase. The data point marked with (*) was produced evaluating only the outer droplet diameter while ignoring the inner droplets. The error bars represent the standard deviation of the droplet size distribution. (D) Total emulsion droplet area $A_{PE,tot}$ for the emulsions prepared with LC18n+ alone and with the addition of the medium cross-linked MG over the total stabilizer mass calculated with eq. (2.10).

In all three cases the curve runs into a plateau for high amount of present MGs and does not decrease further. This limiting value lays around the same value for all three MG types. Figure 6.4 D shows that the total PE interface is also running in a plateau

instead of a linear increase that would be expected when the stabilizer mass is increased. In case of the lowest cross-linked MGs at 15 mg MG content, an oil in water in oil (o/w/o) double emulsion formed (Figure 6.5 A, B) which was not the case for the other two higher cross-linked MGs (Figure 6.5 C, D). By only measuring the outer droplet diameter and ignoring the oil droplets inside the water droplets, a droplet diameter roughly in the trend of the other MG concentration is found. This indicates that the inner droplets are mainly stabilized by the MGs.

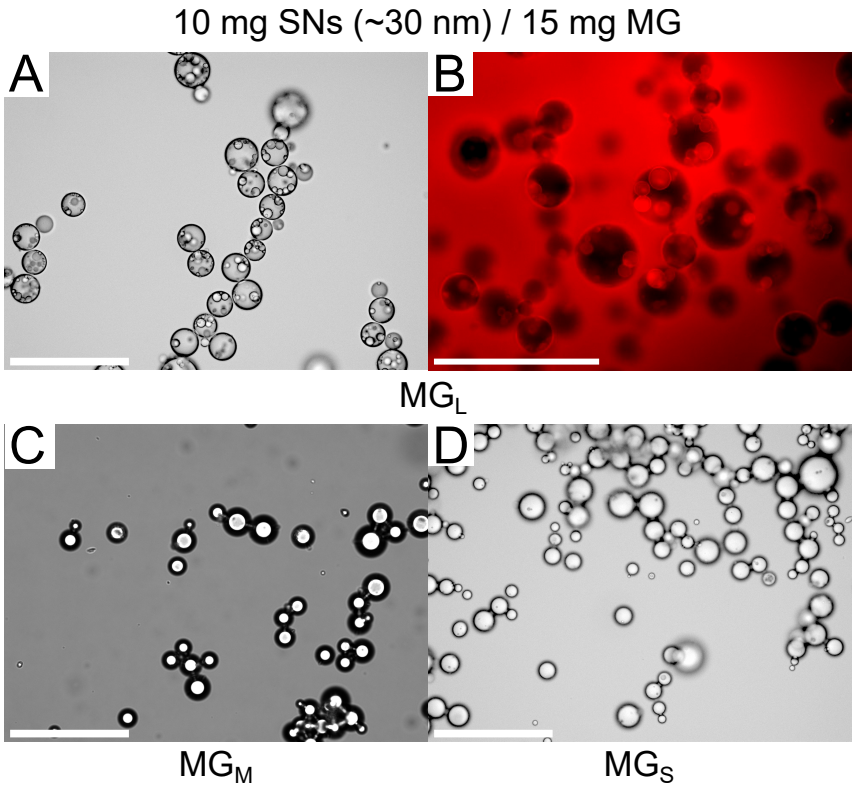

Figure 6.5: Micrographs of the emulsions with the highest amount of present MGs (15 mg). The o/w/o emulsion type for the emulsions prepared with the lowest cross-linked MG (A) was proven by dying the oil phase with nile red (B). For the higher cross-linked MGs (C, D) no double emulsions formed. The white bars represent 200 µm.

Under the assumption that even under the presence of more and more MGs, still all SNs are present at the interface, the individual SN coverage s can be calculated by rearranging eq. (2.13). The rearrangement leads to eq. (6.47):

$$s = \frac{a_{\varnothing} m_{\mathrm{p,tot}}}{6 f_w V_{\mathrm{PE,tot}}} d_{\mathrm{PE}} \tag{6.47}$$

This linear transformation applied to the Sauter mean diameter curves from Figure 6.4 A - C, results in similar shaped curves for the SN coverage (Figure 6.6). The error bars were calculated from the propagation of uncertainty with the estimated uncertainties of $a_{\oslash}$, $m_{\mathrm{p,tot}}$, f_w and $V_{\mathrm{PE,tot}}$. However, the absolute values for the initial and the final values of the SN coverage parameter s reveal further insights in the emulsion structure. For the PE samples without MGs the received values are close to the 2D hcp value of 0.91. The final plateau value s_{limit} was determined using a simple saturation approach (eq. (6.48)) applied as a fit to the data:

$$s = s_{\mathrm{max}} e^{-\beta_s m_{\mathrm{MG}}} + s_{\mathrm{limit}} \tag{6.48}$$

In this empiric approach, s_{max} is a value for the amplitude which is connected to the maximum amount of MG at the interface. β_s is a value for the effectiveness of decreasing the drop size per MG mass and s_{limit} the desired value for the minimum percentage of covered interface by the SNs. This saturation approach describes the data sufficiently. The determined values for s_{limit} lay in the interval between 0.56 and 0.59 for all three MG types. This shows that the cross-linking density has no influence on the final interface composition.

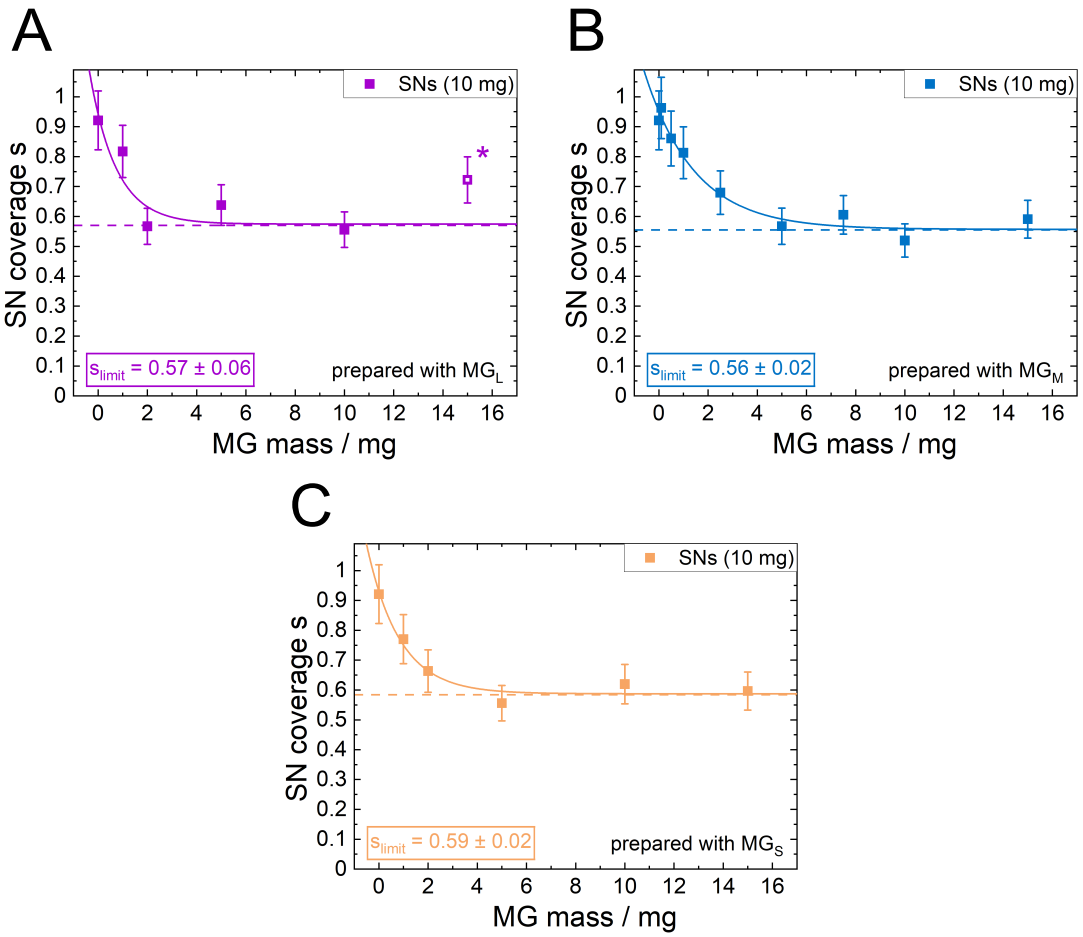

Figure 6.6: Coverage parameter s of the SNs in SN/MG co-stabilized emulsions calculated from the Sauter mean diameters presented in Figure 6.4 A - C using eq. (6.47). All three curves run into a saturation for high amounts of MGs. The final SN coverage s_{limit} was determined using eq. (6.48) and is very similar for all three MG types irrespectively of the cross-linker content.

While the cross-linker content of the MGs had only minor effects on the shape of the Sauter mean diameter curves over the increasing MG content, the size of the SNs changes this behavior significantly. For better comparison between smaller and the larger SNs, the amount of the larger SNs was adjusted so that their amount resembles a similar total particle cross-section $A_{\oslash}$ ($A_{\oslash} = a_{\oslash} \cdot m_{\text{p,tot}}$). Therefore, the experiments with the larger SNs were conducted with a SN mass of 30 mg. This leads to a starting point with a similar Sauter mean droplet diameter. The determined Sauter mean droplet sizes with increasing amount of the medium cross-linked MGs are shown in Figure 6.7 A in comparison to the data for the respective samples with the smaller SNs

already shown in Figure 6.4 B. The addition of MGs also decreases the droplet size when the larger SNs are present but the effect is with a decrease of about 15 µm at 15 mg MG content less strong than for the PEs containing the smaller SNs with more than 25 µm at 15 mg MG content. In contrast to the emulsions with the smaller SNs, the emulsions with the larger SNs do not show a clear saturation with MG, but the droplet sizes are in all cases larger than those of the PEs containing the smaller SNs. The saturation may therefore be better visible at higher MG contents. The calculation of the individual SN coverage s for every sample is shown in Figure 6.7 B. Despite this plot neither shows no clear saturation behavior, it shows that the SN coverage decreases from the hcp value with increasing MG content but always stays above the s_{limit} regime of around 0.56 determined for the smaller SNs. This indicates a saturation for larger MG content.

The emulsions formed with the larger SNs show even more severe droplet clustering with high MG content, which prevents a reliable analysis of even higher MG contents.

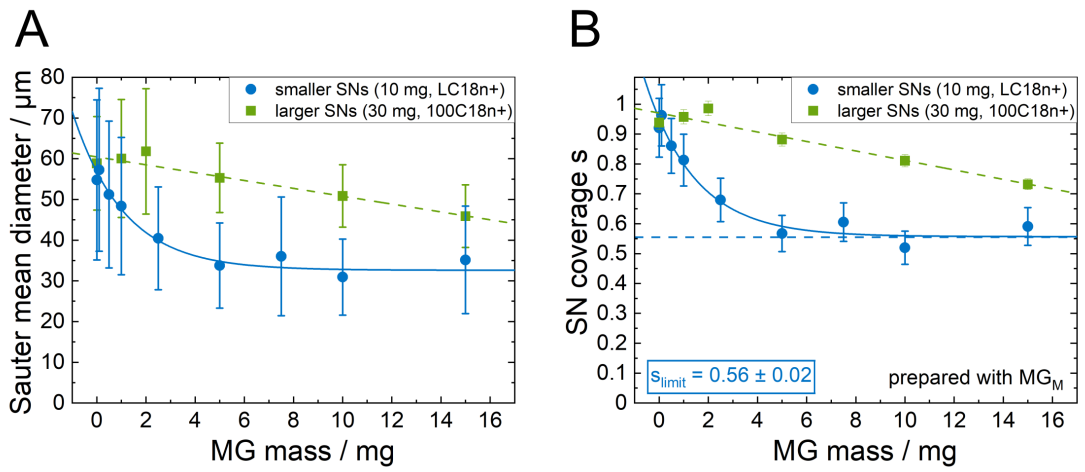

Figure 6.7: Comparison between emulsions stabilized with smaller (LC18n+) and larger (100C18n+) SNs, respectively, with increasing amount of the medium cross-linked MGs ($V_{PE,tot}$=12.55 ml, 20 vol%). The SN mass was adjusted so that both applied particle systems exhibit the same total particle cross-section $A_{\varnothing}$. (A) The Sauter mean droplet diameter decreases in both cases with the present amount of MGs. A saturation behavior is only clearly visible in the case of the smaller SNs. (B) The calculations of the SN coverage parameter s shows that while the fraction of interface covered by the larger SNs decreases with the increasing present amount of MG it never passes the minimum coverage parameter s_{limit} of around 0.56 calculated for the smaller SNs.

6.2.4 Sedimentation Analysis

Figure 6.8 (A - C) shows the PE fraction over time. It was found that the PE fraction shows a single exponential decay:

$$f_{PE} = A \cdot e^{-Bt} + C \tag{6.49}$$

f_{PE} is the emulsion (PE) volume fraction, A is the amplitude ($f_{PE}(t = 0) - C$), B the sedimentation rate and C the final PE volume fraction.
Eq. (6.49) describes the data well and the obtained parameter B characterizes the sedimentation time and therefore was called sedimentation rate. B is linearly connected to

the initial drift velocity $v_{\mathrm{d,i}}$ *via* eq. (6.50):

$$v_{\mathrm{d,i}} = h_{\mathrm{PE}} \cdot \frac{\mathrm{d}}{\mathrm{d}t} f_{\mathrm{PE}}(t = 0) = -A \cdot B \cdot h_{\mathrm{PE}} \tag{6.50}$$

h_{PE} is the total emulsion height. The drift velocity of a single (solid) sphere with density ρ_{P} and diameter d in a medium with a density ρ_{l} and a dynamic viscosity η at low Reynolds numbers under the gravitational force (g: gravitational constant) is given by the Stokes equation (derivation see for example Pal *et al.* [275]):

$$v_{\mathrm{d,\,Stokes}} = \frac{1}{18} \frac{d^2 \cdot (\rho_{\mathrm{P}} - \rho_{\mathrm{l}})}{\eta} \tag{6.51}$$

It was found that the sedimentation rate B shows a linear dependence on the droplet size for both types of stabilization (Figure 6.8 D). But, the emulsions stabilized with SNs and MGs simultaneously sedimented relative to their droplet size faster than the PEs stabilized with SNs only. The case is similar for the initial drift velocity (Figure 6.8 E): While the curve for the single-sphere drift velocity (calculated from eq. (6.51)) describes the data for the emulsions with SNs only quite well, the data for the SN/MG emulsions systematically lays higher than expected, *i. e.*, they even start their sedimentation faster.

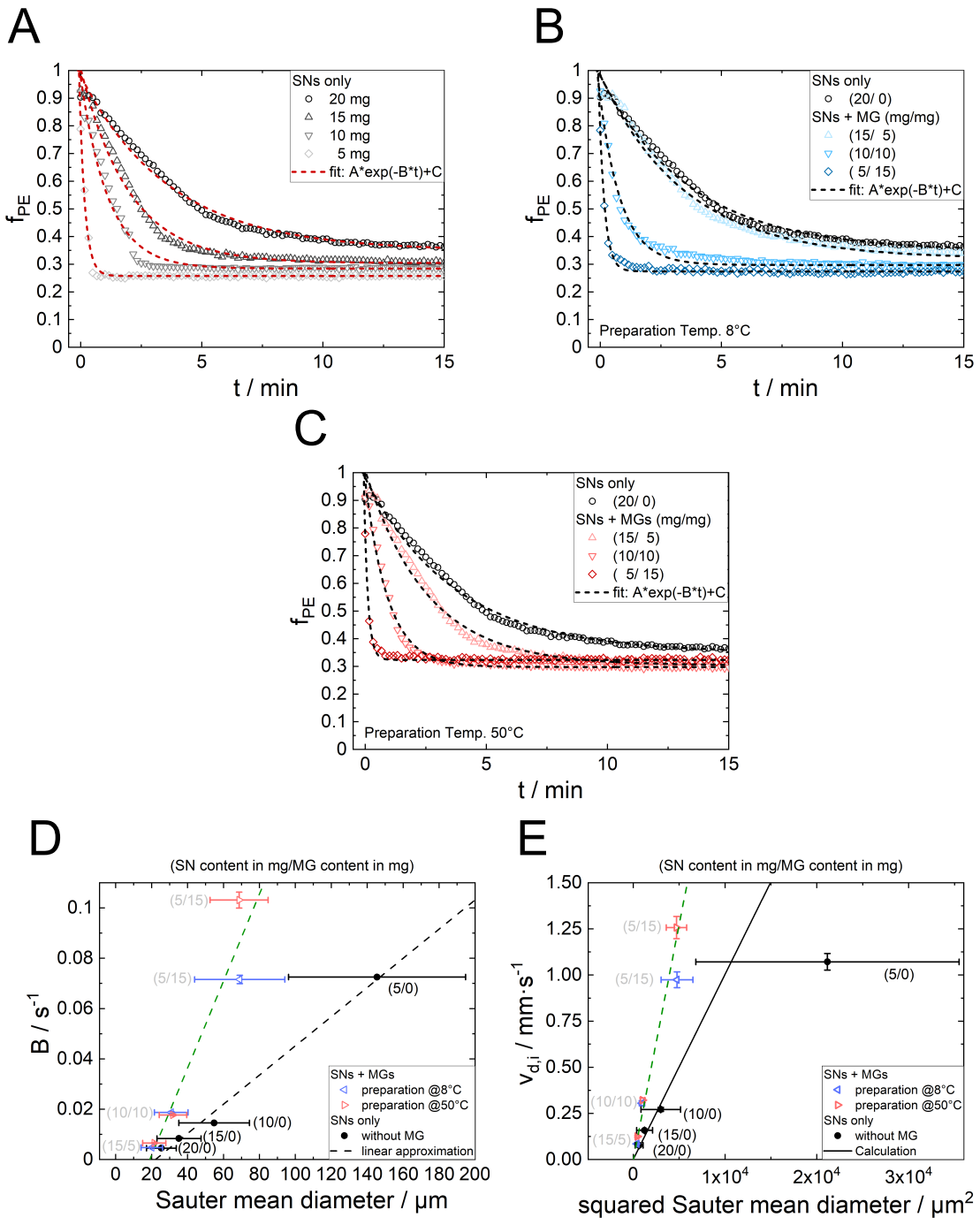

Figure 6.8: Sedimentation curves (PE volume fraction over time) of the different emulsions (V_{tot}=12.55 ml, f_w=20 vol%, at room temperature). The PE volume fraction was evaluated from a series of photos taken every 10 seconds. (A) prepared with SNs only (LC18n+) (B) prepared with SNs (LC18n+) and MGs (MG_M) at 8 °C (C) prepared with SNs (LC18n+) and MGs (MG_M) at 50 °C. Sedimentation rate (D) and initial drift velocity (E) were determined from the fit with eq. (6.49). The straight line in (E) was calculated with stoke equation (eq. (6.51)) The emulsions stabilized with MGs sediment faster than emulsions without MGs relative to their droplet size.

6.3 Discussion

The particle characterization (Chapter 4) shows that both particle types are positively charged in polar solvents. The MGs are hydrophilic, while SNs are hydrophobic. Besides their differences in amphiphilicity, MGs and SNs differ strongly in size. The soft MGs are 10 - 20x larger than the solid SNs.
When it comes to PE formation, both particles follow their nature. The hydrophilic MGs tend to form o/w emulsions, while the hydrophobic SNs form w/o emulsions. But there is more to learn from the attempts to form emulsions with MGs only, because their ability to stabilize emulsions has a water phase fraction dependent and a temperature-dependent component. For some types of amphiphilic particles and some specific oil types a phase inversion may occur when lowering the water volume fraction, *e. g.*, fumed silica in water-toluene emulsions [17]. But, the observed tendency that the number of droplets decreases drastically with decreasing the water fraction from 40 vol% to 20 vol% (Figure 6.1 H, I) indicates that a phase inversion is not possible with the present MGs and the used highly non-polar oil. The strong adhesion between the droplets for the water fraction of 40 % was investigated already in detail by Destribats *et al.* [276] and originates from particle bridging, *i. e.*, two or more droplets share the same MG.
The increase in preparation temperature above the VPTT of the MG prevents the formation of any emulsion phase (Figure 6.1 D, F, J). The temperature induced collapse of emulsions and foams was already studied in detail by various authors [27, 115, 277]. The explanation in the present case may be described as the following: While MGs still may attach to the interface created by stirring, the shrunken MGs are not able to protect the emulsion from coalescence effectively. This leads to an instant and strong coalescence of freshly formed droplets. The MGs attached to the coalescing droplets are rather pushed out of the interface or are increasingly deprived of their free space at the interface. This later case may be comparable to the situation of a MG layer on the 2D interface on a Langmuir-Blodgett-Trough. Under compression of the interface the MGs tend to be squeezed together and crowding effects occur [278]. Therefore, the MGs - now in close contact to each other - agglomerate and accumulate only at the height of the stirrer where the emulsion droplets are formed by sheering and instantly collapse (Figure 6.1 E, G). The same effect may explain the contamination of the upper part of the stirrer during the MGs' durability tests at 50 °C. In this case, the foam formed from stirring induced air bubbles at the water-surface collapses instantly

and the MGs - now in close proximity to each other at the interface - agglomerate and accumulate at the upper part of the stirrer (Figure 4.8). Similar flocculation has been observed by Wiese *et al.* [27] when intentionally destroying PNIPAM MGs stabilized emulsions prepared at room temperature by raising the temperature.
The results change fundamentally when replacing at least 25 % of the MG mass with hydrophobic SNs. The preparation temperature in this case does not play a role anymore. The presence of SNs results in the w/o type in every SN/MG stabilized emulsion that was investigated and the MGs did not agglomerate at the stirrer irrespective of the temperature. Independent from the MG proportion a constant relative shift towards smaller droplet sizes is observed when comparing the PEs with MGs towards those without MGs (Figure 6.2 C). This leads to the conclusion that the MGs are incorporated at the interface structure and stabilize additional interface. Both, the SN stabilized and the SN/MG stabilized emulsions show a reciprocal dependence of the SN mass but no visible correlation with the MG mass - besides the relative decrease in droplet size. This indicates that only a constant relative amount of MGs is incorporated at the interface in dependence of the present number of SNs. Or vice versa, there has to be a sufficient amount of SNs per MG present at the interface. This raises the suspicion that for every MG containing sample (even for the lowest MG concentration) more MG is present than the amount that can be incorporated at the interface. This means a significant amount of excess MG remains in the bulk of the droplets, while only some are integrated into the interface by the SNs. This raises the question if there is a maximum amount of MGs that can be incorporated in between the solid SNs. This question was addressed by increasing the amount of present MG while keeping the amount of used SNs constant.
Instead of an expected reciprocal dependency of the Sauter mean diameter with the increasing amount of present stabilizing material a saturation behavior was found (Figure 6.4). This means that at a certain point the increase of the present amount of MG is not longer decreasing the droplet size and with that is not increasing the total emulsion interface. This means vice versa that at a certain point the MG is rather located in the bulk water phase than adsorbing at the interface where only a maximum amount MG is allowed. This mechanism is illustrated in Figure 6.9.

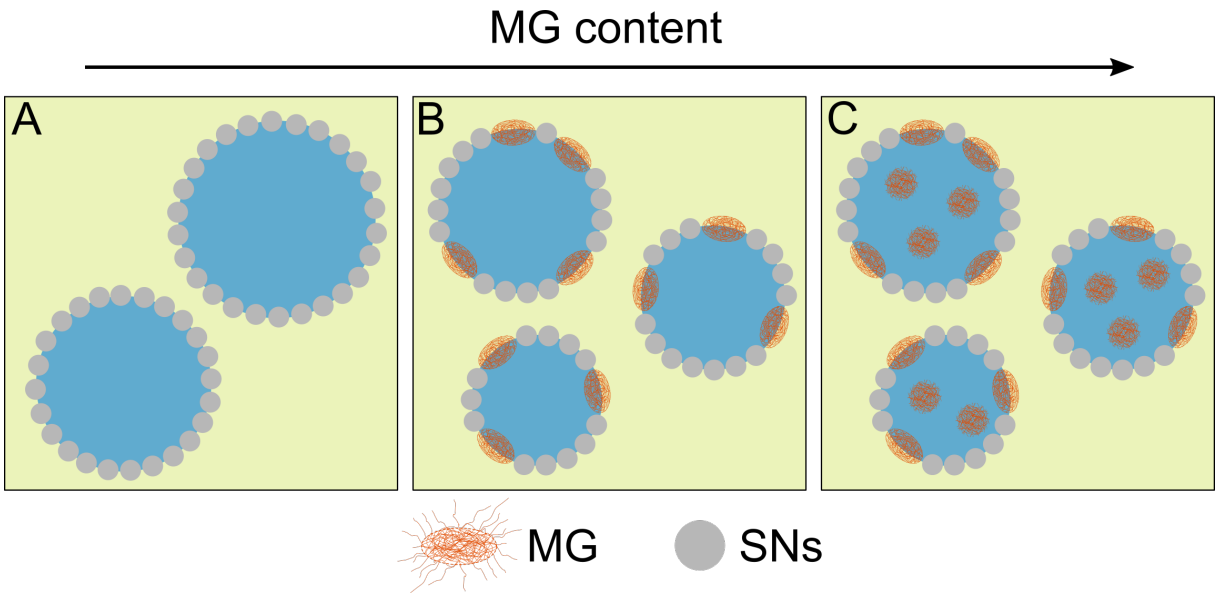

Figure 6.9: With increasing MG content more MG is incorporated at the interface until saturation of the interface. (A) The emulsions stabilized by solid particles only show a tight packing of SNs at the interface. (B) The SN coverage is reduced with increasing amount of present MGs. (C) This incorporation is limited to a minimum SN coverage of around 0.56. Introducing more MG into the system only results in more MG situated in the bulk phase of the water droplets.

Assuming all SNs adsorbing at the interface in presence and absence of the MGs enables the calculation of a SN packing parameter for both cases: This results for SN stabilized emulsions in s(SNs)=0.93±0.03 and is lowered for SN/MG stabilized emulsions to s(SNs/MGs)=0.56±0.02. This result was found independent from the total silica content and temperature (Figure 6.2) as well as from the MG stiffness (Figure 6.6). Only for the larger SNs a larger value for s was found (Figure 6.7). This means with respect to the model above that (a) the MGs stabilize additional interface or act as a "spacer" for the SNs (decrease from s(SNs)=0.93 to s(SNs/MGs)=0.56 for the smaller SNs) but at least $\sim$ 56 % (s(SNs/MGs)) of the droplets surface needs to be covered with SNs for stable emulsion formation.

This model is backed up by the observations in the cryo-SEM studies. The emulsion droplets stabilized by SNs only, in agreement with the previous chapter (Figure 5.5), posses a hexagonal close packed layer of SNs at the interface (Figure 6.3 A - C). This is reflected by the fits of the droplet size curves, which resulted in $s = 0.93 \pm 0.03 \approx s_{\mathrm{hcp}}$.

The images of the droplet interface of the SN/MG stabilized emulsions show the larger MGs forming a presumably hexagonal patterned hyper-structure (Figure 6.3 D - I). In between them the smaller SNs adsorb at the interface or in other words form 2D-shells around the MGs, resulting in the reduction of the SNs' packing parameter. The situation for one MG surrounded by some SNs is depicted in Figure 6.10.
It remains speculative which force results in the particles attaching to MG surface coming from the oil phase and why the charge of the particles is not preventing it. But, it may be explained by the following: It is typical for highly non-polar solvents (like the used one) that particles in it are less charged due to the high energy cost [58, 273]. In the present case, the low ζ-potential of the MGs in water should completely vanish in the oil phase. Also the mediocre ζ-potential of the SNs is presumably reduced there. Therefore, a random attachment at the surface of the MGs seems plausible. This attachment of the hydrophobic SNs onto the hydrophilic MGs may even be energetically favorable, since the energetically unfavorable MG/dodecene interface is replaced by a presumably preferable SN/dodecene interface.

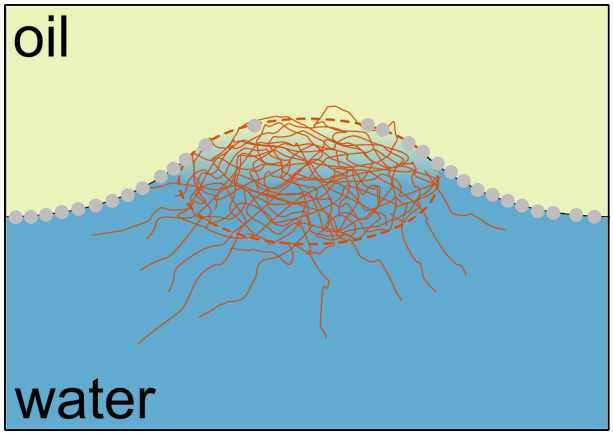

Figure 6.10: The solid and hydrophobic particles attach to the interface from the oil phase, while the hydrophilic MGs attach to the interface from the aqueous phase. Both, the SNs and the MGs adsorb at the interface. SNs are also able to adsorb onto the MGs.This results in protecting shell formation of SNs in the 2D layer around the MGs.

Besides the deviation in droplet size, the SN/MG stabilized emulsions differ from SN stabilized ones in their sedimentation behavior. Figure 6.8 D shows that for both emulsion types a nearly linear dependence of the sedimentation rate over the droplet diameter was found, but the slope in case of SN/MG stabilized emulsions is signif-

icantly steeper. Also the initial sedimentation speed $v_{d,i}$ is higher (Figure6.8 E). This means that SN/MG stabilized emulsions sediment faster relative to their droplet diameter. Since every outer emulsion parameter was held constant and no coalescence was observed, a reasonable explanation is that the droplets that contain MGs are a) more prone to particle bridging and/or b) less prone to surround themselves with the oil molecules, *i. e.*, the emulsions are enthalpically less stable against sedimentation and/or c) are easier to deform. a) Even if no undeniable proof of particle bridging was observed during microscopy this is a commonly observed effect for emulsions stabilized by comparably large and fluffy MGs [96] and would also explain the strong droplet cohesion in the emulsions prepared with MGs only at 8 °C. These bridged droplets may then act as larger "droplets", which themselves sediment faster due to their larger size. b) An additional explanation may be found in the enthalpy of the system. Considering the lower percentage of hydrophobic SNs and the vice versa higher amount of hydrophilic MGs at the interface for SN/MG stabilized emulsions, compared with the SN only stabilized ones, may lead to an overall lower hydrophobicity of the droplets. This leads to a lower affinity of the droplets to surround themselves with oil molecules and, as a result, to drop out of the oil phase faster. Pal [275] suggested in his work that the sedimentation/creaming drift velocity of the droplets is dependent on their contact angle, *i. e.*, their hydrophobicity, which may explain the observed behavior here. c) The influence of the deformability of droplets may also have an effect on the droplets sedimentation behavior. Since the droplets containing MG may be more elastic relative to their droplet size this could have an effect on their fluid mechanics. Faulde *et al.* [279] found this dependence for droplets in the millimeter scale, but the transfer of their models on droplets in the micrometer scale stays speculative.

6.4 Conclusion

Adding hydrophobic SNs to the MG-water-oil system enables the formation of w/o emulsions, which is not possible using MGs only. The droplet size of these SN/MG stabilized emulsions is significantly smaller than for SN only stabilized emulsions, but is governed exclusively by the absolute SN concentration for all investigated MG/SN ratios and MG stiffnesses. It was calculated that an area of ∼56% of the droplets surface is covered by SNs. This may be considered as the minimum coverage by hydrophobic material necessary for a stable w/o emulsion. The excess of MGs remains trapped in

the droplet bulk. Despite it was shown that the used PNIPAM MGs are temperature responsive in their size and charge, the preparation temperature had no influence on any measured emulsion property when investigating the systems after preparation at room temperature: Even if there was an effect of temperature during preparation, the system is reversible afterwards. The cryo-SEM studies of the emulsions revealed the structure formation at the interface: The SNs are located at the interface between the MGs in a very dense packing (presumably hcp) but also adsorbed on their surface in a very lose packing. The use of SNs to enable the stabilization of w/o emulsions with hydrophilic particles present is an easy, convenient and economic strategy to achieve the preferred formation of w/o type emulsions with hydrophilic particles. The new and detailed insights as well as the proposed models provide crucial information for the better understanding of any application where soft hydrophilic particles meet solid hydrophobic ones at the interface of w/o droplets, *e.g.*, in the PE assisted interfacial catalysis.

7 Conclusion and Outlook

7.1 Summary and Conclusion

This thesis aims for a better understanding and controlling of the structure of Pickering emulsions (PEs) for their application as reaction environment for interfacial catalysis and suggests an improved novel emulsion formulation approach. The strategy of this thesis resembles a bottom-up approach that ranges from the synthesis of PE stabilizing particles over the emulsion characterization towards stability and performance experiments.

The silica nanospheres (SNs) are prepared from a sol-gel process and their surface is hydrophobized by silanization. Their size is determined by TEM imaging and their density is calculated from the measured total dispersion density. With density and size, their potential coverage area at the interface, *i. e.*, their specific cross-section, is calculated. Their hydrophobicity is characterized by contact angle determination of a water drop deposited on a spin coated SN layer.

The microgel particles (MGs) are synthesized *via* precipitation polymerization with different amounts of cross-linker. Their size and temperature responsiveness is determined by DLS. The charge of both particle types, MGs and SNs, are determined by ζ-potential measurements.

The characterization of the PE stabilizing particles shows that the establishment of a well defined model system of particles was successful. The SNs are monodisperse and each batch differs from a second only in one of the most important properties, *i. e.*, size, charge and hydrophobicity. A set of SNs can be chosen so that these only differ in size while exhibiting the same hydrophobicity and charge. This is necessary to separate effects resulting from size from those resulting from hydrophobicity and charge. In addition, the measurements show that the density of the particles is essential to determine for the calculation of other important geometric values such as the specific

particle area and cross-section. Complementary to the solid particles, the MGs resemble well understood soft model particles, because they are prepared in a very common procedure from NIPAM and they are also characterized in detail.
These thoroughly studied particles are used for the stabilization of PEs to investigate the resulting PE structure. The structure of the PEs is examined by cryo-SEM studies, the emulsion type is evaluated by fluorescence microscopy and the droplet size is determined by image processing for different particle concentrations, phase compositions and at different temperatures. In addition, the sedimentation behavior of the PEs, the performance in the hydroformylation reaction as well as the subsequent membrane filtration are quantified. Most important, the covered area of the SNs is calculated by comparing the internal PE interface to the potential covered interface of the SNs. This way, a quantitative connection could be drawn between the nanoscopic particle properties and the microscopic emulsion structure. This includes not only the prediction of the resulting droplet size but also the quantification of the particle/oil and water/oil contact-area. Both, Cryo-SEM studies and SN coverage calculation confirm that the SNs show a hexagonal close packing at the droplet interface without additives, but also that the SN coverage is decreased when adding surface active catalyst Rh-SX or MGs. The addition of the catalyst to the system decreases the SN coverage parameter from $\sim$0.91 (hcp) to $\sim$0.69. The negatively charged catalyst occupies particle-free spots in between the SNs but is also present at the interface of positively charged particles but not at the interface of the negatively charged particles.
By normalizing the reaction yield on the respective area where the catalyst is present, the observed reaction yield is quantified relative to both area types (particle/oil or water/oil). It was found, that the reaction takes place equally efficient at the surface of the positively charged particles and in between the particles (irrespective of charge) relative to the respective surface area. Also particle size does not change the resulting conversion rate when the droplet size is kept constant. In summary, the experiments with the SN model systems show that the initial assumption that the reaction yield is exceptionally determined by the droplet size and with that by the magnitude of the interfacial area is insufficient and may only describe the problem on a superficial level. More accurately, in case of solid and not inter-penetrable particle stabilizers, the interfaces (water/oil or particle/oil interface) where the catalyst is present determines the reaction performance. A general conclusion for this and other reactions is, that the interaction of the catalyst with the interface and with the stabilizing particles as well as the resulting PE structure is essential to understand and further improve reaction

performance beyond trial and error.
In the next step, a system was proposed based on the gathered findings, that may improve the PE performance further. MGs at the interface of PEs have the ability to drag catalyst to the interface for a further increase of the catalyst-substrate contact, like demonstrated by Jiang *et al.* [129]. Unfortunately, hydrophilic MGs are not able to stabilize water in highly non-polar oil emulsion alone. Therefore, the synergistic stabilization of w/o emulsions by soft hydrophilic PNIPAM MGs and solid hydrophobic SNs was investigated. The combination of both particles was very successful and in any of the tested combinations w/o emulsions form with a higher interfacial area than those stabilized with SNs alone. For low amounts of added MGs, the droplet size decreases strongly but this effect saturates for larger amounts of added MGs so that the droplet size stays constant. The limit in droplet size of this saturation is dependent of the present amount of SNs. This indicates, that the SNs are responsible for the stabilization while the MGs act as a spacer between the particles. At least 56 % of the surface of the emulsion droplets is always occupied by the SNs even if the present amount of MGs is increased successively. The remaining MGs are probably trapped in the water phase of the droplets. Nonetheless, PEs stabilized by MGs and SNs simultaneously offer exceptional versatility with a large amount of tuning options and therefore represent an overall promising approach for future catalysis experiments. Ultimately, the responsiveness of MGs may also be extendable to the whole PE system.

7.2 Future Perspectives

Future perspectives of this work lay in the technical-chemical application as well as in an even better physical understanding of investigated PE systems.
From the technical-chemical point of view the future focus should lay on the application of the elaborated concepts and systems. First, the limits of the linear connection between applied particle surface area and reaction yield should be tested by testing the systems in a large variety of situations and compositions. Especially, the transfer of the gained knowledge and systems onto different catalysis processes with other substrates (than dodecene) and other catalysts should be targeted. A candidate for a catalytic reaction that may be improved with the gained knowledge is the epoxidation of alkenes with polyoxometalates (POMs) as a catalyst. This novel catalysis approach exhibits

enough similarity to the investigated hydroformylation reaction to compare and evaluate several aspects but is different enough to enable also the gain of new insights and further generalize the concepts: 1-Dodecene is a possible substrate and POMs are macro-molecular metal based catalysts. First proof of concept reactions were already carried out during this thesis and turned out very successful. Another promising catalytic reaction that could be carried out in the derived systems is the enzyme catalyzed transesterification by the enzyme *candida antarctica lipase*. Especially, the incorporation of the MGs should enable the protection of the enzyme during the reaction and this way mitigate its destruction in the rough reaction climate. This may advance the field of bio-catalysis significantly. Ultimately, the aim should be to establish the PE assisted catalysis in industry. Therefore, the systems need to be tested in a mini-plant up to industrial-scale as a step forward to finally commercialize it.

From the physical and material science point of view future research should focus on PEs stabilized by soft particles and PEs stabilized by two or more stabilizers. PEs stabilized by solid (nano-)spheres are vastly understood regarding their formation and structure. Open questions remain regarding PEs that are not in the state of *limited coalescence* and their rheology. However, the derivation of general conclusions is expected to be difficult. Far away from the state of *limited coalescence*, *i. e.*, with high particle concentrations and low energy input, the emulsion structure formation has a very individual and hysteretic dependence of the dispersion strategy. For instance, the understanding of emulsions in stirred tank reactors is essential for the application of PEs in industry. Unfortunately, the modeling is so far restricted to distinct dispersion strategies and struggles with the description of the flow field, the reactor dimensions and its scale up.

PEs stabilized by soft particles lack from fundamental understanding that exceed proof of concept approaches. Difficulties in finding generalizable models are the deformability and compressability of the soft particles at the interface. These particle properties prevent the prediction of the potentially covered interface solely from the properties of the particles in the bulk phase. Finding a connection between experiments on a Langmuir trough and the resulting emulsion properties may enable the finding of paths to predict the droplet sizes and structure of these PEs. Only the understanding of the most important influence factors of the stabilizing particles on the PE structure enables itself the modification or synthesis of tailored soft particles for various applications.

The investigation of PEs stabilized by two or more particle types is the most recent and the most promising field of research. In addition to the characterization of the

particle geometry and adsorption at the interface, the description of these PEs relies on the understanding of the particle interaction at the interface. Of course, this adds an additional dimension of complexity but the strategy to combine several particle systems with complementary properties enables outstanding opportunities for tailoring the PE properties. Therefore, the use of model particles that is presented in this thesis resembles a successful first step in the direction of easy to produce and perfectly application adapted PE systems. Nanoscopic parameters that are not tested yet are the MG size, hydrophobicity and the charge. Macroscopic properties are the influence of the oil-type and fraction. The understanding of those influence factors will enable the application of responsive MG/SN stabilized emulsions in various applications. More important, the gained knowledge and models should be tested on the validity for other soft/solid particle stabilized PEs. The proof of this would lift the understanding of PEs with multiple stabilizers to a new generalized level. Not only the w/o emulsion type may be enabled in more systems where it was inaccessible until now but also a broader understanding of PEs may enable their application in even more fields.

Bibliography

[1] Ramsden, W. Separation of solids in the surface-layers of solutions and 'suspensions' (observations on surface-membranes, bubbles, emulsions, and mechanical coagulation). *Royal Society* **1904**, *72*, 477–486.

[2] Pickering, S. U. Emulsions. *J. Chem. Soc., Trans.* **1907**, *91*, 2001–2021.

[3] Binks, B. P. Particles as surfactants—similarities and differences. *Current Opinion in Colloid & Interface Science* **2002**, *7*, 21–41.

[4] Binks, B. P., Ed. *Colloidal particles at liquid interfaces*; Cambridge University Press: Cambridge, 2006.

[5] Hunter, T. N.; Pugh, R. J.; Franks, G. V.; Jameson, G. J. The role of particles in stabilising foams and emulsions. *Advances in colloid and interface science* **2008**, *137*, 57–81.

[6] Gonzalez Ortiz, D.; Pochat-Bohatier, C.; Cambedouzou, J.; Bechelany, M.; Miele, P. Current Trends in Pickering Emulsions: Particle Morphology and Applications. *Engineering* **2020**, *6*, 468–482.

[7] Yang, Y.; Fang, Z.; Chen, X.; Zhang, W.; Xie, Y.; Chen, Y.; Liu, Z.; Yuan, W. An Overview of Pickering Emulsions: Solid-Particle Materials, Classification, Morphology, and Applications. *Frontiers in pharmacology* **2017**, *8*, 287.

[8] Harman, C. L.; Patel, M. A.; Guldin, S.; Davies, G.-L. Recent developments in Pickering emulsions for biomedical applications. *Current Opinion in Colloid & Interface Science* **2019**, *39*, 173–189.

[9] Linke, C.; Drusch, S. Pickering emulsions in foods - opportunities and limitations. *Critical reviews in food science and nutrition* **2018**, *58*, 1971–1985.

[10] Murray, B. S. Pickering emulsions for food and drinks. *Current Opinion in Food Science* **2019**, *27*, 57–63.

[11] Yan, X.; Ma, C.; Cui, F.; McClements, D. J.; Liu, X.; Liu, F. Protein-stabilized Pickering emulsions: Formation, stability, properties, and applications in foods. *Trends in Food Science & Technology* **2020**, *103*, 293–303.

[12] Niroula, A.; Gamot, T. D.; Ooi, C. W.; Dhital, S. Biomolecule-based pickering food emulsions: Intrinsic components of food matrix, recent trends and prospects. *Food Hydrocolloids* **2021**, *112*, 106303.

[13] Rodriguez, A. M. B.; Binks, B. P. Catalysis in Pickering emulsions. *Soft matter* **2020**, 10221–10243.

[14] Wiley, R. Limited coalescence of oil droplets in coarse oil-in-water emulsions. *Journal of Colloid Science* **1954**, *9*, 427–437.

[15] Binks, B. P.; Lumsdon, S. O. Pickering Emulsions Stabilized by Monodisperse Latex Particles: Effects of Particle Size. *Langmuir* **2001**, *17*, 4540–4547.

[16] Binks, B. P.; Lumsdon, S. O. Stability of oil-in-water emulsions stabilised by silica particles. *Physical Chemistry Chemical Physics* **1999**, *1*, 3007–3016.

[17] Binks, B. P.; Lumsdon, S. O. Catastrophic Phase Inversion of Water-in-Oil Emulsions Stabilized by Hydrophobic Silica. *Langmuir* **2000**, *16*, 2539–2547.

[18] Binks, B. P.; Lumsdon, S. O. Influence of Particle Wettability on the Type and Stability of Surfactant-Free Emulsions. *Langmuir* **2000**, *16*, 8622–8631.

[19] Griffith, C.; Daigle, H. Destabilizing Pickering emulsions using fumed silica particles with different wettabilities. *Journal of colloid and interface science* **2019**, *547*, 117–126.

[20] Arditty, S.; Schmitt, V.; Lequeux, F.; Leal-Calderon, F. Interfacial properties in solid-stabilized emulsions. *The European Physical Journal B* **2005**, *44*, 381–393.

[21] Wang, S.; He, Y.; Zou, Y. Study of Pickering emulsions stabilized by mixed particles of silica and calcite. *Particuology* **2010**, *8*, 390–393.

[22] Owoseni, O.; Zhang, Y.; Su, Y.; He, J.; McPherson, G. L.; Bose, A.; John, V. T. Tuning the Wettability of Halloysite Clay Nanotubes by Surface Carbonization for Optimal Emulsion Stabilization. *Langmuir* **2015**, *31*, 13700–13707.

[23] von Klitzing, R.; Stehl, D.; Pogrzeba, T.; Schomäcker, R.; Minullina, R.; Panchal, A.; Konnova, S.; Fakhrullin, R.; Koetz, J.; Möhwald, H.; Lvov, Y. Halloysites Stabilized Emulsions for Hydroformylation of Long Chain Olefins. *Advanced Materials Interfaces* **2017**, *4*, 1600435.

[24] Stehl, D.; Skale, T.; Hohl, L.; Lvov, Y.; Koetz, J.; Kraume, M.; Drews, A.; von Klitzing, R. Oil-in-Water Pickering Emulsions Stabilized by Halloysite Clay Nanotubes Toward Efficient Filterability. *ACS Applied Nano Materials* **2020**, *3*, 11743–11751.

[25] Zhou, J.; Qiao, X.; Binks, B. P.; Sun, K.; Bai, M.; Li, Y.; Liu, Y. Magnetic Pickering emulsions stabilized by Fe3O4 nanoparticles. *Langmuir : the ACS journal of surfaces and colloids* **2011**, *27*, 3308–3316.

[26] Schmidt, S.; Liu, T.; Rütten, S.; Phan, K.-H.; Möller, M.; Richtering, W. Influence of microgel architecture and oil polarity on stabilization of emulsions by stimuli-sensitive core-shell poly(N-isopropylacrylamide-co-methacrylic acid) microgels: Mickering versus Pickering behavior? *Langmuir : the ACS journal of surfaces and colloids* **2011**, *27*, 9801–9806.

[27] Wiese, S.; Spiess, A. C.; Richtering, W. Microgel-stabilized smart emulsions for biocatalysis. *Angewandte Chemie (International ed. in English)* **2013**, *52*, 576–579.

[28] Destribats, M.; Rouvet, M.; Gehin-Delval, C.; Schmitt, C.; Binks, B. P. Emulsions stabilised by whey protein microgel particles: towards food-grade Pickering emulsions. *Soft matter* **2014**, *10*, 6941–6954.

[29] Fernandez-Rodriguez, M. A.; Martín-Molina, A.; Maldonado-Valderrama, J. Microgels at interfaces, from mickering emulsions to flat interfaces and back. *Advances in colloid and interface science* **2021**, *288*, 102350.

[30] Ogunlaja, S. B.; Pal, R.; Sarikhani, K. Effects of starch nanoparticles on phase inversion of Pickering emulsions. *The Canadian Journal of Chemical Engineering* **2018**, *96*, 1089–1097.

[31] Tao, S.; Jiang, H.; Wang, R.; Yang, C.; Li, Y.; Ngai, T. Ultra-stable Pickering emulsion stabilized by a natural particle bilayer. *Chemical communications (Cambridge, England)* **2020**, *56*, 14011–14014.

[32] Tao, S.; Jiang, H.; Gong, S.; Yin, S.; Li, Y.; Ngai, T. Pickering Emulsions Simultaneously Stabilized by Starch Nanocrystals and Zein Nanoparticles: Fabrication, Characterization, and Application. *Langmuir : the ACS journal of surfaces and colloids* **2021**, 8577–8584.

[33] Cheng, H.; Zhang, H.; Di Li,; Duan, H.; Liang, L. Impact of oil type on the location, partition and chemical stability of resveratrol in oil-in-water emulsions stabilized by whey protein isolate plus gum Arabic. *Food Hydrocolloids* **2020**, *109*, 106119.

[34] Röllig, R.; Plikat, C.; Ansorge-Schumacher, M. B. Efficient and Selective Carboligation with Whole–Cell Biocatalysts in Pickering Emulsion. *Angewandte Chemie* **2019**, *131*, 13094–13097.

[35] Firoozmand, H.; Rousseau, D. Microbial cells as colloidal particles: Pickering oil-in-water emulsions stabilized by bacteria and yeast. *Food Research International* **2016**, *81*, 66–73.

[36] Stock, S.; Kempin, M.; Hohl, L.; Petzold, M.; Hecht, K.; von Klitzing, R.; Drews, A. In *Integrated Chemical Processes in Liquid Multiphase Systems*; Kraume, M., Enders, S., Drews, A., Schomäcker, R., Engell, S., Sundmacher, K., Eds.; DE GRUYTER, 2022; pp 304–337.

[37] Skale, T.; Stehl, D.; Hohl, L.; Kraume, M.; von Klitzing, R.; Drews, A. Tuning Pickering Emulsions for Optimal Reaction and Filtration Conditions. *Chemie Ingenieur Technik* **2016**, *88*, 1827–1832.

[38] Heyse, A.; Plikat, C.; Ansorge-Schumacher, M.; Drews, A. Continuous two-phase biocatalysis using water-in-oil Pickering emulsions in a membrane reactor: Evaluation of different nanoparticles. *Catalysis Today* **2019**, *331*, 60–67.

[39] Heyse, A. Filterability and rheological behavior of lipase containing water-in-oil Pickering emulsions stabilized with silica particles for the application in continuous biphasic biocatalysis in a membrane reactor. Ph.D. thesis, TU Berlin, 2019.

[40] Kempin, M. V.; Stock, S.; von Klitzing, R.; Kraume, M.; Drews, A. Influence of particle type and concentration on the ultrafiltration behavior of nanoparticle stabilized Pickering emulsions and suspensions. *Separation and Purification Technology* **2020**, *252*, 117457.

[41] Kempin, M. V.; Schroeder, H.; Hohl, L.; Kraume, M.; Drews, A. Modeling of water-in-oil Pickering emulsion nanofiltration - Influence of temperature. *Journal of Membrane Science* **2021**, *636*, 119547.

[42] Evans, D. F.; Wennerström, H. *The colloidal domain: Where physics, chemistry, biology, and technology meet*, 2nd ed.; Advances in interfacial engineering series; Wiley-VCH: New York, NY, 1999.

[43] Israelachvili,; N, J. *Intermolecular and Surface Forces*, third edition ed.; 2011.

[44] Tadros, T. F., Ed. *Emulsion formation and stability: Selection of some papers from the Fifth World Congress on Emulsions that was held in Lyon, in October 2010*; Wiley-VCH: Weinheim, 2013.

[45] Arthur T. Hubbard,, Ed. *Encyclopedia of surface and colloid science*; Dekker: New York, 2002; Vol. 3.

[46] Sperling, L. H. *Introduction to physical polymer science*, 4th ed.; Wiley-Interscience: Hoboken, NJ, 2006.

[47] Melin, T.; Rautenbach, R. *Membranverfahren: Grundlagen der Modul- und Anlagenauslegung ; mit 76 Tabellen*, 3rd ed.; VDI-Bücher; Springer: Berlin, 2007.

[48] Albert, C.; Beladjine, M.; Tsapis, N.; Fattal, E.; Agnely, F.; Huang, N. Pickering emulsions: Preparation processes, key parameters governing their properties and potential for pharmaceutical applications. *Journal of controlled release : official journal of the Controlled Release Society* **2019**, *309*, 302–332.

[49] Zhai, X.; Efrima, S. Chemical and Physical Aspects of Macroemulsions Stabilized by Interfacial Colloids. *The Journal of Physical Chemistry* **1996**, *100*, 11019–11028.

[50] Arditty, S.; Whitby, C. P.; Binks, B. P.; Schmitt, V.; Leal-Calderon, F. Some general features of limited coalescence in solid-stabilized emulsions. *The European physical journal. E, Soft matter* **2003**, *11*, 273–281.

[51] Maa, Y.-F.; Hsu, C. Liquid-liquid emulsification by rotor/stator homogenization. *Journal of Controlled Release* **1996**, *38*, 219–228.

[52] Kempin, M. V.; Kraume, M.; Drews, A. W/O Pickering emulsion preparation using a batch rotor-stator mixer – influence on rheology, drop size distribution and filtration behavior. *Journal of colloid and interface science* **2020**, 135–149.

[53] Kempin, M. V.; Drews, A. What Governs Pickering Emulsion Properties During Preparation via Batch Rotor–Stator Homogenizers? *Chemie Ingenieur Technik* **2021**, *93*, 311–317.

[54] Canselier, J. P.; Delmas, H.; Wilhelm, A. M.; Abismaïl, B. Ultrasound Emulsification—An Overview. *Journal of Dispersion Science and Technology* **2002**, *23*, 333–349.

[55] Coulaloglou, C. A.; Tavlarides, L. L. Description of interaction processes in agitated liquid-liquid dispersions. *Chemical Engineering Science* **1977**, *32*, 1289–1297.

[56] Nallamilli, T.; Mani, E.; Basavaraj, M. G. A model for the prediction of droplet size in Pickering emulsions stabilized by oppositely charged particles. *Langmuir* **2014**, *30*, 9336–9345.

[57] Nallamilli, T.; Binks, B. P.; Mani, E.; Basavaraj, M. G. Stabilization of Pickering Emulsions with Oppositely Charged Latex Particles: Influence of Various Parameters and Particle Arrangement around Droplets. *Langmuir* **2015**, *31*, 11200–11208.

[58] Stock, S.; Schlander, A.; Kempin, M.; Geisler, R.; Stehl, D.; Spanheimer, K.; Hondow, N.; Micklethwaite, S.; Weber, A.; Schomäcker, R.; Drews, A.; Gallei, M.; von Klitzing, R. The quantitative impact of fluid vs. solid interfaces on the catalytic performance of pickering emulsions. *Physical chemistry chemical physics : PCCP* **2021**, *23*, 2355–2367.

[59] Binks, B. P.; Philip, J.; Rodrigues, J. A. Inversion of silica-stabilized emulsions induced by particle concentration. *Langmuir* **2005**, *21*, 3296–3302.

[60] Binks, B. P.; Isa, L.; Tyowua, A. T. Direct measurement of contact angles of silica particles in relation to double inversion of pickering emulsions. *Langmuir* **2013**, *29*, 4923–4927.

[61] Bancroft, W. D. The Theory of Emulsification, V. *The Journal of Physical Chemistry* **1913**, *17*, 501–519.

[62] Wu, J.; Ma, G.-H. Recent Studies of Pickering Emulsions: Particles Make the Difference. *Small (Weinheim an der Bergstrasse, Germany)* **2016**, *12*, 4633–4648.

[63] Binks, B. P.; Liu, W.; Rodrigues, J. A. Novel stabilization of emulsions via the heteroaggregation of nanoparticles. *Langmuir* **2008**, *24*, 4443–4446.

[64] Nan, F.; Wu, J.; Qi, F.; Liu, Y.; Ngai, T.; Ma, G. Uniform chitosan-coated alginate particles as emulsifiers for preparation of stable Pickering emulsions with stimulus dependence. *Colloids and Surfaces A: Physicochemical and Engineering Aspects* **2014**, *456*, 246–252.

[65] Qi, F.; Wu, J.; Sun, G.; Nan, F.; Ngai, T.; Ma, G. Systematic studies of Pickering emulsions stabilized by uniform-sized PLGA particles: preparation and stabilization mechanism. *Journal of materials chemistry. B* **2014**, *2*, 7605–7611.

[66] Pushpam, S. D. C.; Basavaraj, M. G.; Mani, E. Pickering emulsions stabilized by oppositely charged colloids: stability and pattern formation. *Physical Review E* **2015**, 5.

[67] Madivala, B.; Vandebril, S.; Fransaer, J.; Vermant, J. Exploiting particle shape in solid stabilized emulsions. *Soft matter* **2009**, *5*, 1717.

[68] Madivala, B.; Fransaer, J.; Vermant, J. Self-assembly and rheology of ellipsoidal particles at interfaces. *Langmuir : the ACS journal of surfaces and colloids* **2009**, *25*, 2718–2728.

[69] Fujii, S.; Okada, M.; Furuzono, T. Hydroxyapatite nanoparticles as stimulus-responsive particulate emulsifiers and building block for porous materials. *Journal of colloid and interface science* **2007**, *315*, 287–296.

[70] Wei, Z.; Wang, C.; Liu, H.; Zou, S.; Tong, Z. Halloysite nanotubes as particulate emulsifier: Preparation of biocompatible drug–carrying PLGA microspheres based on pickering emulsion. *Journal of Applied Polymer Science* **2012**, *125*.

[71] Stehl, D.; Hohl, L.; Schmidt, M.; Hübner, J.; Lehmann, M.; Kraume, M.; Schomäcker, R.; von Klitzing, R. Characteristics of Stable Pickering Emulsions under Process Conditions. *Chemie Ingenieur Technik* **2016**, *88*, 1806–1814.

[72] Stehl, D.; Milojević, N.; Stock, S.; Schomäcker, R.; von Klitzing, R. Synergistic Effects of a Rhodium Catalyst on Particle-Stabilized Pickering Emulsions for the Hydroformylation of a Long-Chain Olefin. *Industrial & Engineering Chemistry Research* **2019**, *58*, 2524–2536.

[73] de Folter, J. W. J.; Hutter, E. M.; Castillo, S. I. R.; Klop, K. E.; Philipse, A. P.; Kegel, W. K. Particle shape anisotropy in pickering emulsions: cubes and peanuts. *Langmuir* **2014**, *30*, 955–964.

[74] Thompson, K. L.; Fielding, L. A.; Mykhaylyk, O. O.; Lane, J. A.; Derry, M. J.; Armes, S. P. Vermicious thermo-responsive Pickering emulsifiers. *Chemical science* **2015**, *6*, 4207–4214.

[75] Yu, Y.-H.; Chen, Y.-P.; Zeng, M.; Cheng, Z. Microwave-assisted rapid synthesis of hexagonal α-zirconium phosphate nanodisks as a Pickering emulsion stabilizer. *Materials Letters* **2016**, *163*, 158–161.

[76] Yamagami, T.; Kitayama, Y.; Okubo, M. Preparation of stimuli-responsive "mushroom-like" janus polymer particles as particulate surfactant by site-selective surface-initiated AGET ATRP in aqueous dispersed systems. *Langmuir : the ACS journal of surfaces and colloids* **2014**, *30*, 7823–7832.

[77] Ridel, L.; Bolzinger, M.-A.; Gilon-Delepine, N.; Dugas, P.-Y.; Chevalier, Y. Pickering emulsions stabilized by charged nanoparticles. *Soft matter* **2016**, *12*, 7564–7576.

[78] Mehrabian, H.; Snoeijer, J. H.; Harting, J. Desorption energy of soft particles from a fluid interface. *Soft matter* **2020**, *16*, 8655–8666.

[79] Stock, S.; von Klitzing, R. Microgels at droplet interfaces of water-in-oil emulsions—challenges and progress. *Current Opinion in Colloid & Interface Science* **2022**, *58*, 101561.

[80] Reculusa, S.; Ravaine, S. Colloidal photonic crystals obtained by the Langmuir–Blodgett technique. *Applied Surface Science* **2005**, *246*, 409–414.

[81] Lotito, V.; Zambelli, T. Pattern Formation in Binary Colloidal Assemblies: Hidden Symmetries in a Kaleidoscope of Structures. *Langmuir : the ACS journal of surfaces and colloids* **2018**, *34*, 7827–7843.

[82] Hummel, M. E. J.; Stelling, C.; Kopera, B. A. F.; Nutz, F. A.; Karg, M.; Retsch, M.; Förster, S. Ordered Particle Arrays via a Langmuir Transfer Process: Access to Any Two-Dimensional Bravais Lattice. *Langmuir : the ACS journal of surfaces and colloids* **2019**, *35*, 973–979.

[83] Razavi, S.; Cao, K. D.; Lin, B.; Lee, K. Y. C.; Tu, R. S.; Kretzschmar, I. Collapse of Particle-Laden Interfaces under Compression: Buckling vs Particle Expulsion. *Langmuir : the ACS journal of surfaces and colloids* **2015**, *31*, 7764–7775.

[84] Jeelani, P. G.; Mulay, P.; Venkat, R.; Ramalingam, C. Multifaceted Application of Silica Nanoparticles. A Review. *Silicon* **2020**, *12*, 1337–1354.

[85] Akhter, F.; Rao, A. A.; Abbasi, M. N.; Wahocho, S. A.; Mallah, M. A.; Anees-ur Rehman, H.; Chandio, Z. A. A Comprehensive Review of Synthesis, Applications and Future Prospects for Silica Nanoparticles (SNPs). *Silicon* **2022**,

[86] Barthel, H.; Rsch, L.; Weis, J. In *Organosilicon chemistry II*; Weis, J., Auner, N., Eds.; VCH: Weinheim Federal Republic of Germany and New York, 1996; pp 761–778.

[87] Stöber, W.; Fink, A.; Bohn, E. Controlled growth of monodisperse silica spheres in the micron size range. *Journal of colloid and interface science* **1968**, *26*, 62–69.

[88] van Der Voort, P.; Vansant, E. F. Silylation of the Silica Surface A Review. *Journal of Liquid Chromatography & Related Technologies* **1996**, *19*, 2723–2752.

[89] Zang, D. Y.; Rio, E.; Delon, G.; Langevin, D.; Wei, B.; Binks, B. P. Influence of the contact angle of silica nanoparticles at the air–water interface on the mechanical properties of the layers composed of these particles. *Molecular Physics* **2011**, *109*, 1057–1066.

[90] ISO/TC 24/SC 4, Representation of results of particle size analysis — Part 2: Calculation of average particle sizes/diameters and moments from particle size distributions. 2014.

[91] Everett, D. H. Manual of Symbols and Terminology for Physicochemical Quantities and Units, Appendix II: Definitions, Terminology and Symbols in Colloid and Surface Chemistry. *Pure and Applied Chemistry* **1972**, *31*, 577–638.

[92] Henschke, M. Determination of a coalescence parameter from batch-settling experiments. *Chemical Engineering Journal* **2002**, *85*, 369–378.

[93] Sacanna, S.; Kegel, W. K.; Philipse, A. P. Thermodynamically stable pickering emulsions. *Physical review letters* **2007**, *98*, 158301.

[94] Huang, Z.; Su, M.; Yang, Q.; Li, Z.; Chen, S.; Li, Y.; Zhou, X.; Li, F.; Song, Y. A general patterning approach by manipulating the evolution of two-dimensional liquid foams. *Nature communications* **2017**, *8*, 14110.

[95] Whitesides, T. H.; Ross, D. S. Experimental and Theoretical Analysis of the Limited Coalescence Process: Stepwise Limited Coalescence. *Journal of colloid and interface science* **1995**, *169*, 48–59.

[96] Destribats, M.; Eyharts, M.; Lapeyre, V.; Sellier, E.; Varga, I.; Ravaine, V.; Schmitt, V. Impact of pNIPAM microgel size on its ability to stabilize Pickering emulsions. *Langmuir* **2014**, *30*, 1768–1777.

[97] Kempin, M. V.; Kraume, M.; Drews, A. W/O Pickering emulsion preparation using a batch rotor-stator mixer - Influence on rheology, drop size distribution and filtration behavior. *Journal of colloid and interface science* **2020**, *573*, 135–149.

[98] Destribats, M.; Lapeyre, V.; Wolfs, M.; Sellier, E.; Leal-Calderon, F.; Ravaine, V.; Schmitt, V. Soft microgels as Pickering emulsion stabilisers: role of particle deformability. *Soft matter* **2011**, *7*, 7689.

[99] Schmitt, V.; Ravaine, V. Surface compaction versus stretching in Pickering emulsions stabilised by microgels. *Current Opinion in Colloid & Interface Science* **2013**, *18*, 532–541.

[100] Tatry, M.-C.; Galanopoulo, P.; Waldmann, L.; Lapeyre, V.; Garrigue, P.; Schmitt, V.; Ravaine, V. Pickering emulsions stabilized by thermoresponsive oligo(ethylene glycol)-based microgels: Effect of temperature-sensitivity on emulsion stability. *Journal of colloid and interface science* **2020**, *589*, 96–109.

[101] Richtering, W. Responsive emulsions stabilized by stimuli-sensitive microgels: emulsions with special non-Pickering properties. *Langmuir : the ACS journal of surfaces and colloids* **2012**, *28*, 17218–17229.

[102] Li, Z.; Harbottle, D.; Pensini, E.; Ngai, T.; Richtering, W.; Xu, Z. Fundamental Study of Emulsions Stabilized by Soft and Rigid Particles. *Langmuir : the ACS journal of surfaces and colloids* **2015**, *31*, 6282–6288.

[103] Kwok, M.-h.; Ngai, T. Emulsions stabilized by pH-responsive PNIPAM-based microgels: Effect of spatial distribution of functional carboxylic groups on the emulsion stability. *Journal of the Taiwan Institute of Chemical Engineers* **2018**, *92*, 97–105.

[104] Navarro Arrebola, I.; Billon, L.; Aguirre, G. Microgels self-assembly at liquid/liquid interface as stabilizers of emulsion: Past, present & future. *Advances in colloid and interface science* **2021**, *287*, 102333.

[105] Zembyla, M.; Lazidis, A.; Murray, B. S.; Sarkar, A. Stability of water-in-oil emulsions co-stabilized by polyphenol crystal-protein complexes as a function of shear rate and temperature. *Journal of Food Engineering* **2020**, *281*, 109991.

[106] Pelton, R. H.; Chibante, P. Preparation of aqueous latices with N-isopropylacrylamide. *Colloids and Surfaces* **1986**, *20*, 247–256.

[107] Pelton, R. Temperature-sensitive aqueous microgels. *Advances in colloid and interface science* **2000**, *85*, 1–33.

[108] Pelton, R. Poly(N-isopropylacrylamide) (PNIPAM) is never hydrophobic. *Journal of colloid and interface science* **2010**, *348*, 673–674.

[109] Pinaud, F.; Geisel, K.; Massé, P.; Catargi, B.; Isa, L.; Richtering, W.; Ravaine, V.; Schmitt, V. Adsorption of microgels at an oil-water interface: correlation between packing and 2D elasticity. *Soft matter* **2014**, *10*, 6963–6974.

[110] Li, Z.; Richtering, W.; Ngai, T. Poly(N-isopropylacrylamide) microgels at the oil-water interface: temperature effect. *Soft matter* **2014**, *10*, 6182–6191.

[111] Style, R. W.; Isa, L.; Dufresne, E. R. Adsorption of soft particles at fluid interfaces. *Soft matter* **2015**, *11*, 7412–7419.

[112] Rey, M.; Hou, X.; Tang, J. S. J.; Vogel, N. Interfacial arrangement and phase transitions of PNiPAm microgels with different crosslinking densities. *Soft matter* **2017**, *13*, 8717–8727.

[113] Kwok, M.-h.; Ngai, T. Comparing the Relative Interfacial Affinity of Soft Colloids With Different Crosslinking Densities in Pickering Emulsions. *Frontiers in chemistry* **2018**, *6*, 148.

[114] Kwok, M.-h.; Sun, G.; Ngai, T. Microgel Particles at Interfaces: Phenomena, Principles, and Opportunities in Food Sciences. *Langmuir* **2019**, *35*, 4205–4217.

[115] Rey, M.; Fernandez-Rodriguez, M. A.; Karg, M.; Isa, L.; Vogel, N. Poly-N-isopropylacrylamide Nanogels and Microgels at Fluid Interfaces. *Accounts of chemical research* **2020**, *53*, 414–424.

[116] Zhang, J.; Pelton, R. Poly(N -isopropylacrylamide) Microgels at the Air−Water Interface. *Langmuir* **1999**, *15*, 8032–8036.

[117] Li, Z.; Geisel, K.; Richtering, W.; Ngai, T. Poly(N-isopropylacrylamide) microgels at the oil–water interface: adsorption kinetics. *Soft matter* **2013**, *9*, 9939.

[118] Wu, Y.; Wiese, S.; Balaceanu, A.; Richtering, W.; Pich, A. Behavior of temperature-responsive copolymer microgels at the oil/water interface. *Langmuir : the ACS journal of surfaces and colloids* **2014**, *30*, 7660–7669.

[119] Tatry, M. C.; Laurichesse, E.; Perro, A.; Ravaine, V.; Schmitt, V. Kinetics of spontaneous microgels adsorption and stabilization of emulsions produced using microfluidics. *Journal of colloid and interface science* **2019**, *548*, 1–11.

[120] Karg, M.; Pich, A.; Hellweg, T.; Hoare, T.; Lyon, L. A.; Crassous, J. J.; Suzuki, D.; Gumerov, R. A.; Schneider, S.; Potemkin, I. I.; Richtering, W. Nanogels and Microgels: From Model Colloids to Applications, Recent Developments, and Future Trends. *Langmuir : the ACS journal of surfaces and colloids* **2019**, *35*, 6231–6255.

[121] Scotti, A.; Schulte, M. F.; Lopez, C. G.; Crassous, J. J.; Bochenek, S.; Richtering, W. How Softness Matters in Soft Nanogels and Nanogel Assemblies. *Chemical reviews* **2022**,

[122] Picard, C.; Garrigue, P.; Tatry, M.-C.; Lapeyre, V.; Ravaine, S.; Schmitt, V.; Ravaine, V. Organization of Microgels at the Air-Water Interface under Compression: Role of Electrostatics and Cross-Linking Density. *Langmuir : the ACS journal of surfaces and colloids* **2017**, *33*, 7968–7981.

[123] Harrer, J.; Ciarella, S.; Rey, M.; Löwen, H.; Janssen, L. M. C.; Vogel, N. Collapse-induced phase transitions in binary interfacial microgel monolayers. *Soft matter* **2021**, *17*, 4504–4516.

[124] Destribats, M.; Lapeyre, V.; Sellier, E.; Leal-Calderon, F.; Schmitt, V.; Ravaine, V. Water-in-oil emulsions stabilized by water-dispersible poly(N-isopropylacrylamide) microgels: understanding anti-Finkle behavior. *Langmuir* **2011**, *27*, 14096–14107.

[125] Schneider, C. Interaktion zwischen weichen und harten Nanopartikeln an der Wasser-Luft Grenzfläche bei steigendem Lateraldruck. bachelor thesis, TU Darmstadt, Darmstadt, 27.07.2022.

[126] Brugger, B.; Rosen, B. A.; Richtering, W. Microgels as stimuli-responsive stabilizers for emulsions. *Langmuir* **2008**, *24*, 12202–12208.

[127] Lefroy, K. S.; Murray, B. S.; Ries, M. E.; Curwen, T. D. A natural, cellulose-based microgel for water-in-oil emulsions. *Food Hydrocolloids* **2021**, *113*, 106408.

[128] Zhang, T.; Ngai, T. One-Step Formation of Double Emulsions Stabilized by PNIPAM-based Microgels: The Role of Co-monomer. *Langmuir : the ACS journal of surfaces and colloids* **2021**, *37*, 1045–1053.

[129] Jiang, H.; Liu, L.; Li, Y.; Yin, S.; Ngai, T. Inverse Pickering Emulsion Stabilized by Binary Particles with Contrasting Characteristics and Functionality for Interfacial Biocatalysis. *ACS applied materials & interfaces* **2020**, *12*, 4989–4997.

[130] Watanabe, T.; Takizawa, M.; Jiang, H.; Ngai, T.; Suzuki, D. Hydrophobized nanocomposite hydrogel microspheres as particulate stabilizers for water-in-oil emulsions. *Chemical communications (Cambridge, England)* **2019**, *55*, 5990–5993.

[131] Zembyla, M.; Lazidis, A.; Murray, B. S.; Sarkar, A. Water-in-Oil Pickering Emulsions Stabilized by Synergistic Particle-Particle Interactions. *Langmuir* **2019**, *35*, 13078–13089.

[132] Stock, S.; Jakob, F.; Röhl, S.; Gräff, K.; Kühnhammer, M.; Hondow, N. S.; Micklethwaite, S.; Kraume, M.; von Klitzing, R. Exploring Water in Oil Emulsions simultaneously stabilized by solid hydrophobic Silica Nanospheres and hydrophilic soft PNIPAM Microgel. *Soft matter* **2021**, *17*, 8258–8268.

[133] Ellis, A. L.; Mills, T. B.; Norton, I. T.; Norton-Welch, A. B. The hydrophobic modification of kappa carrageenan microgel particles for the stabilisation of foams. *Journal of colloid and interface science* **2019**, *538*, 165–173.

[134] Haney, B.; Werner, J. G.; Weitz, D. A.; Ramakrishnan, S. Stimuli responsive Janus microgels with convertible hydrophilicity for controlled emulsion destabilization. *Soft matter* **2020**, *16*, 3613–3620.

[135] Bonham, J. A.; Faers, M. A.; van Duijneveldt, J. S. Non-aqueous microgel particles: synthesis, properties and applications. *Soft matter* **2014**, *10*, 9384–9398.

[136] Zembyla, M.; Murray, B. S.; Sarkar, A. Water-in-oil emulsions stabilized by surfactants, biopolymers and/or particles: a review. *Trends in Food Science & Technology* **2020**, *104*, 49–59.

[137] Zembyla, M.; Murray, B. S.; Radford, S. J.; Sarkar, A. Water-in-oil Pickering emulsions stabilized by an interfacial complex of water-insoluble polyphenol crystals and protein. *Journal of colloid and interface science* **2019**, *548*, 88–99.

[138] Zhang, S.; Murray, B. S.; Suriyachay, N.; Holmes, M.; Ettelaie, R.; Sarkar, A. Synergistic Interactions of Plant Protein Microgels and Cellulose Nanocrystals at the Interface and Their Inhibition of the Gastric Digestion of Pickering Emulsions. *Langmuir : the ACS journal of surfaces and colloids* **2021**, *37*, 827–840.

[139] Chorkendorff, I.; Niemantsverdriet, J. W. *Concepts of modern catalysis and kinetics*; Wiley-VCH: Weinheim, 2003.

[140] Pera-Titus, M.; Leclercq, L.; Clacens, J.-M.; de Campo, F.; Nardello-Rataj, V. Pickering interfacial catalysis for biphasic systems: from emulsion design to green reactions. *Angewandte Chemie (International ed. in English)* **2015**, *54*, 2006–2021.

[141] Kraume, M., Enders, S., Drews, A., Schomäcker, R., Engell, S., Sundmacher, K., Eds. *Integrated Chemical Processes in Liquid Multiphase Systems: From Chemical Reaction To Process Design and Operation*, 1st ed.; DE GRUYTER, 2022.

[142] Chang, F.; Vis, C. M.; Ciptonugroho, W.; Bruijnincx, P. C. A. Recent developments in catalysis with Pickering Emulsions. *Green Chemistry* **2021**, 2575–2594.

[143] Ni, L.; Yu, C.; Wei, Q.; Liu, D.; Qiu, J. Pickering Emulsion Catalysis: Interfacial Chemistry, Catalyst Design, Challenges, and Perspectives. *Angewandte Chemie* **2022**,

[144] Wu, C.; Bai, S.; Ansorge-Schumacher, M. B.; Wang, D. Nanoparticle cages for enzyme catalysis in organic media. *Advanced materials (Deerfield Beach, Fla.)* **2011**, *23*, 5694–5699.

[145] Wei, L.; Zhang, M.; Zhang, X.; Xin, H.; Yang, H. Pickering Emulsion as an Efficient Platform for Enzymatic Reactions without Stirring. *ACS Sustainable Chemistry & Engineering* **2016**, *4*, 6838–6843.

[146] Zhang, M.; Wei, L.; Chen, H.; Du, Z.; Binks, B. P.; Yang, H. Compartmentalized Droplets for Continuous Flow Liquid-Liquid Interface Catalysis. *Journal of the American Chemical Society* **2016**, *138*, 10173–10183.

[147] Zhang, M.; Ettelaie, R.; Yan, T.; Zhang, S.; Cheng, F.; Binks, B. P.; Yang, H. Ionic Liquid Droplet Microreactor for Catalysis Reactions Not at Equilibrium. *Journal of the American Chemical Society* **2017**, *139*, 17387–17396.

[148] Qu, Y.; Huang, R.; Qi, W.; Qu, Q.; Su, R.; He, Z. Structural Insight into Stabilization of Pickering Emulsions with Fe 3 O 4 @SiO 2 Nanoparticles for Enzyme

Catalysis in Organic Media. *Particle & Particle Systems Characterization* **2017**, *34*, 1700117.

[149] Jiang, H.; Li, Y.; Hong, L.; Ngai, T. Submicron Inverse Pickering Emulsions for Highly Efficient and Recyclable Enzymatic Catalysis. *Chemistry, an Asian journal* **2018**, *13*, 3533–3539.

[150] Yu, S.; Zhang, D.; Jiang, J.; Cui, Z.; Xia, W.; Binks, B. P.; Yang, H. Biphasic biocatalysis using a CO 2 -switchable Pickering emulsion. *Green Chemistry* **2019**, *136*, 7498.

[151] Heyse, A.; Kraume, M.; Drews, A. The impact of lipases on the rheological behavior of colloidal silica nanoparticle stabilized Pickering emulsions for biocatalytical applications. *Colloids and surfaces. B, Biointerfaces* **2020**, *185*, 110580.

[152] Crossley, S.; Faria, J.; Shen, M.; Resasco, D. E. Solid nanoparticles that catalyze biofuel upgrade reactions at the water/oil interface. *Science (New York, N.Y.)* **2010**, *327*, 68–72.

[153] Yang, X.; Liang, Y.; Cheng, Y.; Song, W.; Wang, X.; Wang, Z.; Qiu, J. Hydrodeoxygenation of vanillin over carbon nanotube-supported Ru catalysts assembled at the interfaces of emulsion droplets. *Catalysis Communications* **2014**, *47*, 28–31.

[154] Han, Z.; Peng, L.; Li, Q.; Hao, Y. An Interfacially Active Pd/C Catalyst Enhanced Hydrogenation of Aromatic Compounds in Pickering Emulsion. *Catalysis Letters* **2017**, *147*, 1615–1621.

[155] Hao, Y.; Liu, Y.; Yang, R.; Zhang, X.; Liu, J.; Yang, H. A pH-responsive TiO2-based Pickering emulsion system for in situ catalyst recycling. *Chinese Chemical Letters* **2018**, *29*, 778–782.

[156] Han, C.; Meng, P.; Waclawik, E. R.; Zhang, C.; Li, X.-H.; Yang, H.; Antonietti, M.; Xu, J. Palladium/Graphitic Carbon Nitride (g-C 3 N 4) Stabilized Emulsion Microreactor as a Store for Hydrogen from Ammonia Borane for Use in Alkene Hydrogenation. *Angewandte Chemie* **2018**, *130*, 15073–15077.

[157] Xue, B.; Xu, T.; Li, D.; Xu, J.; Li, Y.; Wang, F.; Zhu, J. A Pickering emulsion of a bifunctional interface prepared from Pd nanoparticles supported on silicane-modified graphene oxide: an efficient catalyst for water-mediated catalytic hydrogenation. *Catalysis Science & Technology* **2020**, *10*, 1096–1105.

[158] Chen, H.; Zou, H.; Hao, Y.; Yang, H. Flow Pickering Emulsion Interfaces Enhance Catalysis Efficiency and Selectivity for Cyclization of Citronellal. *ChemSusChem* **2017**, *10*, 1989–1995.

[159] Peng, F.; Xu, J.; Zeng, X.; Feng, G.; Bao, H. Metal–Decorated Pickering Emulsion for Continuous Flow Catalysis. *Particle & Particle Systems Characterization* **2020**, *37*, 1900382.

[160] Tang, X.; Hou, Y.; Meng, Q. B.; Zhang, G.; Liang, F.; Song, X.-M. Heteropoly acids-functionalized Janus particles as catalytic emulsifier for heterogeneous acylation in flow ionic liquid-in-oil Pickering emulsion. *Colloids and Surfaces A: Physicochemical and Engineering Aspects* **2019**, *570*, 191–198.

[161] Zhang, X.; Hou, Y.; Ettelaie, R.; Guan, R.; Zhang, M.; Zhang, Y.; Yang, H. Pickering Emulsion-Derived Liquid-Solid Hybrid Catalyst for Bridging Homogeneous and Heterogeneous Catalysis. *Journal of the American Chemical Society* **2019**, *141*, 5220–5230.

[162] Heyse, A.; Plikat, C.; Grün, M.; Delaval, S.; Ansorge-Schumacher, M.; Drews, A. Impact of enzyme properties on drop size distribution and filtration of water-in-oil Pickering emulsions for application in continuous biocatalysis. *Process Biochemistry* **2018**, *72*, 86–95.

[163] Vis, C. M.; Nieuwelink, A.-E.; Weckhuysen, B. M.; Bruijnincx, P. Continuous Flow Pickering Emulsion Catalysis in Droplet Microfluidics Studied with In-situ Raman Microscopy. *Chemistry (Weinheim an der Bergstrasse, Germany)* **2020**,

[164] Dedovets, D.; Li, Q.; Leclercq, L.; Nardello-Rataj, V.; Leng, J.; Zhao, S.; Pera-Titus, M. Multiphase Microreactors Based on Liquid–Liquid and Gas–Liquid Dispersions Stabilized by Colloidal Catalytic Particles. *Angewandte Chemie* **2022**, *134*.

[165] Tao, L.; Zhong, M.; Chen, J.; Jayakumar, S.; Liu, L.; Li, H.; Yang, Q. Heterogeneous hydroformylation of long-chain alkenes in IL-in-oil Pickering emulsion. *Green Chemistry* **2018**, *20*, 188–196.

[166] Zhou, W.-J.; Fang, L.; Fan, Z.; Albela, B.; Bonneviot, L.; de Campo, F.; Pera-Titus, M.; Clacens, J.-M. Tunable catalysts for solvent-free biphasic systems: pickering interfacial catalysts over amphiphilic silica nanoparticles. *Journal of the American Chemical Society* **2014**, *136*, 4869–4872.

[167] Xu, M.; Richard, F.; Corbet, M.; Marion, P.; Clacens, J.-M. Pickering emulsions assisted synthesis of fatty acetal over phenyl sulfonic groups grafted on activated charcoal. *Applied Catalysis A: General* **2020**, *597*, 117543.

[168] Li, Y.; Zhao, G.; Hong, B.; Zhao, S.; Han, X.; Pera-Titus, M. Unraveling Particle Size and Roughness Effects on the Interfacial Catalytic Properties of Pickering Emulsions. *Colloids and Surfaces A: Physicochemical and Engineering Aspects* **2020**, *599*, 124800.

[169] Zapata, P. A.; Faria, J.; Ruiz, M. P.; Jentoft, R. E.; Resasco, D. E. Hydrophobic zeolites for biofuel upgrading reactions at the liquid-liquid interface in water/oil emulsions. *Journal of the American Chemical Society* **2012**, *134*, 8570–8578.

[170] Mohaghegh, N.; Tasviri, M.; Rahimi, E.; Gholami, M. R. A novel p–n junction Ag 3 PO 4 /BiPO 4 -based stabilized Pickering emulsion for highly efficient photocatalysis. *RSC Advances* **2015**, *5*, 12944–12955.

[171] Fessi, N.; Nsib, M. F.; Chevalier, Y.; Guillard, C.; Dappozze, F.; Houas, A.; Palmisano, L.; Parrino, F. Photocatalytic Degradation Enhancement in Pickering Emulsions Stabilized by Solid Particles of Bare TiO2. *Langmuir : the ACS journal of surfaces and colloids* **2019**, *35*, 2129–2136.

[172] Bago Rodriguez, A. M.; Schober, L.; Hinzmann, A.; Gröger, H.; Binks, B. P. Effect of Particle Wettability and Particle Concentration on the Enzymatic Dehydration of n-Octanaloxime in Pickering Emulsions. *Angewandte Chemie (International ed. in English)* **2021**, *60*, 1450–1457.

[173] Leclercq, L.; Mouret, A.; Proust, A.; Schmitt, V.; Bauduin, P.; Aubry, J.-M.; Nardello-Rataj, V. Pickering emulsion stabilized by catalytic polyoxometalate nanoparticles: a new effective medium for oxidation reactions. *Chemistry (Weinheim an der Bergstrasse, Germany)* **2012**, *18*, 14352–14358.

[174] Leclercq, L.; Company, R.; Mühlbauer, A.; Mouret, A.; Aubry, J.-M.; Nardello-Rataj, V. Versatile eco-friendly pickering emulsions based on substrate/native cyclodextrin complexes: a winning approach for solvent-free oxidations. *ChemSusChem* **2013**, *6*, 1533–1540.

[175] Mouret, A.; Leclercq, L.; Mühlbauer, A.; Nardello-Rataj, V. Eco-friendly solvents and amphiphilic catalytic polyoxometalate nanoparticles: a winning combination for olefin epoxidation. *Green Chem* **2014**, *16*, 269–278.

[176] Zhang, W.; Fu, L.; Yang, H. Micrometer-scale mixing with Pickering emulsions: biphasic reactions without stirring. *ChemSusChem* **2014**, *7*, 391–396.

[177] Xue, F.; Zhang, Y.; Zhang, F.; Ren, X.; Yang, H. Tuning the Interfacial Activity of Mesoporous Silicas for Biphasic Interface Catalysis Reactions. *ACS applied materials & interfaces* **2017**, *9*, 8403–8412.

[178] Lv, G.; Wang, F.; Zhang, X.; Binks, B. P. Surface-Active Hollow Titanosilicate Particles as a Pickering Interfacial Catalyst for Liquid-Phase Alkene Epoxidation Reactions. *Langmuir* **2018**, *34*, 302–310.

[179] Wang, Z.; van Oers, M. C. M.; Rutjes, F. P. J. T.; van Hest, J. C. M. Polymersome colloidosomes for enzyme catalysis in a biphasic system. *Angewandte Chemie (International ed. in English)* **2012**, *51*, 10746–10750.

[180] Jiang, Y.; Liu, X.; Chen, Y.; Zhou, L.; He, Y.; Ma, L.; Gao, J. Pickering emulsion stabilized by lipase-containing periodic mesoporous organosilica particles: a robust biocatalyst system for biodiesel production. *Bioresource technology* **2014**, *153*, 278–283.

[181] Yang, B.; Leclercq, L.; Clacens, J.-M.; Nardello-Rataj, V. Acidic/amphiphilic silica nanoparticles: new eco-friendly Pickering interfacial catalysis for biodiesel production. *Green Chemistry* **2017**, *19*, 4552–4562.

[182] Zhang, S.; Hong, B.; Fan, Z.; Lu, J.; Xu, Y.; Pera-Titus, M. Aquivion-Carbon Composites with Tunable Amphiphilicity for Pickering Interfacial Catalysis. *ACS applied materials & interfaces* **2018**, *10*, 26795–26804.

[183] Wang, M.; Wang, M.; Zhang, S.; Chen, J. Pickering gel emulsion stabilized by enzyme immobilized polymeric nanoparticles: a robust and recyclable biocatalyst system for biphasic catalysis. *Reaction Chemistry & Engineering* **2019**, *4*, 1459–1465.

[184] Wang, L.; Liu, X.; Jiang, Y.; Liu, P.; Zhou, L.; Ma, L.; He, Y.; Li, H.; Gao, J. Silica Nanoflowers-Stabilized Pickering Emulsion as a Robust Biocatalysis Platform for Enzymatic Production of Biodiesel. *Catalysts* **2019**, *9*, 1026.

[185] Yang, X.; Wang, Y.; Bai, R.; Ma, H.; Wang, W.; Sun, H.; Dong, Y.; Qu, F.; Tang, Q.; Guo, T.; Binks, B. P.; Meng, T. Pickering emulsion-enhanced interfacial biocatalysis: tailored alginate microparticles act as particulate emulsifier and enzyme carrier. *Green Chemistry* **2019**, *21*, 2229–2233.

[186] Yang, L.; Zhao, X.; Lei, M.; Sun, J.; Yang, L.; Shen, Y.; Zhao, Q. Facile construction of thermo-responsive Pickering emulsion for esterification reaction in phase transfer catalysis system. *Molecular Catalysis* **2021**, *500*, 111335.

[187] Zhang, H.; Yu, S.; Cao, S.; Liu, X.; Tang, J.; Zhu, L.; Ji, J.; Wang, J. Stabilizing Triglyceride in Methanol Emulsions via a Magnetic Pickering Interfacial Catalyst for Efficient Transesterification under Static Conditions. *ACS omega* **2021**, *6*, 14138–14147.

[188] Zhu, Z.; Tan, H.; Wang, J.; Yu, S.; Zhou, K. Hydrodeoxygenation of vanillin as a bio-oil model over carbonaceous microspheres-supported Pd catalysts in the aqueous phase and Pickering emulsions. *Green Chem* **2014**, *16*, 2636–2643.

[189] Hao, P.; Schwartz, D. K.; Medlin, J. W. Effect of Surface Hydrophobicity of Pd/Al_2O_3 on Vanillin Hydrodeoxygenation in a Water/Oil System. *ACS Catalysis* **2018**, *8*, 11165–11173.

[190] Zhao, Y.; Zhang, X.; Sanjeevi, J.; Yang, Q. Hydroformylation of 1-octene in Pickering emulsion constructed by amphiphilic mesoporous silica nanoparticles. *Journal of Catalysis* **2016**, *334*, 52–59.

[191] Stehl, D. Hydroformylation of Long Chain Olefins in Pickering Emulsions. Ph.D. thesis, TU Darmstadt, Darmstadt, 2019.

[192] Faria, J.; Ruiz, M. P.; Resasco, D. E. Phase-Selective Catalysis in Emulsions Stabilized by Janus Silica-Nanoparticles. *Advanced Synthesis & Catalysis* **2010**, *352*, 2359–2364.

[193] Zapata, P. A.; Faria, J.; Pilar Ruiz, M.; Resasco, D. E. Condensation/Hydrogenation of Biomass-Derived Oxygenates in Water/Oil Emulsions Stabilized by Nanohybrid Catalysts. *Topics in Catalysis* **2012**, *55*, 38–52.

[194] Yang, H.; Zhou, T.; Zhang, W. A strategy for separating and recycling solid catalysts based on the pH-triggered Pickering-emulsion inversion. *Angewandte Chemie (International ed. in English)* **2013**, *52*, 7455–7459.

[195] Fu, L.; Li, S.; Han, Z.; Liu, H.; Yang, H. Tuning the wettability of mesoporous silica for enhancing the catalysis efficiency of aqueous reactions. *Chemical communications (Cambridge, England)* **2014**, *50*, 10045–10048.

[196] Huang, J.; Yang, H. A pH-switched Pickering emulsion catalytic system: high reaction efficiency and facile catalyst recycling. *Chemical communications (Cambridge, England)* **2015**, *51*, 7333–7336.

[197] Zhang, Y.; Zhang, M.; Yang, H. Tuning Biphasic Catalysis Reaction with a Pickering Emulsion Strategy Exemplified by Selective Hydrogenation of Benzene. *ChemCatChem* **2018**, *10*, 5224–5230.

[198] Li, D.-D.; Jiang, J.-Z.; Cai, C. Palladium nanoparticles anchored on amphiphilic Janus-type cellulose nanocrystals for Pickering interfacial catalysis. *Chemical communications (Cambridge, England)* **2020**, *56*, 9396–9399.

[199] Herrera, C.; Fuentealba, D.; Ghampson, I. T.; Sepulveda, C.; García-Fierro, J. L.; Canales, R. I.; Escalona, N. Selective conversion of biomass-derived furfural to cyclopentanone over carbon nanotube-supported Ni catalyst in Pickering emulsions. *Catalysis Communications* **2020**, *144*, 106092.

[200] Zhang, Y.; Ettelaie, R.; Binks, B. P.; Yang, H. Highly Selective Catalysis at the Liquid–Liquid Interface Microregion. *ACS Catalysis* **2021**, *11*, 1485–1494.

[201] Liu, J.; Lan, G.; Peng, J.; Li, Y.; Li, C.; Yang, Q. Enzyme confined in silica-based nanocages for biocatalysis in a Pickering emulsion. *Chemical communications (Cambridge, England)* **2013**, *49*, 9558–9560.

[202] Chen, Z.; Ji, H.; Zhao, C.; Ju, E.; Ren, J.; Qu, X. Individual surface-engineered microorganisms as robust Pickering interfacial biocatalysts for resistance-minimized phase-transfer bioconversion. *Angewandte Chemie (International ed. in English)* **2015**, *54*, 4904–4908.

[203] Peng, L.; Feng, A.; Liu, S.; Huo, M.; Fang, T.; Wang, K.; Wei, Y.; Wang, X.; Yuan, J. Electrochemical Stimulated Pickering Emulsion for Recycling of Enzyme in Biocatalysis. *ACS applied materials & interfaces* **2016**, *8*, 29203–29207.

[204] Shi, J.; Wang, X.; Zhang, S.; Tang, L.; Jiang, Z. Enzyme-conjugated ZIF-8 particles as efficient and stable Pickering interfacial biocatalysts for biphasic biocatalysis. *Journal of materials chemistry. B* **2016**, *4*, 2654–2661.

[205] Chen, Z.; Zhao, C.; Ju, E.; Ji, H.; Ren, J.; Binks, B. P.; Qu, X. Design of Surface-Active Artificial Enzyme Particles to Stabilize Pickering Emulsions for High-Performance Biphasic Biocatalysis. *Advanced materials (Deerfield Beach, Fla.)* **2016**, *28*, 1682–1688.

[206] Xue, L.-H.; Xie, C.-Y.; Meng, S.-X.; Bai, R.-X.; Yang, X.; Wang, Y.; Wang, S.; Binks, B. P.; Guo, T.; Meng, T. Polymer–Protein Conjugate Particles with Biocatalytic Activity for Stabilization of Water-in-Water Emulsions. *ACS Macro Letters* **2017**, *6*, 679–683.

[207] Meng, T.; Bai, R.; Wang, W.; Yang, X.; Guo, T.; Wang, Y. Enzyme-Loaded Mesoporous Silica Particles with Tuning Wettability as a Pickering Catalyst for Enhancing Biocatalysis. *Catalysts* **2019**, *9*, 78.

[208] Huang, X.-M.; Luo, Z.-J.; Guo, J.; Ruan, Q.-J.; Wang, J.-M.; Yang, X.-Q. Enzyme-Adsorbed Chitosan Nanogel Particles as Edible Pickering Interfacial Biocatalysts and Lipase-Responsive Phase Inversion of Emulsions. *Journal of agricultural and food chemistry* **2020**, *68*, 8890–8899.

[209] Yang, H.; Fu, L.; Wei, L.; Liang, J.; Binks, B. P. Compartmentalization of incompatible reagents within Pickering emulsion droplets for one-pot cascade reactions. *Journal of the American Chemical Society* **2015**, *137*, 1362–1371.

[210] Xue, N.; Zhang, G.; Zhang, X.; Yang, H. A reinforced Pickering emulsion for cascade reactions. *Chemical communications (Cambridge, England)* **2018**, *54*, 13014–13017.

[211] Sadgar, A. L.; Deore, T. S.; Jayaram, R. V. Pickering Interfacial Catalysis-Knoevenagel Condensation in Magnesium Oxide-Stabilized Pickering Emulsion. *ACS omega* **2020**, *5*, 12224–12235.

[212] Gao, Y.; Sun, C.; Qi, C. Ionic liquid-containing non-aqueous Pickering emulsions prepared with sterically-stabilized polymer nanoparticles: A highly efficient platform for Knoevenagel reaction. *Colloids and Surfaces A: Physicochemical and Engineering Aspects* **2021**, *626*, 126995.

[213] Tang, J.; Cao, S.; Wang, J. CO2-switchable Pickering emulsions: efficient and tunable interfacial catalysis for alcohol oxidation in biphasic systems. *Chemical communications (Cambridge, England)* **2019**, *55*, 11079–11082.

[214] Deng, C.; Xu, M.; Dong, Z.; Li, L.; Yang, J.; Guo, X.; Peng, L.; Xue, N.; Zhu, Y.; Ding, W. Exclusively catalytic oxidation of toluene to benzaldehyde in an O/W emulsion stabilized by hexadecylphosphate acid terminated mixed-oxide nanoparticles. *Chinese Journal of Catalysis* **2020**, *41*, 341–349.

[215] Tan, H.; Zhang, P.; Wang, L.; Yang, D.; Zhou, K. Multifunctional amphiphilic carbonaceous microcapsules catalyze water/oil biphasic reactions. *Chemical communications (Cambridge, England)* **2011**, *47*, 11903–11905.

[216] Fang, Z.; Yang, D.; Gao, Y.; Li, H. pH-responsible Pickering emulsion and its catalytic application for reaction at water–oil interface. *Colloid and Polymer Science* **2015**, *293*, 1505–1513.

[217] Zhao, H.; Li, J.; Wang, L.; Li, C.; Zhang, S. Pickering emulsion stabilized by dual stabilizer: A novel reaction/separation system for methacrolein synthesis. *Chemical Engineering Science* **2021**, *229*, 116038.

[218] Xie, H.; Zhao, W.; Ali, D. C.; Zhang, X.; Wang, Z. Interfacial biocatalysis in bacteria-stabilized Pickering emulsions for microbial transformation of hydrophobic chemicals. *Catalysis Science & Technology* **2021**, 2816–2826.

[219] Zhao, W.; Xie, H.; Zhang, X.; Wang, Z. Crystal substrate inhibition during microbial transformation of phytosterols in Pickering emulsions. *Applied microbiology and biotechnology* **2022**, *106*, 2403–2414.

[220] van Leeuwen, P. W. N. M. *Rhodium Catalyzed Hydroformylation*; Catalysis by metal complexes; Kluwer Academic Publishers: Hingham, 2000; Vol. v. 22.

[221] Bohnen, H.-W.; Cornils, B. Hydroformylation of alkenes: An industrial view of the status and importance. *Advances in Catalysis* **2002**, *47*, 1–64.

[222] Frey, G. D. 75 Years of oxo synthesis – The success story of a discovery at the OXEA Site Ruhrchemie. *Journal of Organometallic Chemistry* **2014**, *754*, 5–7.

[223] Brown, C. K.; Wilkinson, G. Homogeneous hydroformylation of alkenes with hydridocarbonyltris-(triphenylphosphine)rhodium(I) as catalyst. *Journal of the Chemical Society A: Inorganic, Physical, Theoretical* **1970**, 2753.

[224] Pittman, J. C.; Honnick, W. Rhodium-Catalyzed Hydroformylation of Allyl Alcohol. A Potential Route to1,4-Butanediol. *The Journal of Organic Chemistry* **1980**, *45*, 2132–2139.

[225] Pittman, C. U.; Honnick, W. D.; Yang, J. J. Hydroformylation of methyl methacrylate catalyzed by homogeneous and polymer-attached rhodium complexes. *The Journal of Organic Chemistry* **1980**, *45*, 684–689.

[226] Nicolas Maximilian Kaiser, Dynamic optimization based reactor synthesis and design under uncertainty for liquid multiphase processes. Ph.D. thesis, Otto-von-Guericke-Universität Magdeburg, Magdeburg, 2018.

[227] Tudor, R.; Ashley, M. Enhancement of Industrial Hydroformylation Processes by the Adoption of Rhodium-Based Catalyst: Part I. *Platinum Metals Review* **2007**, *51*, 116–126.

[228] Tudor, B. R.; Ashley, M. Enhancement of Industrial Hydroformylation Processes by the Adoption of Rhodium-Based Catalyst: Part II. *Platinum Metals Review* **2007**, *51*, 164–171.

[229] Schäfer, E.; Brunsch, Y.; Sadowski, G.; Behr, A. Hydroformylation of 1-Dodecene in the Thermomorphic Solvent System Dimethylformamide/Decane. Phase Behavior–Reaction Performance–Catalyst Recycling. *Industrial & Engineering Chemistry Research* **2012**, *51*, 10296–10306.

[230] McBride, K.; Sundmacher, K. Data Driven Conceptual Process Design for the Hydroformylation of 1-Dodecene in a Thermomorphic Solvent System. *Industrial & Engineering Chemistry Research* **2015**, *54*, 6761–6771.

[231] Bianga, J.; Künnemann, K. U.; Gaide, T.; Vorholt, A. J.; Seidensticker, T.; Dreimann, J. M.; Vogt, D. Thermomorphic Multiphase Systems: Switchable Solvent Mixtures for the Recovery of Homogeneous Catalysts in Batch and Flow Processes. *Chemistry (Weinheim an der Bergstrasse, Germany)* **2019**, *25*, 11586–11608.

[232] Keßler, T.; Kunde, C.; Linke, S.; McBride, K.; Sundmacher, K.; Kienle, A. Systematic Selection of Green Solvents and Process Optimization for the Hydroformylation of Long-Chain Olefines. *Processes* **2019**, *7*, 882.

[233] Linke, S.; McBride, K.; Sundmacher, K. Systematic Green Solvent Selection for the Hydroformylation of Long-Chain Alkenes. *ACS Sustainable Chemistry & Engineering* **2020**,

[234] Alsalahi, W.; Trzeciak, A. M. Rhodium-catalyzed hydroformylation under green conditions: Aqueous/organic biphasic, "on water", solventless and Rh nanoparticle based systems. *Coordination Chemistry Reviews* **2021**, *430*, 213732.

[235] Behr, A.; Henze, G.; Schomaecker, R. Thermoregulated Liquid/Liquid Catalyst Separation and Recycling. *ChemInform* **2006**, *37*.

[236] Schwarze, M.; Pogrzeba, T.; Volovych, I.; Schomäcker, R. Microemulsion systems for catalytic reactions and processes. *Catalysis Science & Technology* **2015**, *5*, 24–33.

[237] Pogrzeba, T.; Schmidt, M.; Milojevic, N.; Urban, C.; Illner, M.; Repke, J.-U.; Schomäcker, R. Understanding the Role of Nonionic Surfactants during Catalysis in Microemulsion Systems on the Example of Rhodium-Catalyzed Hydroformylation. *Industrial & Engineering Chemistry Research* **2017**, *56*, 9934–9941.

[238] Ünveren, H. H. Y.; Schomäcker, R. Rhodium catalyzed hydroformylation of 1-octene in microemulsion: comparison with various catalytic systems. *Catalysis Letters* **2006**, *110*, 195–201.

[239] Illner, M.; Müller, D.; Esche, E.; Pogrzeba, T.; Schmidt, M.; Schomäcker, R.; Wozny, G.; Repke, J.-U. Hydroformylation in Microemulsions: Proof of Concept in a Miniplant. *Industrial & Engineering Chemistry Research* **2016**, *55*, 8616–8626.

[240] Sigma Aldrich / Merck, price of mesopourous silica beads. (last checked: 24.06.2022 13:00); `https://www.sigmaaldrich.com/DE/en/product/aldrich/748161`.

[241] Sigma Aldrich / Merck, price fumed silica. (last checked 24.06.22 13:00); `https://www.sigmaaldrich.com/DE/en/product/sigma/s5505`.

[242] Evans, D.; Osborn, J. A.; Wilkinson, G. Hydroformylation of alkenes by use of rhodium complex catalysts. *Journal of the Chemical Society A: Inorganic, Physical, Theoretical* **1968**, 3133.

[243] Hamerla, T.; Rost, A.; Kasaka, Y.; Schomäcker, R. Hydroformylation of 1-Dodecene with Water-Soluble Rhodium Catalysts with Bidentate Ligands in Multiphase Systems. *ChemCatChem* **2013**, *5*, 1854–1862.

[244] Kiedorf, G.; Hoang, D. M.; Müller, A.; Jörke, A.; Markert, J.; Arellano-Garcia, H.; Seidel-Morgenstern, A.; Hamel, C. Kinetics of 1-dodecene hydroformylation in a thermomorphic solvent system using a rhodium-biphephos catalyst. *Chemical Engineering Science* **2014**, *115*, 31–48.

[245] Deshpande, R. M.; Kelkar, A. A.; Sharma, A.; Julcour-Lebigue, C.; Delmas, H. Kinetics of hydroformylation of 1-octene in ionic liquid-organic biphasic media using rhodium sulfoxantphos catalyst. *Chemical Engineering Science* **2011**, *66*, 1631–1639.

[246] Garland, M.; Pino, P. Kinetics of the formation and hydrogenolysis of acylrhodium tetracarbonyl. *Organometallics* **1991**, *10*, 1693–1704.

[247] van der Slot, S. C.; Kamer, P. C. J.; van Leeuwen, P. W. N. M.; Iggo, J. A.; Heaton, B. T. Mechanistic Studies of the Hydroformylation of 1-Alkenes Using a Monodentate Phosphorus Diamide Ligand. *Organometallics* **2001**, *20*, 430–441.

[248] Skale, T.; Hohl, L.; Kraume, M.; Drews, A. Feasibility of w/o Pickering emulsion ultrafiltration. *Journal of Membrane Science* **2017**, *535*, 1–9.

[249] Schreuder Goedheijt, M.; Kamer, P. C.; van Leeuwen, P. W. A water-soluble diphosphine ligand with a large 'natural' bite angle for two-phase hydroformylation of alkenes. *Journal of Molecular Catalysis A: Chemical* **1998**, *134*, 243–249.

[250] Graf, C.; van Blaaderen, A. Metallodielectric Colloidal Core−Shell Particles for Photonic Applications. *Langmuir* **2002**, *18*, 524–534.

[251] Barisik, M.; Atalay, S.; Beskok, A.; Qian, S. Size Dependent Surface Charge Properties of Silica Nanoparticles. *The Journal of Physical Chemistry C* **2014**, *118*, 1836–1842.

[252] Hoare, T.; Pelton, R. Highly pH and Temperature Responsive Microgels Functionalized with Vinylacetic Acid. *Macromolecules* **2004**, *37*, 2544–2550.

[253] Garcia, A.; Marquez, M.; Cai, T.; Rosario, R.; Hu, Z.; Gust, D.; Hayes, M.; Vail, S. A.; Park, C.-D. Photo-, thermally, and pH-responsive microgels. *Langmuir : the ACS journal of surfaces and colloids* **2007**, *23*, 224–229.

[254] Sanson, N.; Rieger, J. Synthesis of nanogels/microgels by conventional and controlled radical crosslinking copolymerization. *Polymer Chemistry* **2010**, *1*, 965.

[255] Helmholtz, H. Ueber einige Gesetze der Vertheilung elektrischer Ströme in körperlichen Leitern mit Anwendung auf die thierisch-elektrischen Versuche. *Annalen der Physik* **1853**, *165*, 211–233.

[256] Helmholtz, H. Studien über electrische Grenzschichten. *Annalen der Physik* **1879**, *243*, 337–382.

[257] Gouy, M. Sur la constitution de la charge électrique à la surface d'un électrolyte. *Journal de Physique Théorique et Appliquée* **1910**, *9*, 457–468.

[258] Chapman, D. L. LI. A contribution to the theory of electrocapillarity. *The London, Edinburgh, and Dublin Philosophical Magazine and Journal of Science* **1913**, *25*, 475–481.

[259] Tadros, T. *Encyclopedia of Colloid and Interface Science*; Springer Berlin Heidelberg: Berlin, Heidelberg, 2013.

[260] Berne, B. J.; Pecora, R. *Dynamic light scattering: With applications to chemistry, biology, and physics*, dover ed. ed.; Dover Publications: Mineola, NY, 2000.

[261] Huh, C.; Mason, S. G. A rigorous theory of ring tensiometry. *Colloid and Polymer Science* **1975**, *253*, 566–580.

[262] Stock, S.; Röhl, S.; Mirau, L.; Kraume, M.; von Klitzing, R. Maximum Incorporation of Soft Microgel at Interfaces of Water in Oil Emulsion Droplets Stabilized by Solid Silica Spheres. *Nanomaterials* **2022**, *12*, 2649.

[263] Godin, M.; Bryan, A. K.; Burg, T. P.; Babcock, K.; Manalis, S. R. Measuring the mass, density, and size of particles and cells using a suspended microchannel resonator. *Applied Physics Letters* **2007**, *91*, 123121.

[264] Alheshibri, M.; Craig, V. S. J. Differentiating between Nanoparticles and Nanobubbles by Evaluation of the Compressibility and Density of Nanoparticles. *The Journal of Physical Chemistry C* **2018**, *122*, 21998–22007.

[265] Adamov, G. A. Measurement of density and specific weight of suspensions, boiling layers, liquids and gases in ascending flow. *Measurement Techniques* **1960**, *1*, 426–433.

[266] Aminabhavi, T. M.; Joshi, S. S.; Balundgi, R. H.; Shukla, S. S. Densities and viscosities of binary and ternary liquid mixtures at 25 °C. *Canadian Journal of Chemistry* **1991**, *69*, 1028–1032.

[267] Aralaguppi, M. I.; Aminabhavi, T. M.; Balundgi, R. H. Excess molar volume, excess isentropic compressibility and excess molar refraction of binary mixtures of methyl acetoacetate with benzene, toluene, m-xylene, mesitylene and anisole. *Fluid Phase Equilibria* **1992**, *71*, 99–112.

[268] Skinner, B.; Appleman, D. E. Melanophlogite, a cubic polymorph of silica. *American Mineralogist* **1963**, *48*, 854–867.

[269] Kimoto, S.; Dick, W. D.; Hunt, B.; Szymanski, W. W.; McMurry, P. H.; Roberts, D. L.; Pui, D. Y. H. Characterization of nanosized silica size standards. *Aerosol Science and Technology* **2017**, *51*, 936–945.

[270] Mirau, L. Charakterisierung der beschleunigten Adsorptionskinetik von PNIPAM Mikrogelen an der Wasser-Öl-Grenzfläche durch Ultraschall. bachelor thesis, TU Darmstadt, Darmstadt, 16.06.2022.

[271] Gruen, D. W.; Wolfe, J. Lateral tensions and pressures in membranes and lipid monolayers. *Biochimica et Biophysica Acta (BBA) - Biomembranes* **1982**, *688*, 572–580.

[272] Low, L. E.; Siva, S. P.; Ho, Y. K.; Chan, E. S.; Tey, B. T. Recent advances of characterization techniques for the formation, physical properties and stability of Pickering emulsion. *Advances in colloid and interface science* **2020**, *277*, 102117.

[273] Lee, J.; Zhou, Z.-L.; Alas, G.; Behrens, S. H. Mechanisms of Particle Charging by Surfactants in Nonpolar Dispersions. *Langmuir : the ACS journal of surfaces and colloids* **2015**, *31*, 11989–11999.

[274] Witt, M. U.; Hinrichs, S.; Möller, N.; Backes, S.; Fischer, B.; von Klitzing, R. Distribution of CoFe2O4 Nanoparticles Inside PNIPAM-Based Microgels of Different Cross-linker Distributions. *The journal of physical chemistry. B* **2019**, *123*, 2405–2413.

[275] Pal, R. Modeling of Sedimentation and Creaming in Suspensions and Pickering Emulsions. *Fluids* **2019**, *4*, 186.

[276] Destribats, M.; Lapeyre, V.; Sellier, E.; Leal-Calderon, F.; Ravaine, V.; Schmitt, V. Origin and control of adhesion between emulsion drops stabilized by thermally sensitive soft colloidal particles. *Langmuir* **2012**, *28*, 3744–3755.

[277] Horiguchi, Y.; Kawakita, H.; Ohto, K.; Morisada, S. Temperature-responsive Pickering foams stabilized by poly(N -isopropylacrylamide) nanogels. *Advanced Powder Technology* **2018**, *29*, 266–272.

[278] Rauh, A.; Rey, M.; Barbera, L.; Zanini, M.; Karg, M.; Isa, L. Compression of hard core-soft shell nanoparticles at liquid-liquid interfaces: influence of the shell thickness. *Soft matter* **2016**, *13*, 158–169.

[279] Faulde, M.; Siemes, E.; Wöll, D.; Jupke, A. Fluid Dynamics of Microgel-Covered Drops Reveal Impact on Interfacial Conditions. *Polymers* **2018**, *10*, 809.

Wissenschaftlicher Werdegang

07/2018 - heute	Wissenschaftlicher Mitarbeiter am Institut für Physik kondensierter Materie an der Technischen Universität Darmstadt in der AG von Prof. Dr. Regine von Klitzing
04/2016 - 06/2018	Studium der Physik (M. Sc.) an der Technischen Universität Darmstadt mit Schwerpunkt ″Physik weicher/kondensierter Materie″
	Masterarbeit in der Gruppe von PD Ingo Alig am Fraunhofer-Institut für Betriebsfestigkeit und Systemzuverlässigkeit mit dem Thema: ″Niederfeld-NMR zur Untersuchung des Einflusses von Dehnung, Nukleierung und Vernetzung auf Dynamik und Struktur von Polymeren″
10/2012 - 03/2016	Studium der Physik (B. Sc.) an der Technischen Universität Darmstadt
	Bachelorarbeit in der AG von Prof. Dr. Michael Vogel mit dem Thema: ″Untersuchung der Diffusion von Wasser an Proteinmatrizen mit Hilfe von Feldgradienten NMR″